


# 國立交通大學

應用化學所

博士論文

合成不同插層劑對高分子/黏土奈米複合材料  
物理性質之影響



Effect of Various Synthesized Intercalation Agents on  
Physical Properties of Polymer/Clay Nanocomposites

研究生：葉定儒

指導老師：張豐志 教授

中華民國九十四年九月

合成不同插層劑對高分子/黏土奈米複合材料  
物理性質之影響

Effect of Various Synthesized Intercalation Agents on  
Physical Properties of Polymer/Clay Nanocomposites

研究生：葉定儒

Student : Ting-Ju Yeh

指導教授：張豐志

Advisor : Feng-Chih Chang



A Dissertation  
Presented to Institute of Applied Chemistry  
College of Science  
National Chiao Tung University  
In Partial Fulfillment of the Requirements  
For the Degree of  
Doctor of Philosophy  
In  
Applied Chemistry  
September 2004  
Hsinchu, Taiwan, Republic of China

中華民國九十四年九月

## 誌 謝

從未中斷的求學之路暫時要告一段落了，對我而言這一路走來真的很辛苦，幸運地我遇到許多貴人的幫助，才使得我能順利拿到博士學位。我要感謝我的指導教授張豐志博士，這些年勞心勞力修改學生的論文，以及提供良好的研究環境使我能專心在研究上，老師培養我具備獨立思考的能力與自動自發的精神，老師的待人處世與領導統御皆值得我學習的地方。感謝口試委員：段葉芳教授、芮祥鵬教授、邱顯堂教授、葉正濤教授、廖建勛教授、吳震裕教授、韋光華教授與黃華宗教授提供寶貴的意見，使學生的論文更臻完善。

感謝實驗室的學長郭紹偉博士、黃智峰博士、陳文億博士與蘇一哲博士在實驗上的幫忙與親身經驗的傳承使我獲益良多。我要感謝與我共同奮鬥的同學老隆、muscle、阿錫、凱方，有你們真好，讓我研究所生活多采多姿。謝謝阿明、寶寶、小呆、阿吉與加菲貓，因為你們的搞笑使得實驗室生氣勃勃。感謝我帶的學弟丫廣實驗上的協助，使我順利完成論文。謝謝婉君、小杜、漢清、芷伶為實驗室辛苦的付出，管帳、大陸學者來台、實驗室計畫有勞你們。感謝學弟妹英傑、DiDi、怡婷、佩儀、春雄維持實驗儀器正常的運轉、藥品目錄清楚、採買實驗室必需品，我才能順利畢業，感謝實驗室所有成員。

感謝大學的專題老師段葉芳教授，在大學什麼都不懂的情況下訓練我具備基礎的研究能力。謝謝大學好友誌民、誌銘、福特豐富我大學生活，且時常關心我、幫助我，真的非常謝謝你們。我還要感謝在大學期間非常照顧我的叔叔和嬸嬸，因為有他們的幫忙，我才能快速適應台北的生活。

我要感謝一直陪在我身邊默默支持我的女朋友瑜芝，因為你我對唸書不在排斥，因為你我繼續求上進，很高興能與你在一起，認識你是我這輩子最快樂的事。

我最感謝我的家人，沒有他們的栽培，我無法完成博士學位，我的榮耀獻給最偉大的父母親。

# Outline of Contents

Outline of Contents	I
List of Tables	VI
List of Schemes	VII
List of Figures	VIII
Abstract (in Chinese)	XIV
Abstract (in English)	XVI
Chapter 1 Introduction	1
1.1 Introduction	1
1.2 Organically Modified Clay	6
1.3 Polymer/Clay Nanocomposite Processing	10
1.4 Surface-Initiated Polymerization (SIP)	14
1.5 Types of Polymer Matrix	20
1.5.1 Polyamide Matrices	20
1.5.2 Polyimide Matrices	20
1.5.3 Polypropylene and Polyethylene Matrices	22
1.5.4 Polymethylmethacrylate/Polystyrene Matrices	22
1.5.5 Epoxy and Polyurethane Matrices	23
1.5.6 Polyelectrolyte Matrices	24
1.5.7 Rubber Matrices	25
1.5.8 Others	25
1.6 Properties of Nanocomposites	26
1.6.1 Dimensional Stability	26
1.6.2 Thermal Stability and Flammability	28
1.6.3 Mechanical Properties	30

1.6.4 Gas Barrier Properties	34
1.6.5 Electrical and Optical Properties	35
1.7 Summary	37
References	38
Chapter 2 Enhanced Thermal Properties of PS Nanocomposites formed from Inorganic POSS-Treated Montmorillonite	43
Abstract	43
2.1 Introduction	44
2.2 Experimental	46
2.2.1 Materials	46
2.2.2 Preparation of CPC-Modified Clays	46
2.2.3 Preparation of POSS-Modified Clays	46
2.2.4 Preparation of Polystyrene/Clay Nanocomposites	47
2.2.5 Instrumentations	47
2.3 Results and Discussion	49
2.3.1 X-Ray Diffractions	49
2.3.2 TEM Measurements on the Nanocomposites	51
2.3.3 Infrared Spectroscopy	52
2.3.4 Analyzing Glass Transition Temperatures	52
2.3.5 Molecular Weights of the Nanocomposites	52
2.3.6 Characterization by TGA	53
2.4 Conclusions	55
References	56

Chapter 3 Thermal Properties of Exfoliated Polystyrene Nanocomposites formed from Rigid Intercalation Agents-Treated Montmorillonite	66
Abstract	66
3.1 Introduction	67
3.2 Experimental	69
3.2.1 Materials	69
3.2.2 Synthesis of Intercalation Agent of 4-(4-adamantylphenoxy)-1-butanamine (APB)	69
3.2.3 Preparation of Modified Clays	70
3.2.4 Preparation of Polystyrene/Clay Nanocomposites	70
3.2.5 Instrumentations	71
3.3 Results and Discussion	73
3.3.1 Preparation of 4-(4-adamantylphenoxy)-1-butanamine (APB)	73
3.3.2 X-Ray Diffractions	73
3.3.3 TEM Measurements on the Nanocomposites	75
3.3.4 Analyzing Glass Transition Temperatures	75
3.3.5 Molecular Weights of the Nanocomposites	75
3.3.6 Coefficient of Thermal Expansion	76
3.3.7 Characterization by TGA	76
3.4 Conclusions	78
References	79
Chapter 4 Enhanced Thermal Properties of PS Nanocomposites formed from Montmorillonite Treated with a Surfactant/Cyclodextrin Inclusion Complex	89

Abstract	89
4.1 Introduction	90
4.2 Experimental	92
4.2.1 Materials	92
4.2.2 Preparation of Inclusion Complex	92
4.2.3 Preparation of Surfactant-Modified Clays	93
4.2.4 Preparation Polystyrene/Clay Nanocomposites	93
4.2.5 Instrumentations	94
4.3 Results and Discussion	95
4.3.1 X-Ray Diffraction	95
4.3.2 TEM Characterization	96
4.3.3 Stoichiometry of the Complex	97
4.3.4 Solid State <sup>13</sup> C NMR Spectroscopic Analysis	97
4.3.5 Glass Transition Temperatures	98
4.3.6 Characterization by TGA	99
4.4 Conclusions	100
References	101
Chapter 5 Synthesis of a Novel Benzoxazine Monomer-Intercalated Montmorillonite and the Curing Kinetics of Polybenzoxazine/Clay Hybrid Nanocomposites	111
Abstract	111
5.1 Introduction	112
5.2 Experimental	114
5.2.1 Materials	114

5.2.2 Synthesis of Monofunctional benzoxazine Monomer (MBM)	114
5.2.3 Preparation of MBM-Modified Clays	115
5.2.4 Preparation of Polybenzoxazine/Clay Nanocomposites	115
5.2.5 Isothermal Curing	115
5.2.6 Dynamic Curing	116
5.2.7 Instrumentation	116
5.3 Results and Discussion	118
5.3.1 Preparation of Monofunctional Benzoxazine Monomer (MBM)	118
5.3.2 X-Ray Diffractions	118
5.3.3 TEM Measurements of the Nanocomposites	119
5.3.4 Investigating the Curing Behavior of PBZ/Clay Nanocomposites Using DSC	119
5.3.5 Kinetic Analysis	121
5.3.5.1 Dynamic Kinetic Method	122
5.3.5.2 Isothermal Kinetic Analysis (Autocatalytic Model)	123
5.3.6 Analyzing Glass Transition Temperatures	124
5.3.7 Thermal Stability of PBZ/Clay Nanocomposites	125
5.4 Conclusions	126
References	127
Chapter 6 Conclusions and Future Outlook	143
List of Publications	146
Introduction to Author	148



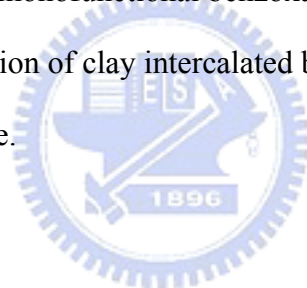
## List of Tables

Table 2-1	Results of TGA and DSC for Polystyrene Nanocomposites	58
Table 2-2	Molecular Weights of Polystyrene Nanocomposites	58
Table 3-1	Results of TGA and DSC for Polystyrene Nanocomposites	81
Table 3-2	Molecular Weights of Polystyrene Nanocomposites	81
Table 4-1	Results of TGA and DSC Data for the Polystyrene Nanocomposites	103
Table 5-1	Activation energies obtained using the Kissinger and Ozawa methods for PBZ/clay nanocomposites.	130
Table 5-2	Results obtained from isothermal experiments on the PBZ/clay nanocomposites.	130
Table 5-3	TGA and DSC data for PBZ/clay nanocomposites.	130



## List of Schemes

Scheme 2-1	Chemical structures of the surfactants used to prepare the modified clays.	59
Scheme 2-2	Schematic drawing of the clay intercalated by the POSS and polystyrene.	60
Scheme 3-1	Structures of Intercalation Agent (a) APP (b) APB.	82
Scheme 3-2	Preparation of Intercalation Agent (APB).	83
Scheme 4-1	Schematic representation of clay intercalated by the CPC/ $\alpha$ -CD inclusion complexes.	104
Scheme 5-1	Preparation of polybenzoxazine (PBZ).	133
Scheme 5-2	Preparation of the monofunctional benzoxaine monomer (MBM).	134
Scheme 5-3	Schematic illustration of clay intercalated by the MBM and polybenzoxazine.	135



## List of Figures

Figure 1-1	Schematic of nanoscale fillers	2
Figure 1-2	Schematic representation of various methods used to prepare polymer-layered-silicate nanocomposites.	4
Figure 1-3	Schematically illustration of three different types of thermodynamically achievable polymer/layered silicate nanocomposites.	5
Figure 1-4	Structures of the salts used to prepare the organically modified clays.	6
Figure 1-5	Structure of triphenylhexadecylstibonium trifluoromethylsulfonate.	7
Figure 1-6	Structure of VDAC used to prepare the organically modified clay.	7
Figure 1-7	Chemical structures of the surfactants used to prepare the modified clays.	8
Figure 1-8	The structures of intercalation agent (a) CPC and (b) CPC/ $\alpha$ -CD inclusion complex.	9
Figure 1-9	Schematic of the basic steps in processing clay-filled polymers	11
Figure 1-10	X-ray diffraction data showing the diffraction patterns that result from (a), (b) exfoliated clays, (c) intercalated clays, (d) organically modified clays.	12
Figure 1-11	Schematic of the microstructures that can develop in clay-filled polymer composites.	13
Figure 1-12	(a) Synthetic scheme and structure of the bicationic free radical initiator. (b) Synthetic Scheme and structure of the monocationic free radical initiator.	15
Figure 1-13	X-ray powder diffraction patterns of pure clay and two intercalated clay samples.	16

Figure 1-14	(a-c) Schematic diagrams of the intercalation: (a) original clay, (b) clay intercalated with bicationic initiator, and (c) clay intercalated with monocationic initiator.	17
Figure 1-15	XRD spectra of the two SIP nanocomposites showing degree of exfoliation.	18
Figure 1-16	Schematic of the synthesis of polyimide-clay hybrid film.	21
Figure 1-17	PS and PS/clay nanocomposites after dimension stability test. Clay loading is 5 wt % for all nanocomposites.	27
Figure 1-18	TGA curves for polystyrene, PS, and the nanocomposites.	28
Figure 1-19	Peak heat release rates for polystyrene and the three nanocomposites.	29
Figure 1-20	Storage modulus of (a) pure PS, (b) PS/MMT-1, (c) PS/MMT-2 and (d) PS/MMT-3.	31
Figure 1-21	Tan $\delta$ values of (a) pure PS, (b) PS/MMT-1, (c) PS/MMT-2 and (d) PS/MMT-3.	31
Figure 1-22	(a) Tensile strengths, (b) Young's modulus and (c) elongations at break of PS/MMT nanocomposites.	33
Figure 1-23	Formation of tortuous path in PLS nanocomposites.	34
Figure 1-24	Dependence of diffusion coefficient of water on clay content for montmorillonite with a layer width of 100 nm, and saponite with a layer width of 50 nm.	35
Figure 2-1	XRD spectra of materials featuring various ratios of the organic ammonium salt.	61
Figure 2-2	X-Ray powder diffraction patterns of pure POSS, pure clay, and intercalated clay.	61

Figure 2-3	XRD spectra of the two surfactant-containing nanocomposites, indicating the degree of exfoliation.	62
Figure 2-4	TEM micrographs of (a, top) the CPC-treated nanocomposite and (b, bottom) the POSS-treated nanocomposite.	63
Figure 2-5	IR spectra of pure clay, pure POSS, and intercalated clay.	64
Figure 2-6	DSC curves for determining the glass transition temperature of the nanocomposites.	64
Figure 2-7	TGA traces of (a) pure clay, (b) clay intercalated with the POSS, and (c) clay intercalated with CPC.	65
Figure 2-8	TGA curves for the nanocomposites under a nitrogen atmosphere: (a) pure PS, (b) the nanocomposite formed with CPC, and (c) the nanocomposite formed with POSS.	65
Figure 3-1	Proton NMR spectra of intercalation agent (APB)	84
Figure 3-2	X-ray diffraction patterns of (a) pure clay, (b) the APP-intercalated clay, (c) the APB-intercalated clay.	84
Figure 3-3	WAXD analysis of PS nanocomposites prepared by emulsion polymerization: (a) APB treatment; (b) APP treatment.	85
Figure 3-4	TEM images of the APP-treated nanocomposite at low (left) and high (right) magnifications.	86
Figure 3-5	TEM images of APB-treated nanocomposite at low (left) and high (right) magnifications.	86
Figure 3-6	DSC curves for determining the glass transition temperature of (a) PS, (b) the nanocomposite formed using APP, and (c) the nanocomposite formed using APB	87

Figure 3-7	Coefficient of thermal expansion of nanocomposites.	87
Figure 3-8	TGA curves of (a) pure APP (b) pure APB.	88
Figure 3-9	TGA curves of the nanocomposites recorded under nitrogen atmospheres: (a) pure PS, (b) the nanocomposite formed using APB, and (c) the nanocomposite formed using APP.	88
Figure 4-1	X-Ray diffraction patterns of (a) $\alpha$ -CD, (b) the CPC/ $\alpha$ -CD inclusion complex, and (c) clay intercalated by the CPC/ $\alpha$ -CD inclusion complex.	105
Figure 4-2	X-Ray diffraction patterns of (a) pure clay, (b) the CPC-intercalated clay, and (c) the CPC/ $\alpha$ -CD intercalated clay.	105
Figure 4-3	WAXD analysis of PS nanocomposites prepared by emulsion polymerization: (a) CPC treatment; (b) CPC/ $\alpha$ -CD treatment.	106
Figure 4-4	TEM images of the CPC-treated nanocomposite at low (left) and high (right) magnifications.	107
Figure 4-5	TEM images of CPC/ $\alpha$ -CD-treated nanocomposite at low (left) and high (right) magnifications.	107
Figure 4-6	$^1\text{H}$ NMR spectrum (500 MHz) of the CPC/ $\alpha$ -CD complex in $\text{DMSO-}d_6$ .	108
Figure 4-7	$^{13}\text{C}$ CP/MAS NMR spectra of (a) $\alpha$ -CD, (b) CPC/ $\alpha$ -CD, and (c) CPC/ $\alpha$ -CD intercalated clay.	108
Figure 4-8	DSC curves for determining the glass transition temperature of (a) PS, (b) the nanocomposite formed using CPC, and (c) the nanocomposite formed using CPC/ $\alpha$ -CD.	109

Figure 4-9	TGA curves of (a) pure CPC and (b) the CPC/ $\alpha$ -CD inclusion complex.	109
Figure 4-10	TGA curves of the nanocomposites recorded under nitrogen atmospheres: (a) pure PS, (b) the nanocomposite formed using CPC, and (c) the nanocomposite formed using CPC/ $\alpha$ -CD.	110
Figure 5-1	$^1\text{H}$ NMR spectrum of MBM.	136
Figure 5-2	XRD patterns of (a) pure clay and (b) the clay intercalated by MBM.	136
Figure 5-3	XRD patterns of the (a) 3, (b) 6, (c) 10, and (d) 15% clay nanocomposites.	137
Figure 5-4	TEM micrographs of the (a) 3 and (b) 6% clay nanocomposites.	138
Figure 5-5	Dynamic exothermal curves of the PBZ/clay nanocomposites recorded at a heating rate of $20^\circ\text{C}/\text{min}$ .	139
Figure 5-6	Dynamic DSC exothermic curves of pure PBZ recorded at different scan rates.	139
Figure 5-7	Plots of reaction rate versus curing time for pure PBZ at different curing temperatures.	140
Figure 5-8	Plots of conversion as a function of cure time for the PBZ/clay nanocomposites cured at isothermal curing temperature of $200^\circ\text{C}$ .	140
Figure 5-9	Plots of reaction rate as a function of conversion for the nanocomposites cured at different temperatures.	141
Figure 5-10	Representations of Ozawa's and Kissinger's methods of calculating the activation energy from non-isothermal data for pure PBZ ( $T_p$ , temperature at maximum reaction rate; $\beta$ , heating rate).	141

Figure 5-11 DSC curves for determining the glass transition temperatures of the nanocomposites. 142

Figure 5-12 TGA curves of the PBZ/clay nanocomposites recorded under a nitrogen atmosphere. 142





## 摘要

蒙托土應用於高分子材料上，改善了原有高分子的物理性質，例如：熱穩定性、機械性質、阻氣性、尺寸安定性等。這些物理性質改善的程度取決於蒙托土在高分子基材的分散程度，分散程度越好性質提升越顯著，反之則不然。本篇論文分成四部份，主要探討不同插層劑對奈米複合材料物理性質的影響。

1. 本實驗利用乳化聚合的方法製備聚苯乙烯/蒙托土奈米複材，在蒙托土含量 3%時為脫層結構，在實驗當中使用 POSS 與 CPC 兩種插層劑改質蒙托土，由 X-ray 鑑定出 POSS 與 CPC 都有成功插層進入蒙托土，在 TGA 實驗中，POSS 有效地增加奈米複材的熱穩定性，主要因素是 POSS 較 CPC 具有剛性結構，有別於市售的插層劑，其具有長的碳烷鏈較不受熱。GPC 分子量分析得知蒙托土會妨礙高分子聚合反應的進行，分子量分布也較廣。
2. 我們合成插層劑 APB，其具有金剛烷的官能基，去改質蒙托土製備聚苯乙烯/蒙托土奈米複材，先前文獻利用含磷的官能基作插層劑，目的提升奈米複材的熱穩定性，本實驗研究金剛烷可否取代磷的官能基，作為插層劑另一種選擇。TGA 結果顯示金剛烷確實較含磷的插層劑穩定，XRD 說明我們所製備的複合材料具有奈米尺寸的分散程度，DSC 得知有添加蒙托土的奈米複材玻璃轉移溫度較高，熱膨脹係數也下降 44~55%，證實蒙托土有助奈米複材的尺寸安定性。

3. 研究一般商業用插層劑CPC經過改質，套入環糊精對奈米複材的影響。研究結果顯示CPC套環糊精有助將長的碳烷鏈拉直，避免它糾結在一起影響插層效果，在 $^1\text{H}$  NMR得知一個CPC的分子鏈能夠套入兩個環糊精，由XRD與 $^{13}\text{C}$  NMR可以確定CPC確實有套入環糊精，TGA實驗證實有套環糊精的CPC熱裂解溫度提升  $50^\circ\text{C}$  左右，主要原因是環糊精保護了CPC的碳烷鏈提升了裂解溫度。
4. 我們首先合成插層劑 MBM 其具有 Benzoxazine 官能基，可以進行開環交聯反應，促使蒙托土達到奈米分散程度。我們使用溶劑的摻混方法將 Benzoxazine 單體與改質後的蒙托土均勻混合，並進行恆溫與非恆溫的交聯動力學實驗，結果得知有添加蒙托土會促進交聯反應提早發生，原因是因為蒙托土表面有催化交聯反應，反應的級數在 2.4~2.8 之間，活化能隨著蒙托土的含量增加而降低。在 3%的蒙托土含量時為脫層結構，大於 3%時為插層結構。

## Abstract

Nanoclay-filled polymeric systems offer the prospect of greatly improving many of the properties of their mother polymers. In the recent literature, there have been reports of nanoclay-filled polymeric systems that display significant improvements in tensile and thermal properties, heat distortion temperatures, and resistance to flammability and reduced permeability to small molecules and reduced solvent uptake. A common observation emerging from these studies is that the magnitude of improvement depends strongly on the state of dispersion of the clay layers in the polymer matrix. The experiment work in this dissertation was divided into four areas:

1. We have prepared polystyrene/clay nanocomposites using an emulsion polymerization technique. The nanocomposites were exfoliated at up to a 3 wt % content of pristine clay relative to the amount of polystyrene (PS). We used two different surfactants for the montmorillonite: the aminopropylisobutyl polyhedral oligomeric silsesquioxane (POSS) and the ammonium salt of cetylpyridinium chloride (CPC). The nanocomposite prepared from the clay treated with the POSS containing surfactant is exfoliated, while an intercalated clay was obtained from the CPC-treated surfactant. The value of  $T_g$  of the PS component in the nanocomposite is 8 °C higher than the virgin PS and its thermal decomposition temperature (21 °C) is also higher significantly. The presence of the POSS unit in the MMT enhances the thermal stability of the polystyrene.
2. We synthesized intercalation agent APB and prepared polystyrene/clay nanocomposites using an emulsion polymerization technique. We used two different intercalation agents to treat clay: the phosphonium salt (APP) and the ammonium salt (APB). We expected that the intercalation agent APB containing rigid adamantane group also has high thermal stability besides phosphonium

group. The molecular weights of polystyrene (PS) obtained from the nanocomposite is slightly lower than the virgin PS formed under similar polymerization conditions. The coefficient of thermal expansion (CTE) was obtained from thermomechanical analysis. A 44~55 % decrease of CTE is observed for APB- and APP-intercalated clay nanocomposites relative to the pure PS.

3. We employed two surfactants for the montmorillonite: cetylpyridinium chloride (CPC) and the CPC/ $\alpha$ -CD inclusion complex. The inclusion complex was characterized by X-ray diffraction,  $^{13}\text{C}$  CP/MAS NMR spectra, and  $^1\text{H}$  NMR spectroscopy, and TGA. The  $^1\text{H}$  NMR spectra of the complexes indicate that the stoichiometry of the complexes is 1:2 (i.e., one CPC molecule and two  $\alpha$ -CD units). The CPC/ $\alpha$ -CD-treated clay is more effective than is virgin CPC-treated clay at enhancing the thermal stability of polystyrene.
4. We have used the solvent blending method to prepare polybenzoxazine/clay nanocomposites possessing various clay contents. We synthesized a monofunctional benzoxazine monomer (MBM) and then treated the clay with this intercalation agent. To better understand the curing kinetics of the polybenzoxazine/clay nanocomposites, we performed dynamic and isothermal differential scanning calorimetry (DSC) measurements. The Kissinger and Ozawa methods gave fairly close results for the calculated activation energies, which decreased upon increasing the clay content. The Kamal method—based on an autocatalytic model—suggested a total reaction order of between 2.4 and 2.8.

# Chapter 1

## Introduction

### 1.1 Introduction

Polymer composites are important commercial materials with applications that include filled elastomers for damping, electrical insulators, thermal conductors, and high-performance composites for use in aircraft. Materials with synergistic properties are chosen to create composites with tailored properties; for example, high-modulus but brittle carbon fibers are added to low-modulus polymers to create a stiff, lightweight composite with some degree of toughness. In recent years, however, we have reached the limits of optimizing composite properties of traditional micrometer-scale composite fillers, because the properties achieved usually involve compromises. Stiffness is traded for toughness, or toughness is obtained at the cost of optical clarity. In addition, macroscopic defects due to regions of high or low volume fraction of filler often lead to breakdown or failure.

Nanoscale fillers come in many shapes and sizes. For ease of discussion, we have grouped nanofillers into three categories (Figure 1-1). Fiber or tube fillers have a diameter  $<100$  nm and an aspect ratio of at least 100. The aspect ratios can be as high as  $10^6$  (carbon nanotubes). Plate-like nanofillers (Figure 1-1) are layered materials typically with a thickness on the order of 1 nm, but with an aspect ratio in the other two dimensions of at least 25. Three dimensional (3D) nanofillers are relatively equi-axed particles  $<100$  nm in their largest dimension. This is a convenient way to discuss polymer nanocomposites, because the processing methods used and the properties achieved depend strongly on the geometry of the fillers.

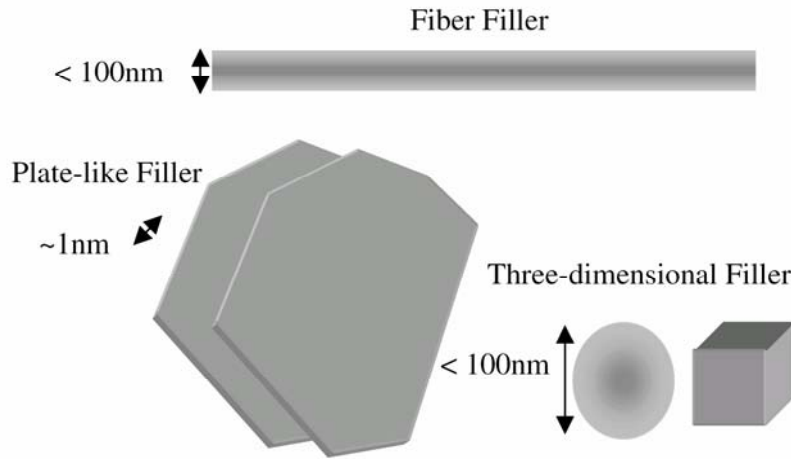


Figure 1-1 Schematic of nanoscale fillers.

Recently, a large window of opportunity has opened to overcome the limitations of traditional micrometer-scale polymer composites – nanoscale filled polymer composites – in which the filler is <100 nm in at least one dimension (Figure 1-1). Although some nanofilled composites have been used for more than a century, research and development of nanofilled polymers has greatly increased in recent years, for several reasons. First, unprecedented combinations of properties have been observed in some polymer nanocomposites. For example, the inclusion of equi-axed nanoparticles in thermoplastics, and particularly in semicrystalline thermoplastics, increases the yield stress, the tensile strength, and Young’s modulus compared to pure polymer. A volume fraction of only 0.04 mica-type silicates (MTS) in epoxy increases the modulus below the glass transition temperature by 58% and the modulus in the rubbery region by 450%. In addition, the permeability of water in poly( $\epsilon$ -caprolactone) decreases by an order of magnitude with the addition of 4.8% silicate by volume. Yano et al. showed a 50% decrease in the permeability of polyimides at a 2% loading of MTS. Many of these nanocomposites are optically transparent and/or optically active.

A second reason for the large increase in research and development efforts was the ‘discovery’ of carbon nanotubes in the early 1990s. Although more careful review has shown that nanotubes have been observed since the 1960s, it was only in the mid-1990s that they were made in the quantities required for property evaluation of composites. The properties of these carbon nanotubes, particularly strength and electrical properties, are significantly different from those of graphite and offer exciting possibilities for new composite materials.

Third, significant development in the chemical processing of nanoparticles and in the in situ processing of nanocomposites has led to unprecedented control over the morphology of such composites. It has also created an almost unlimited ability to control the interface between the matrix and the filler.

Thus, this is an exciting time to study nanocomposites, because of the unique combinations of properties that are achievable and because of the high potential for successful commercial development. Although the technical community has made advances in the processing of nanocomposites, we are just beginning to assemble the interdisciplinary teams required to understand, tailor, and optimize properties. We have at our fingertips, however, the ability to change the size, shape, volume fraction, interface, and degree of dispersion or aggregation. Thus, the opportunities may well become limitless when theory and experiment have assembled enough information to guide further development.

Polymerization of vinyl monomers intercalating into the montmorillonite (MMT) clay [1] were first reported in literature as early as 1961. The most recent methods to prepare polymer-layered-silicate nanocomposites have primarily been developed by several other groups. In general these methods (shown in Figure 1-2) are able to achieve molecular-level incorporation of the layered silicate (e.g. montmorillonite clay or synthetic layered silicate) in the polymer matrix by addition of a modified

silicate either to a polymerization reaction (in situ method), [2-4] to a solvent-swollen polymer (solution blending), [5] or to a polymer melt (melt blending). [6,7] Recently, a method has been developed to prepare the layered silicate by polymerizing silicate precursors in the presence of a polymer. [8]

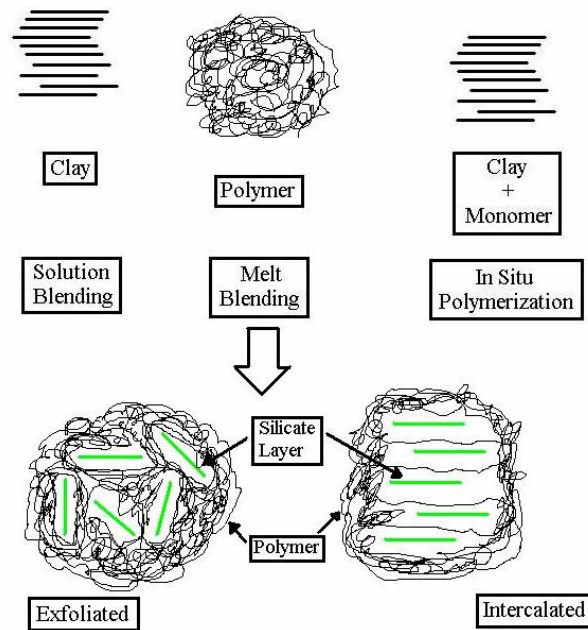


Figure 1-2. Schematic representation of various methods used to prepare polymer-layered-silicate nanocomposites. [41]

In general, layered silicates have layer thickness on the order of 1 nm and very high aspect ratio (e.g. 10~1000). A few weight percent of layered silicates that are properly dispersed throughout the polymer matrix thus create much higher surface area for polymer/filler interaction as compared to conventional composites. Depending on the strength of interfacial interactions between the polymer matrix and layered silicate (modified or not), three different types of polymer/layered silicate (PLS) nanocomposites are thermodynamically achievable (see Figure 1-3):

- a. *Intercalated nanocomposites*: in intercalated nanocomposites, the insertion of a polymer matrix into the layered silicate structure occurs in a crystallographically regular fashion, regardless of the clay to polymer ratio.



Intercalated nanocomposites are normally interlayer by a few molecular layers of polymer. Properties of the composites typically resemble those of ceramic materials.

- b. *Flocculated nanocomposites*: conceptually this is same as intercalated nanocomposites. However, silicate layers are some times flocculated due to hydroxylated edge-edge interaction of the silicate layers.
- c. *Exfoliated nanocomposites*: in an exfoliated nanocomposite, the individual clay layers are separated in a continuous polymer matrix by an average distances that depends on clay loading. Usually, the clay content of an exfoliated nanocomposite is much lower than that of an intercalated nanocomposite.

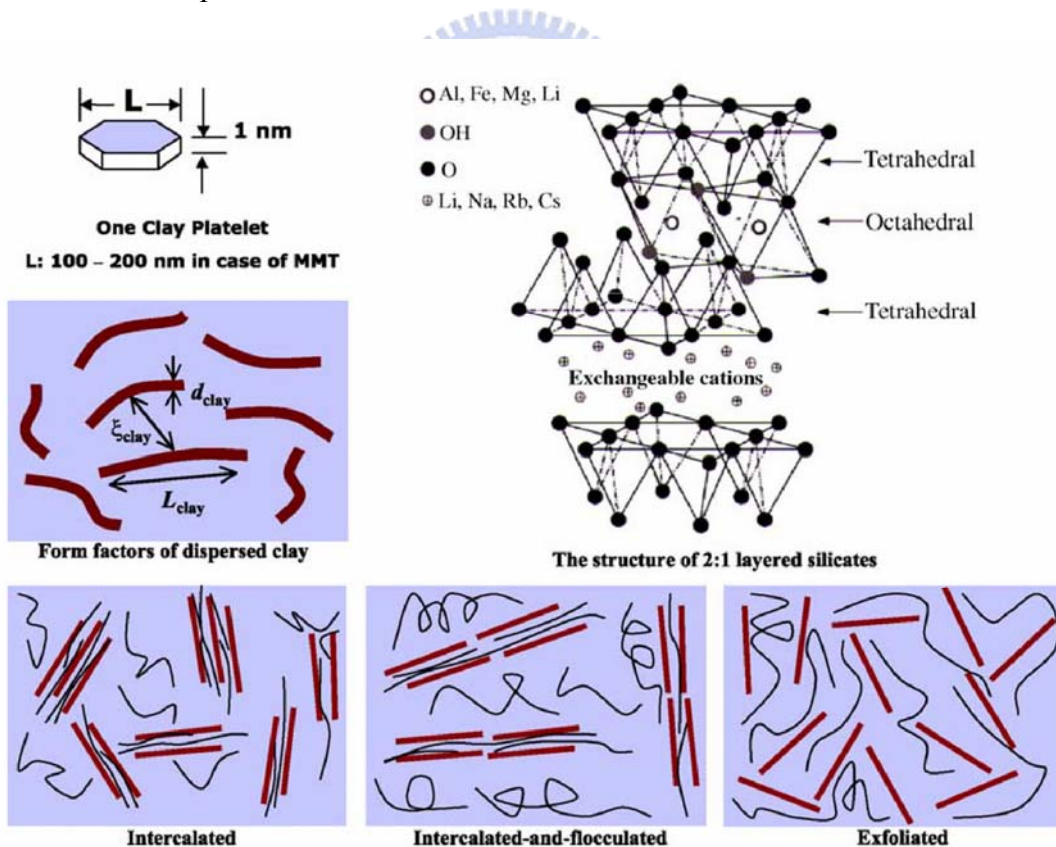


Figure 1-3 Schematically illustration of three different types of thermodynamically achievable polymer/layered silicate nanocomposites.

## 1.2 Organically modified clay

Zhu and co-workers [21] reported the preparation of three new organically modified clays and their corresponding preparation of PS/clay nanocomposites from these clays by bulk polymerization. Two are functionalized ammonium salts while the third is a phosphonium salt and structures of these salts are shown in Figure 1-4. TGA/FTIR showed that the phosphonium treatment results in the most thermally stable treatment when compared to the two ammonium salts.

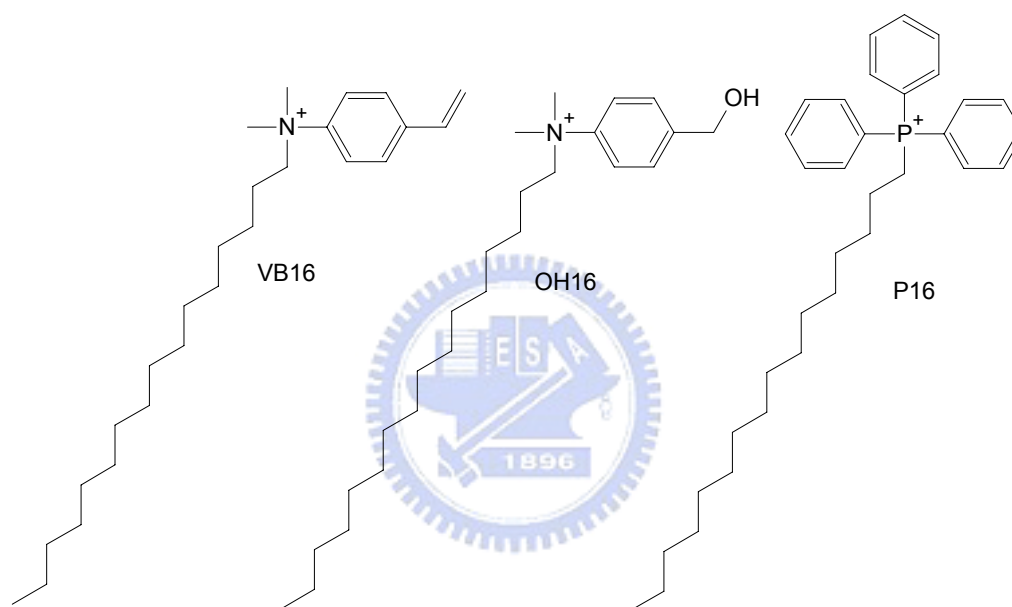


Figure 1-4. Structures of the salts used to prepare the organically modified clays. [21]

Wang [22] used two different organic modifications of the montmorillonite, one contains a styryl monomer on the ammonium ion while the other contains no double bond. A double bond that may be involved in the polymerization reaction is present in the cation of the clay. Polystyrene-clay nanocomposite has been prepared by bulk, solution, suspension, and emulsion polymerization as well as by melt blending. The organic modification as well as the mode of preparation may determine whether the composite is either exfoliated or intercalated. Exfoliation is more likely to occur if the ammonium ion contains a double bond which can participate in the polymerization reaction. However, the mere presence of this double bond is not sufficient to always

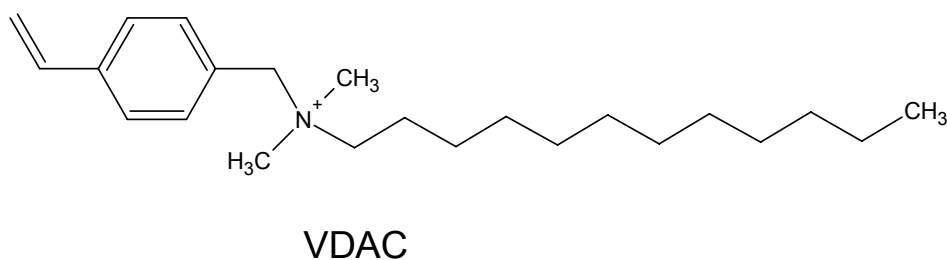
produce an exfoliated system.

In addition, Wang and Wilkie [23] also reported the preparation and characterization of an antimony-containing clay and the preparation of polystyrene nanocomposites from this clay. The structure of antimony is shown in Figure 1-5. The objective of this study is to determine if this clay is more thermally stable than the common ammonium clays and thus could be used at higher temperatures for the processing of polymers, such as polycarbonate, that require processing at higher temperature.



Figure 1-5. Structure of triphenylhexadecylstibonium trifluoromethylsulfonate. [23]

Fu and Qutubuddin [24] reported the synthesis of exfoliated polystyrene-clay nanocomposite. A reactive cation surfactant vinylbenzyltrimethylammonium chloride (VDAC) was synthesized and used for ion exchange with sodium ions in MMT. The structure of VDAC is shown in Figure 1-6. The exfoliated polystyrene-clay nanocomposite was prepared by direct dispersion of organophilic MMT in styrene monomer followed by free radical polymerization.



VDAC

Figure 1-6. Structure of VDAC used to prepare the organically modified clay.

Chang and co-workers [27] reported the preparation of two types of nanocomposites formed from cetylpyridinium chloride (CPC)- and aminopropylisobutyl polyhedral oligomeric silsesquioxane (POSS)-treated clays (Figure 1-7). The PS/clay nanocomposite formed using the CPC-treated clay exhibited no significant improvement in thermal properties. [28-32] The major advantage of choosing POSS molecules is its thermal stability up to 300 °C, higher than the thermal degradation temperatures of most organic molecules. POSS consists of a rigid cubic silica core with 0.53 nm side length, to which organic functional groups can be attached at the vertices for further reactions. POSS derivatives containing amine functional groups can play the role of surfactants for the treatment of clay and the thermal stability of the resulting nanocomposite is enhanced.

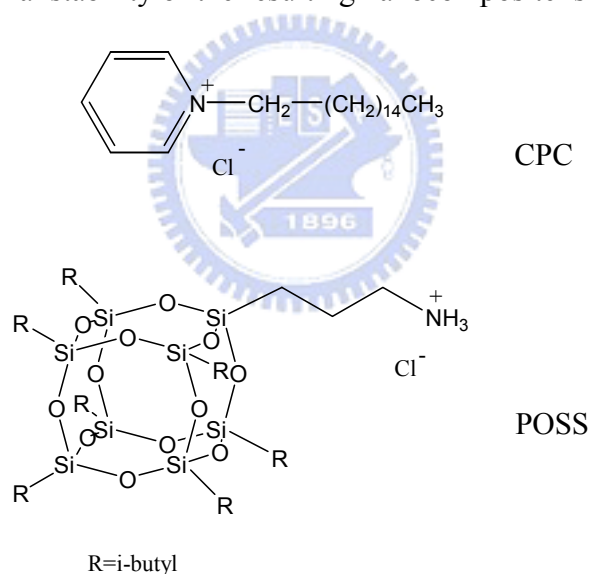


Figure 1-7. Chemical structures of the surfactants used to prepare the modified clays. [27]

In addition, chang and co-workers also reported the preparation of two types of PS/clay nanocomposites formed from clays treated with either cetylpyridinium chloride (CPC) or the CPC/ $\alpha$ -CD inclusion complex. [26] The structures of two intercalation agents were shown in Figure 1-8. We found that CPC, a linear aliphatic surfactant, is able to form a crystalline complex with cyclodextrin. Including CPC

within CD channels improves the thermal stability of the virgin CPC. The linear aliphatic chain within the CPC/ $\alpha$ -CD cannot bend within the galleries of the clay and the  $d$  spacing of clay intercalated by the CPC/ $\alpha$ -CD inclusion complex is significantly higher than that formed using pure CPC. The CPC/ $\alpha$ -CD inclusion complex can promote exfoliated structure of clay.

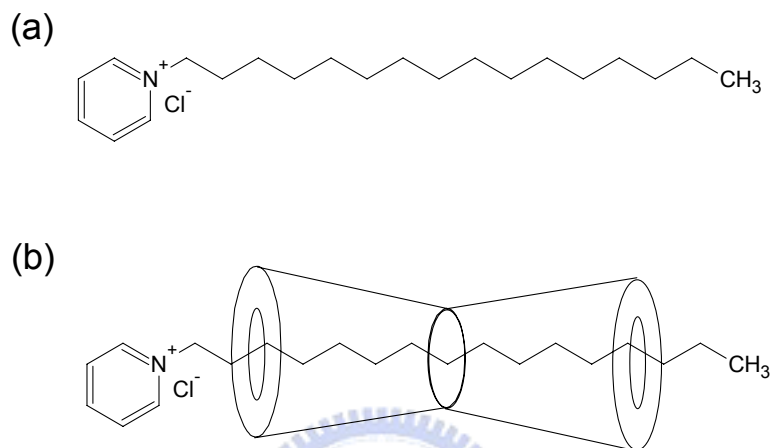


Figure 1-8. The structures of intercalation agent (a) CPC and (b) CPC/ $\alpha$ -CD inclusion complex.

### 1.3 Polymer/clay nanocomposite processing

Scientists have known for about 40 years that polymers interact strongly with montmorillonite and that the clay surface can act as an initiator for polymerization. Patents for clay/Nylon 6 composites were not issued until the 1980s, at which point the clay/polymer nanocomposites were commercialized. [83] The improvement that led to commercialization was the appropriate dispersion of the clays at the nanometer scale.

The first step in achieving nanoscale dispersion of clays in polymers is to open the galleries and to match the polarity of the polymer or monomer so that it will intercalate between the layers. This is done by exchanging an organic cation for an inorganic cation (Figure 1-9). The larger organic cations swell the layers and increase the hydrophobic properties of the clay (Figure 1-9), resulting in an organically modified clay. The organically modified clay can then be intercalated with polymer by several routes. Solution processing involves dispersion of both the organically modified clay and the polymer in a common solution. Variations on this process include emulsion or suspension polymerization. [84] Highly polar polymers such as Nylon and polyimides are more easily intercalated than nonpolar polymers such as polypropylene, because polar polymers have a higher affinity for the polar clay galleries. In situ polymerization intercalates monomer directly into the organically modified clay galleries, and the monomer can either adsorb onto the layer surface or be anchored by free radical techniques. Melt intercalation involves mixing the clay and a polymer melt, with or without shear. The success of melt intercalation is surprising, given that the gallery spacing is only about 2 nm and the radius of gyration of the polymer is significantly larger than this. Even more surprising is that the speed of melt intercalation is faster than that of self diffusion of polymers and scales with

the inverse of the molecular weight.

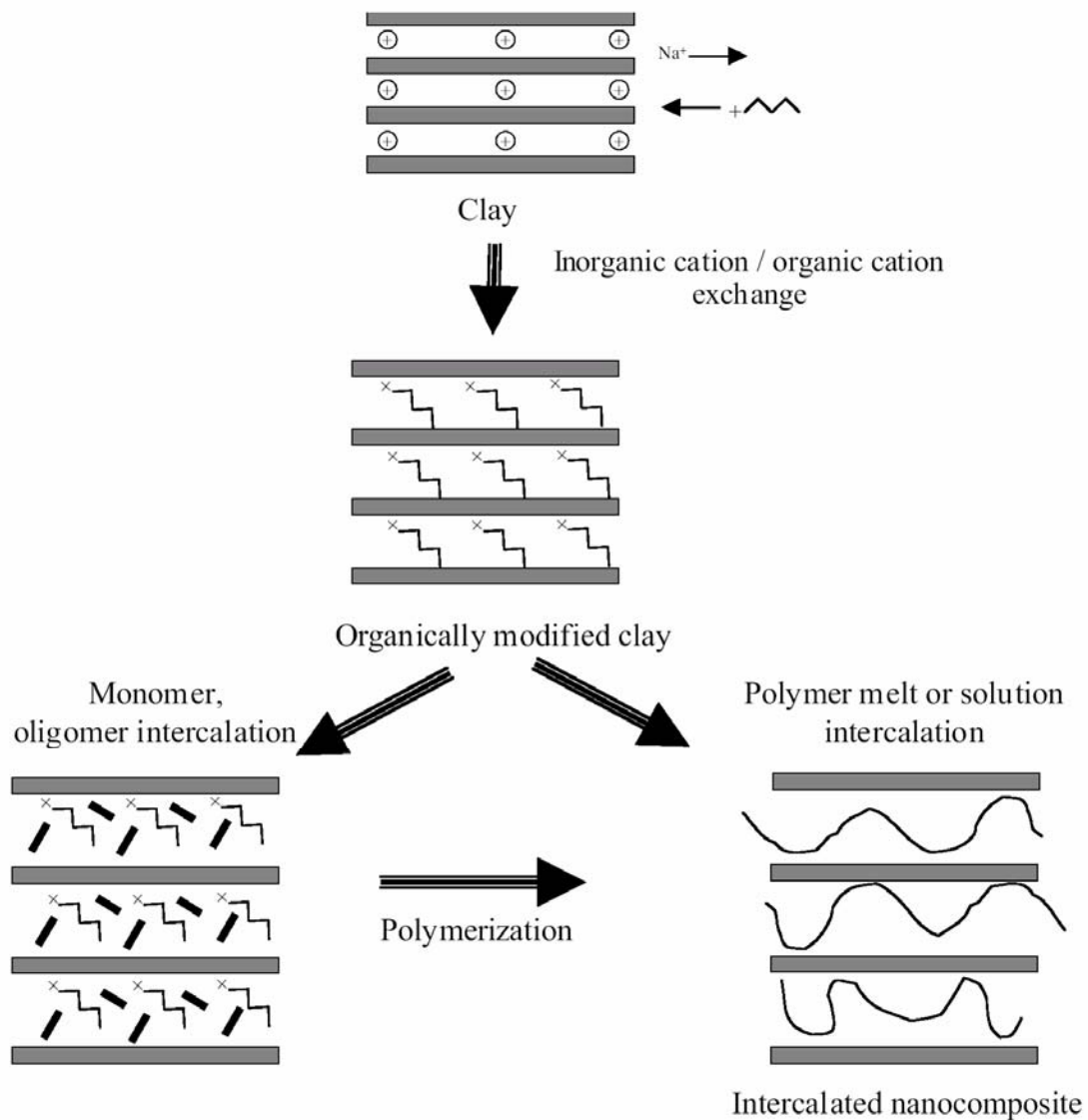


Figure 1-9 Schematic of the basic steps in processing clay-filled polymers.

As the layer spacing increases, the process can be monitored by x-ray diffraction (XRD). Intense peaks between  $3^\circ$  and  $9^\circ$  indicate an intercalated composite, but if the peaks are extremely broad or disappear completely, this indicates complete exfoliation. Figure 1-10 shows the XRD pattern of organically modified montmorillonite (d), an intercalated montmorillonite (c), and two exfoliated montmorillonite nanocomposites (a, b).

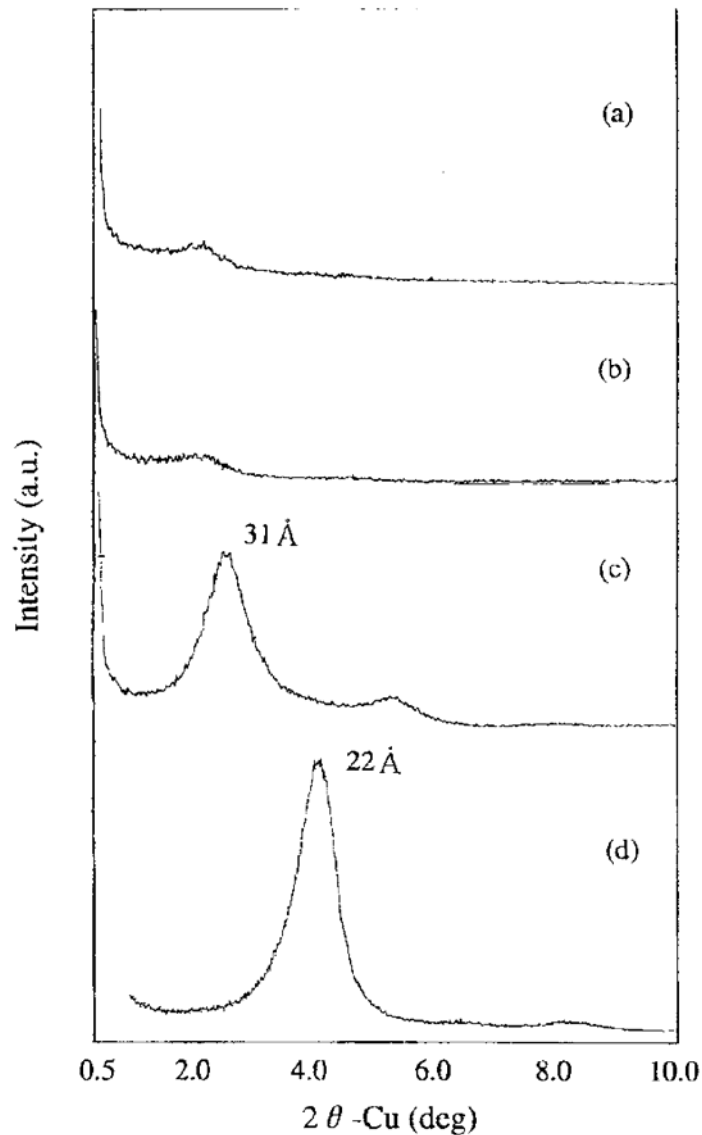


Figure 1-10 X-ray diffraction data showing the diffraction patterns that result from (a), (b) exfoliated clays, (c) intercalated clays, (d) organically modified clays.

The resulting nanocomposites can have several structures (Figure 1-11). The structure of an intercalated nanocomposite is a tactoid with expanded interlayer spacing, but the clay galleries have a fixed interlayer spacing. Exfoliated nanocomposites are formed when the individual clay layers break off the tactoid and are either randomly dispersed in the polymer (a disordered nanocomposite) or left in an ordered array.



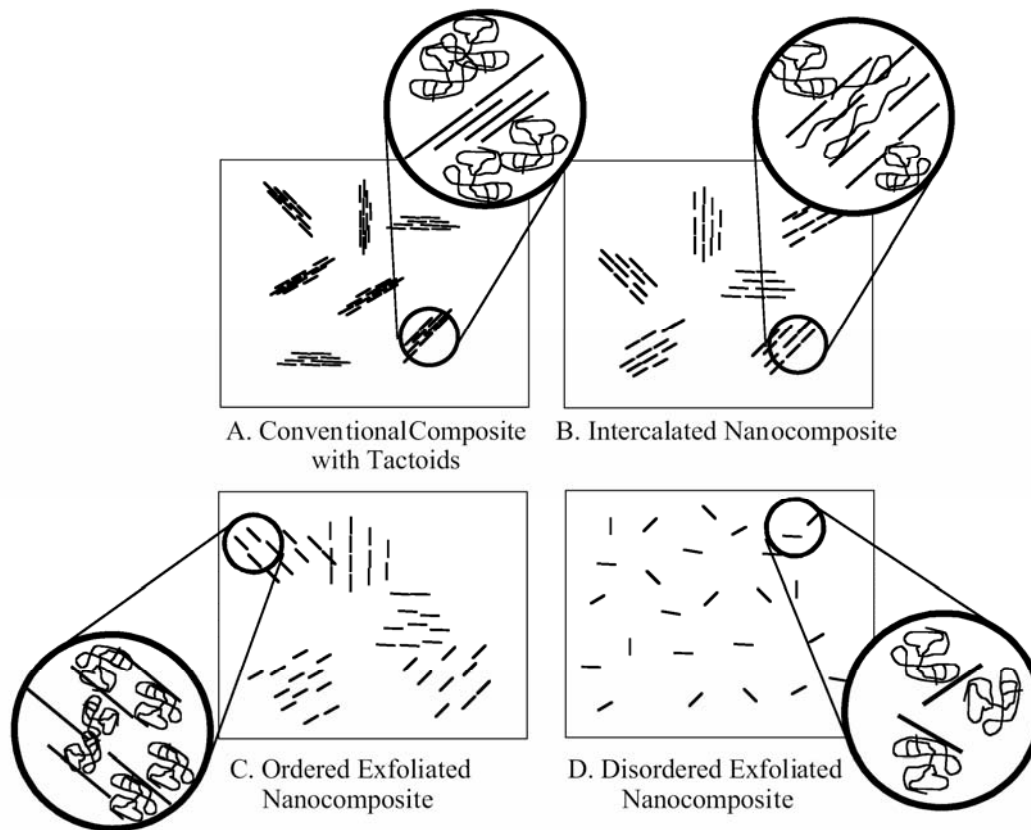


Figure 1-11 Schematic of the microstructures that can develop in clay-filled polymer composites.

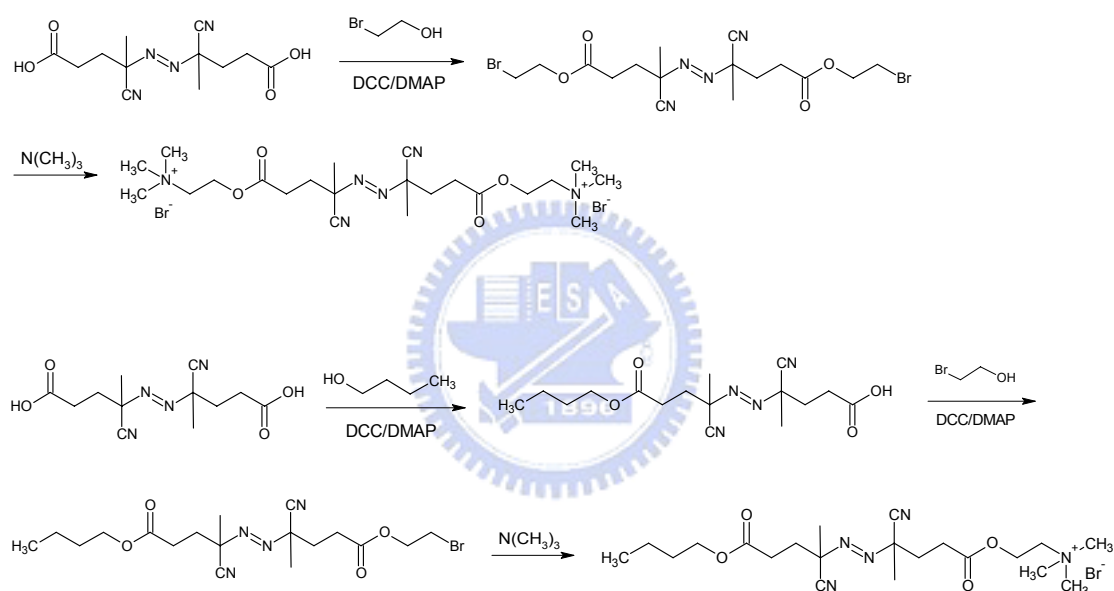


#### 1.4 Surface-initiated polymerization (SIP)

Rather than modifying the clay with organic quaternized ammonium salts, cationically modified polymerization initiators can also be used to prepare organophilic clays. In this method, in situ polymerization is initiated by the activation of these initiators which are *ionically bound* to the clay particle surfaces, that is, through a surface-initiated polymerization (SIP) process. The advantage of SIP is based on the assumption that as the polymer chain grows through surface initiation, the ordered silicate layers can be gradually pushed apart, ultimately exfoliating to discrete laths, resulting in a well-dispersed structure of the final product. Also, theoretically, if all initiators are tethered to clay surfaces, a higher efficiency of intergallery polymerization is expected compared to that of free, or unattached initiators. Exfoliated polystyrene-clay nanocomposites with controllable MW have been prepared by intercalating a charged living free radical polymerization (LFRP) initiator into montmorillonite. [33] A (1,1-diphenylethylene) DPE derivative initiator was used to synthesize polystyrene-clay nanocomposite materials through living anionic surface-initiated polymerization (LASIP). [34,35] However, only intercalated structures were obtained.

In efforts to conduct SIP from clay surfaces, Xiaowu and co-workers [36] recently synthesized two initiators for free radical SIP, both contain quaternized amine endgroups for cation exchange with montmorillonite particles. The initiator molecule design is as follow: (1) *symmetric*, with two cationic groups at both chain ends (named bicationic free radical initiator hereafter) and (2) *asymmetric*, with one cationic group at one end (named monocationic free radical initiator hereafter). The synthetic schemes and structures of these initiators are shown in Figures 1-12a and 12b. They are both AIBN-analogue initiators for free radical polymerization. The use

of another symmetric bicationic azo compound, 2,2'-azobis(isobutyramidine hydrochloride) (AIBN), has also been proven to be feasible for styrene SIP on high surface area mica powder. [37] However, no structural information for these SIP products has been reported. Asymmetric azo initiators in the form of silanes have also been successfully employed to free radically polymerize styrene from spherical silica gel surfaces. [38,39] To the best of our knowledge, there have been no reports on a direct free radical SIP approach from surface-bound monocationic azo initiators on individual clay nanoparticles.



X-ray powder diffraction patterns of the pristine clay and two initiator-intercalated clay samples are shown in Figure 13. Lamellar periodicity was maintained on the organophilic clay despite the rigorous sonication-centrifugation procedure to intercalate the initiators. By using the Bragg equation,  $n \lambda = 2d \sin \theta$ , the  $d$  spacing values of these samples were calculated and shown beside each peak.

The basal spacing of the pure montmorillonite  $\text{Na}^+$  is 1.16 nm, which is in

accordance with data from other sources. [40] The XRD patterns of the intercalated clays indicate the successful insertion of the initiator molecules into the galleries of the silicate platelets since both intercalated clay samples gave increased  $d$  spacing values. In addition, the sharper shape and the higher diffraction intensities of these peaks after intercalation provide the evidence of a better-ordered swollen structure than that of the original clay. This result demonstrates that the layered framework of inorganic clay can accommodate the AIBN derivative molecules of various functionalities with better long-range periodicity.

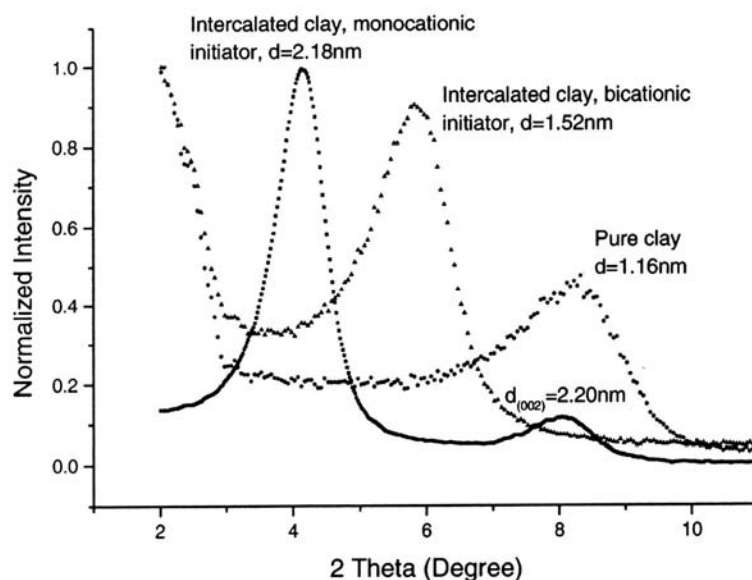


Figure 1-13. X-ray powder diffraction patterns of pure clay and two intercalated clay samples. [36]

On further analysis, the  $d$  spacing values seemed to be inconsistent with the steric sizes of the two initiators. The  $d$  spacing of bicationic intercalated clay (1.52 nm) is substantially smaller than that of the monocationic intercalated clay although their molecular dimensions are comparable (both chain length values are 2.20 nm, as estimated by Chem 3D software). The bicationic initiator molecule possesses charged groups on both ends that can have two intercalation possibilities: (1) these two cationic endgroups interact electrostatically with two different but neighboring

platelets' surfaces, or (2) they interact on the same side surface of a single clay particle. The combination of these two possibilities makes the intercalated structure less spatially ordered which accounts for the broadened reflection for this sample as compared with the peak of the clay intercalated by the monocationic initiator. Furthermore, since XRD collects the average information from a large area of a powder sample, a synergic effect of these two possibilities accounts for an intermediate  $d$  spacing value. This interpretation is schematically shown in Figure 1-14. The interlamellar height shown in the figure is calculated by  $\Delta d = d$  spacing – thickness of one platelet ( $\sim 1.0$  nm).

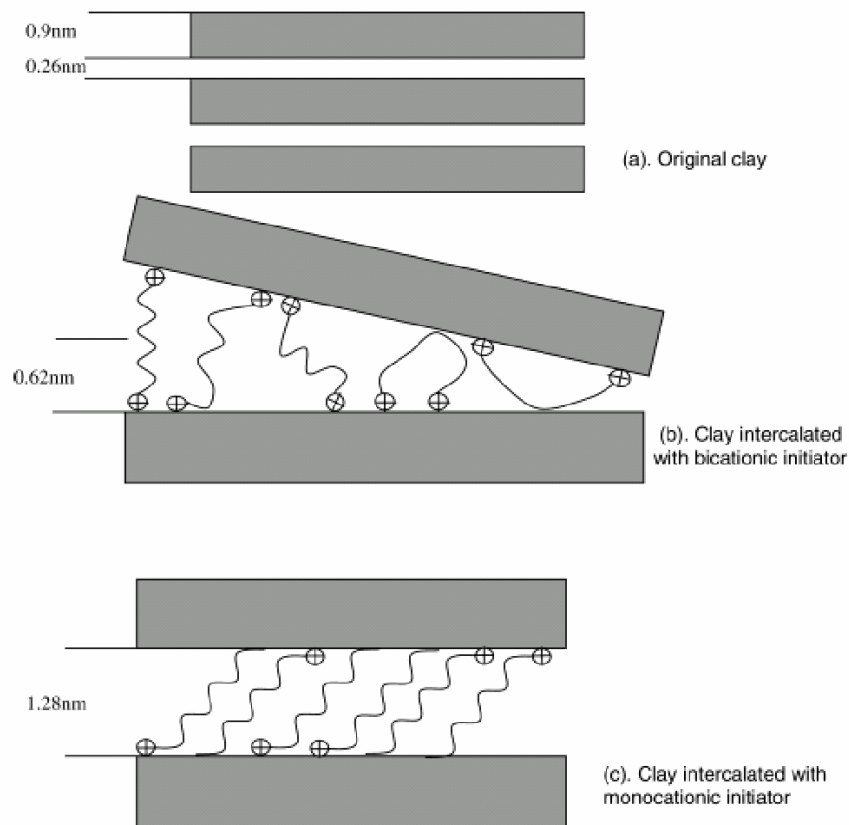


Figure 1-14. (a-c) Schematic diagrams of the intercalation: (a) original clay, (b) clay intercalated with bicationic initiator, and (c) clay intercalated with monocationic initiator. [36]

The X-ray diffractograms of the two final SIP products are shown in Figure 1-15. The broad peaks of both samples at the higher angle regime are believed to be related

to the long-range order of the polystyrene matrix. Similar broad peaks were also observed in the diffractogram of the PS-0 reference sample (not shown). Sample bi-PS-M-2 shows a small peak at  $2\theta = 5.9^\circ$ , which is about the same as the peak position of the corresponding intercalated clay (Figure 1-8), implying that this product still contains fraction of the intercalated clay structure. On the contrary, there is no peak on the XRD trace of the mono-PS-M-2 sample, indicating that a completely exfoliated structure was achieved in this sample.

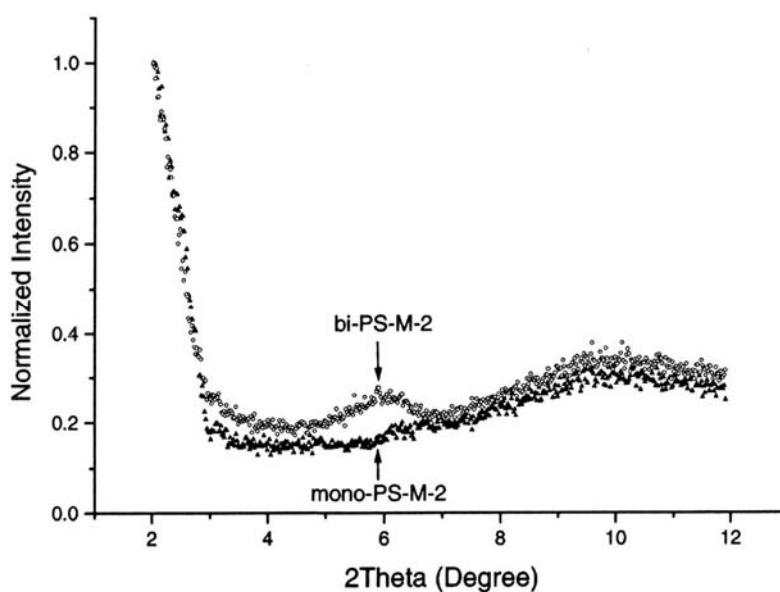


Figure 1-15. XRD spectra of the two SIP nanocomposites showing degree of exfoliation. [36]

This observed result is quite unexpected. We would anticipated that these adjacent clay layers in the clay/bicationic initiator system will be gradually pushed apart during SIP, if these two immobilized free radicals are simultaneously generated. As a result, the intercalated clay stacks would be totally delaminated, forming a fully exfoliated nanocomposite product. However, the polymer can only grow within the clay gallery when monomer molecules are able to diffuse and make contact with effectively with the tethered radicals within the interlayer spacing. The time scale of diffusion is such that access to the monomer from within the layers is limited.

Considering the rapid kinetics for free radical polymerization in solution, this intercalative monomer diffusion is significantly slower toward monomer addition. Thus, free initiators exhaust the monomers while SIP inside clay lamellar is delayed by diffusion. Furthermore, there is also competition from the surface-perimeter-attached initiators of the clay particles. Even if some of the bication initiators were activated and grew to become oligomers, the growing chains will likely be terminated by recombination or disproportionation by nearby immobilized growing chains/initiators in the same gallery. Hence the low molecular weight and high polydispersity obtained by bi-PS-M-2 can be explained.

By comparison, an intercalated monocationic initiator is easier to be delaminated than a bicationic initiator. The monocationic initiator molecule is also more organophilic. The weaker van der Waals interaction between the alkyl headgroups of the monocationic initiator and clay surfaces makes the intercalated clay easier to be swelled by the solvent and monomer. Once the clay intercalated with monocationic initiator is exfoliated by sonicating and stirring, the attached initiators have more accessibility to monomer and thus results in better monomer intercalative diffusion.

## 1.5 Types of Polymer matrix

### 1.5.1 Polyamide Matrices

Nylon-6/Nylon-12/clay hybrid composites were the first exfoliated smectic clay composites made. [40] Montmorillonite, with a CEC of 119 mEq/100 g, was intercalated with 12-aminolauric acid, which increased the intergallery spacing from 1.0 to 1.7 nm. This '12-montmorillonite' was then mixed with  $\epsilon$ -caprolactam, which increased the intergallery spacing even further, to 4.0 nm, indicating that the  $\epsilon$ -caprolactam had intercalated into the galleries. Heating to 250 °C led to polymerization, forming a clay/Nylon-6 nanocomposite. Further research [41] determined that  $\epsilon$ -caprolactam could intercalate directly into the galleries of montmorillonite in a hydrochloric acid solution and, upon intercalation, becomes oriented vertically in the galleries. The modified montmorillonite then mixed easily with additional molten  $\epsilon$ -caprolactam and 6-aminocaproic acid, yielding a Nylon-6 homopolymer/clay nanocomposite. The montmorillonite was completely exfoliated. Recently [42], montmorillonite/Nylon 6 nanocomposites were processed by melt intercalation. Although the degree of exfoliation was not as high as in nanocomposites produced by the above methods, at weight fractions less than 0.1 the composites were primarily exfoliated.

### 1.5.2 Polyimide Matrices

The preparation of polyimide matrix clay nanocomposites involves several steps [43] (Figure 1-16). By intercalating montmorillonite with the ammonium salt of dodecylamine, it becomes soluble in dimethylacetamide (DMAC). DMAC is also a solvent for 4,4'-diaminodiphenylether and pyromellitic dianhydride, the precursors for polyamic acid and, as such, polyimides. After intercalation of the ammonium salt of dodecylamine, x-ray studies [44] showed that hectrite (CEC = 55 mEq/100 g) has



one monolayer of organic material between the layers, whereas saponite, montmorillonite, and synthetic mica (all with CEC > 100 mEq/100 g) have two. After composite formation, however, only the montmorillonite and the synthetic mica have exfoliated completely, but the hecrite and saponite remain in a somewhat aggregated state. Lan et al. [45] found aggregates of montmorillonite after using a similar procedure. More recently, P-phylenediamine in an HCl solution was also found to form organic-modified montmorillonite that dissolves in DMAC. [46] This same study showed that the presence of a small amount of nanoscale organoclay can decrease the imidization temperature by 50 °C (from 300 °C to 250 °C), and at 250 °C the imidization time decreased by 15 min. The activation energy decreased by 20 %. Clearly, the organoclay surface is acting as a catalyst.

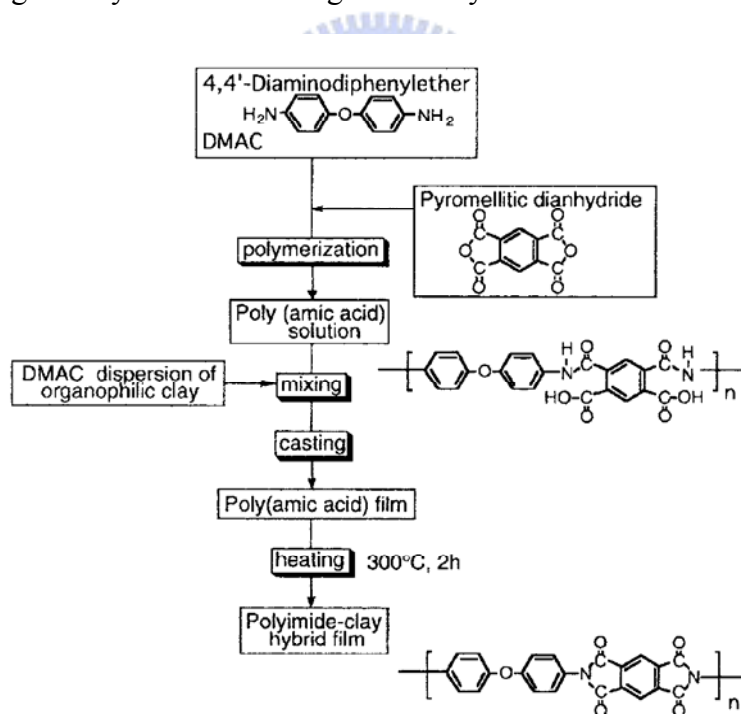
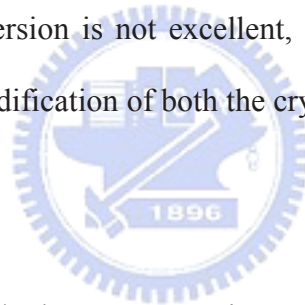


Figure 1-16 Schematic of the synthesis of polyimide-clay hybrid film. [40]

### 1.5.3 Polypropylene and Polyethylene Matrices

Nonpolar polymers are very difficult to intercalate into smectic clays, because the clays are strongly polar. This challenge has been met [47, 48] by first intercalating stearylamine into montmorillonite and synthetic mica. Melt-mixing the organoclays with maleic anhydride-modified polypropylene oligomers results in PP-MA intercalation. The modified organoclay is then melt-mixed with a polypropylene matrix. There is a balance between creating a polar oligomer with enough maleic anhydride to intercalate well, but nonpolar enough to mix with the polypropylene. Unfortunately, the oligomer limits the extent of property improvement achieved to date. Polyethylene has also been successfully melt-mixed with modified montmorillonite and saponite after ion exchange with dioctadecyldimethylammonium bromide. The degree of dispersion is not excellent, and the layers are certainly not exfoliated; yet, significant modification of both the crystal structure and properties has been observed. [49]



### 1.5.4 Polymethylmethacrylate/Polystyrene Matrices

The processing of clay/PMMA or clay/PS composites was first done by directly intercalating the monomer into the clay, followed by polymerization. [50] This method was not successful in exfoliating the clays. At issue again is the compatibility between the clay and the monomer. One solution for PMMA has been to use appropriate ammonium salts, [51, 52] which may be reactive. Another solution is to use a comonomer as a compatibilizer. [53] A similar solution was found for polystyrene by using the reactive cationic surfactant vinylbenzyltrimethylammonium as the intercalant. Exfoliated graphite/polystyrene composites have been made by similar processing methods. Recently, a commercially viable process was developed [54] for polystyrene in which

montmorillonite intercalated with octadecyl trimethyl ammonium chloride was melt-mixed with a styrene methylvinylloxazoline copolymer. This process resulted in complete exfoliation, which could not be achieved with pure polystyrene. The hypothesis is that the hybridization is due to strong hydrogen bonding between the oxazoline groups and oxygen groups in the silicate clays.

#### 1.5.5 Epoxy and Polyurethane Matrices

Epoxy is a widely used thermoset, with applications ranging from household glues to high-performance composites. To improve performance, increasing the  $T_g$  of epoxy and improving its properties above the  $T_g$  are desirable. Adding clays and layered silicic acids to epoxy [55-57] can greatly improve its mechanical performance, particularly at temperatures above  $T_g$ . The processing has been studied in detail. In the smectic clay/epoxy composites, the length of the intercalated organic amine determines the ease of exfoliation, and only clays with primary and secondary onium ions form exfoliated nanocomposites. After intercalation of the organic amines, the epoxy resin or a combination of resin and curing agent can be intercalated into the smectic clays or layered silicic acids. If enough resin and curing agent are intercalated and the curing process is controlled, exfoliated nanocomposites result. The acidic onium ions catalyze the intragallery polymerization or curing of the resin. If this reaction occurs more rapidly than extragallery curing, then the clay exfoliates. Otherwise, an intercalated nanocomposite results. Therefore, careful control of temperature and time is required, or the ratio of resin to curing agent must be significantly less than the stoichiometric ratio in order to achieve exfoliation. An approach similar to that used for epoxy composites was used to make intercalated montmorillonite/polyurethane composites.

### 1.5.6 Polyelectrolyte Matrices

Polyelectrolytes can be used in electrochemical devices such as solid-state batteries, electrochromic devices, and sensors. [69] The addition of layered silicates to polyelectrolytes increases the conductivity, improves the mechanical stability, and improves the interfacial stability with electrode materials. Polyelectrolytes are characterized by a large number of ionizable groups and thus are highly polar. This makes them excellent candidates for intercalation into smectic clays. Polyvinylpyridines are of particular interest because of the variety of processing methods available. Intercalated nanocomposites can be formed easily from the water-soluble hydrobromide salt of the 1,2 or 1,6 polyelectrolyte (1,2 or 2,6 polyvinylpyridinium cations). However, only a single layer of polymer intercalates, and exfoliation does not occur. A slower, but ultimately more effective process, uses neutral poly-4-vinylpyridine and results in an exfoliated composite. A second method involves intercalation of 4-vinylpyridinium salts, followed by polymerization.

Poly(ethylene oxide) (PEO) matrix composites have also been processed both by intercalating PEO in solution into organically modified smectic clays [69] and by melt-mixing clay with PEO and PEO/PMMA mixtures. [70, 71] In neither case does an exfoliated composite result. Aranda and Ruiz-Hitzky [69] dissolved PEO in acrylonitrile and found that the structure of the PEO changed when the interlayer cation was changed. Use of  $\text{Na}^+$  montmorillonite or  $\text{NH}_4^+$  montmorillonite resulted in either a helical PEO or a bilayer zigzag PEO structure in the galleries. The PEO arrangement was reversible with exchange of the interlayer cations.

### 1.5.7 Rubber Matrices

Several applications of rubbers might benefit from inclusion of exfoliated clays. Their greatly reduced permeability [72] would be useful for the inner liners of tires and inner tubes. [73] In addition, modification of the glass transition temperature and/or the loss modulus might be useful in a variety of damping applications. Montmorillonite has been ion-exchanged with a protonated form of butadiene and acrylonitrile copolymer. This was subsequently mixed with nitrile butadiene rubber in the presence of crosslinking agents and resulted in highly dispersed nanocomposites. Nanocomposites have also been prepared from dioctadecyldimethyl ammonium-exchanged montmorillonite in poly(styrene-b-butadiene) matrices. [74]

### 1.5.8 Others

Clay/polymer nanocomposites that include poly( $\epsilon$ -caprolactone) have been made via in-situ polymerization. Composites that include poly(p-phenylenevinylene) have been made via intercalation of poly(xylylenedimethylsulfonium bromide) and subsequent elimination of the dimethylsulfide and HBR. [75] Those including cyclic polycarbonate [76] or polyethyleneterephthalate have been made via monomer intercalation and subsequent polymerization; and those including polyaniline via in-situ polymerization of aniline monomer. [77]

## 1.6 Properties of Nanocomposites

### 1.6.1 Dimensional Stability

Dimensional stability is critical in many applications. For example, if the layers of a microelectronic chip have different thermal or environmental dimensional stabilities, then residual stresses can develop and cause premature failure. Poor dimensional stability can also cause warping or other changes in shape that affect the function of a material. Nanocomposites provide methods for improving both thermal and environmental dimensional stability. The possible mechanism by which nanofillers can affect the coefficient of thermal expansion (CTE) of a polymer has also been observed in traditional fillers.

The dimension stability of nanocomposites was studied by Zeng and Lee. [58] Figure 1-17 shows the shape changes of injection molded PS and PS/clay nanocomposites under the aforementioned thermal cycle (50 °C, 1 h; 75 °C, 1 h; 105 °C, 1 h; and 135 °C, 1h). The original sample shape is shown in the first row. Pure PS and the extruded PS/20A (dimethyl dehydrogenated tallow ammonium montmorillonite, 20A) nanocomposite are shown in the second row for comparison. The third row shows the in-situ polymerized pure PS, PS/20A, and PS/MHABS (2-methacryloyloxyethylhexadecyldimethylammonium bromide, MHABS) nanocomposites. All the nanocomposites contain 5 wt % clay. In the absence of clay, the sample shrank greatly, and the shape became highly irregular. Dimension stability at elevated temperature was improved significantly when 5 wt % of clay was present in the in-situ polymerized nanocomposites, as shown in the third row. The exfoliate PS/MHABS exhibited the best dimensional stability. After the heating cycle, although the sample shrank to a certain extent, the original shape and surface smoothness remained. It is noteworthy that the PS/20A nanocomposite prepared by extrusion

compounding did not show much improvement in dimension stability at elevated temperature, as compared to the in-situ polymerized PS/20A nanocomposite with the same clay content.

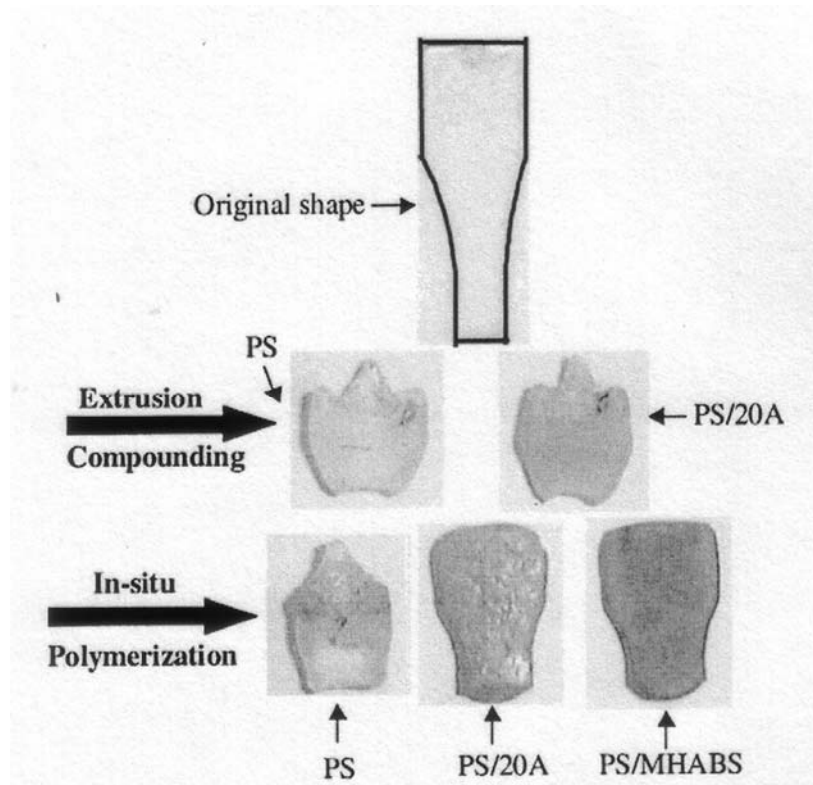


Figure 1-17. PS and PS/clay nanocomposites after dimension stability test. Clay loading is 5 wt % for all nanocomposites. [58]

### 1.6.2 Thermal Stability and Flammability

Delaminated composites have significantly higher degradation temperatures than intercalated nanocomposites or traditional clay composites [61]. Some speculate that this increase in stability is due to the improved barrier properties of the composites. If oxygen cannot penetrate, then it cannot cause oxidation of the resin [62]. In addition, the inorganic phase can act as a radical sink to prevent polymer chains from decomposing. The improved thermal stability of some composites may be limited by the lower thermal stability of alkylammonium ions. For example, in intercalated clay/polystyrene composites, the intercalating agent decomposes at about 250 °C. Bonding the intercalating ion to the polystyrene matrix noticeably improved the thermal stability.

Jin and co-worker investigated thermal property of polymer-clay nanocomposites by TGA and cone calorimetry. [21] The thermal stability of the nanocomposite is enhanced relative to that of virgin polystyrene and this is shown in Figure 1-18. Typically, the onset temperature of the degradation is about 50 °C higher for the nanocomposites than for virgin polystyrene.

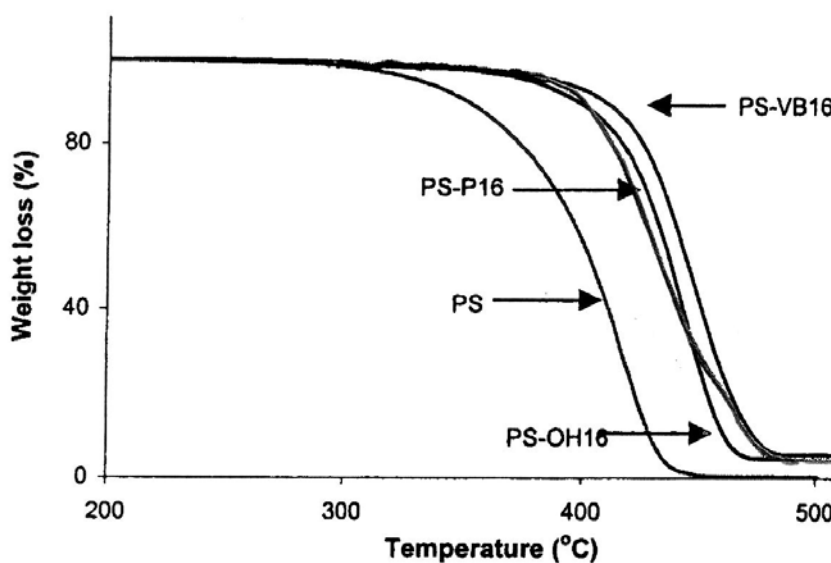


Figure 1-18. TGA curves for polystyrene, PS, and the nanocomposites. [21]



One invariably finds that nanocomposites have a much lower peak heat release rate (PHRR) than the virgin polymer. The peak heat release rate for polystyrene and the three nanocomposites are also shown graphically in Figure 1-19. P16-3 means that the nanocomposite was formed using 3 % of P16 clay with polystyrene. The peak heat release rate falls as the amount of clay was increased. The suggested mechanism by which clay nanocomposites function involves the formation of a char that serves as a barrier to both mass and energy transport. [59] It is reasonable that as the fraction of clay increases, the amount of char that can be formed increases and the rate at which heat is released is decreased. There has been a suggestion that an intercalated material is more effective than is an exfoliated material in fire retardancy. [21]

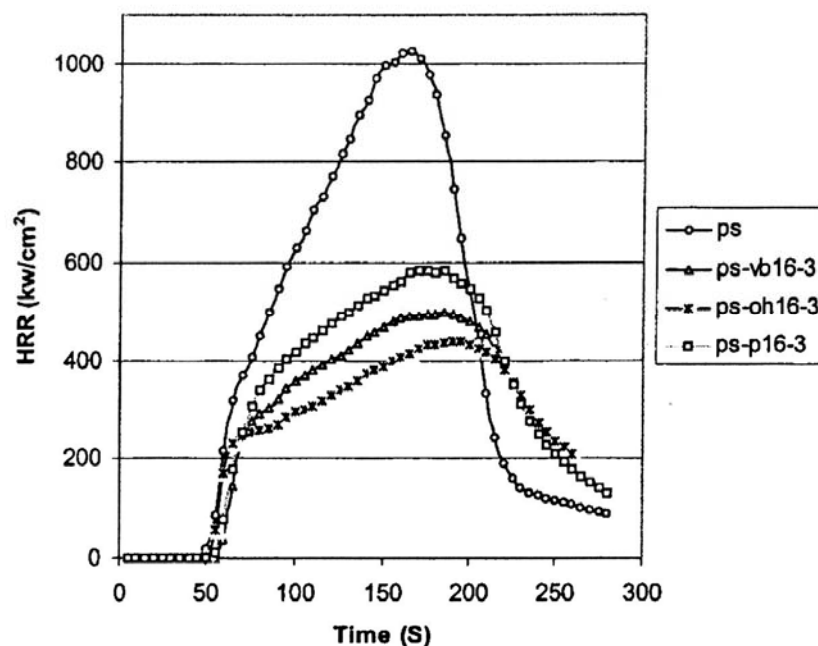


Figure 1-19. Peak heat release rates for polystyrene and the three nanocomposites. [21]

The production of a char barrier must serve to retain some of the polymer and thus both the energy released and the mass loss rate decrease. The amount of smoke evolved, specific extinction area, also decreases with the formation of the nanocomposite. There is some variability in the smoke production but apparently the

formation of the nanocomposite gives a reduction in smoke, however, the presence of additional clay does not decrease smoke.

### 1.6.3 Mechanical Properties

The cyclic deformation of PS/MMT nanocomposites as a function of temperature was measured by DMA. The temperature dependence of storage modulus and  $\tan\delta$  were shown in Figure 1-20 and 21, respectively. The storage modulus of PS/MMT nanocomposites were greater than that of pure PS and monotonically increased with the clay content in both the glassy and rubbery regions. However, the improvements in the rubbery region were much greater than those in the glassy region. This behavior indicates that the restricted segmental motions at the organic-inorganic interface are due to large aspect ratios of the clay platelets, and the polymer chains were also well confined inside the clay galleries at the nanoscale level. [63,64] The storage modulus of PS/MMT-3 was 1.2 times higher than that of pure PS, which is comparable to the earlier reported data (1.4 times improvement). [63] The  $T_g$ s of the nanocomposites were estimated from the peak values of  $\tan\delta$  in Figure 1-18, which were shifted towards higher temperature with increasing the clay content. These results indicate that nanoscale clay platelets strongly restrict the polymer segmental motions, resulting in the significant increase in  $T_g$ . This improvement in  $T_g$  is higher than those of other researchers even though the smaller clay content was used in this experiment. [65,66]

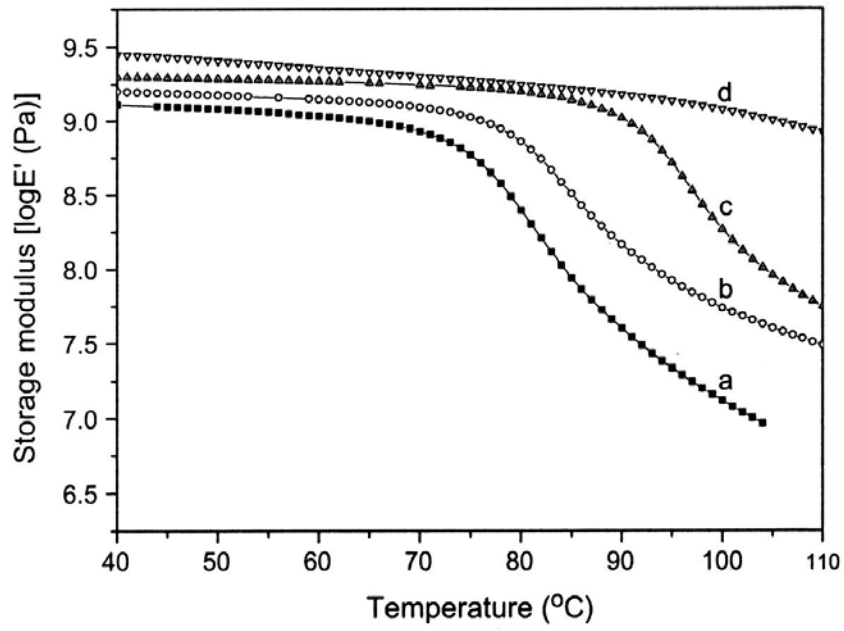


Figure 1-20. Storage modulus of (a) pure PS, (b) PS/MMT-1, (c) PS/MMT-2 and (d) PS/MMT-3.

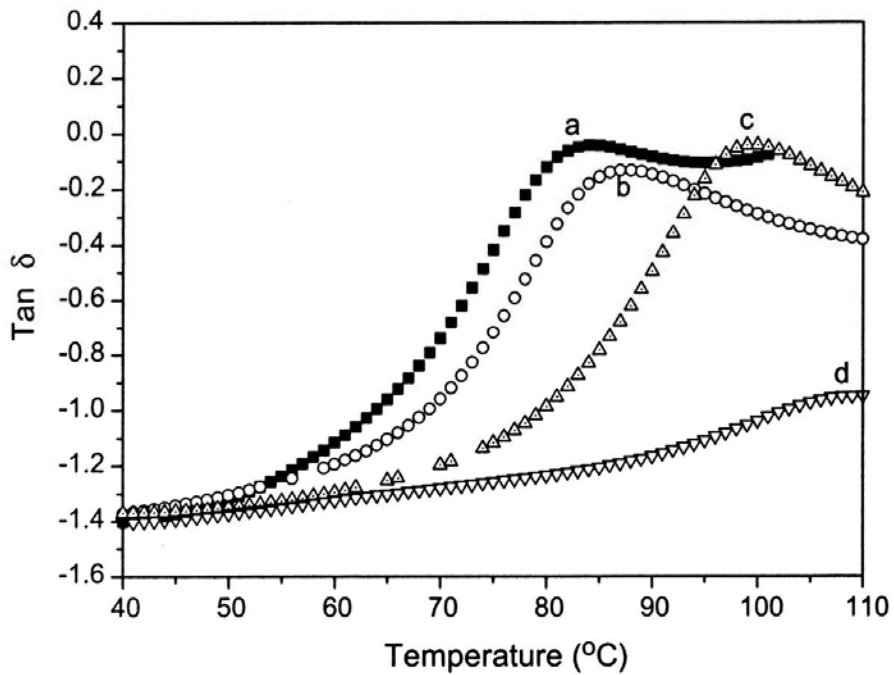


Figure 1-21.  $\text{Tan } \delta$  values of (a) pure PS, (b) PS/MMT-1, (c) PS/MMT-2 and (d) PS/MMT-3.

The effects of clay loadings on tensile properties of the PS/MMT nanocomposites are shown in Figure 1-22. The tensile strength and Young's modulus were significantly enhanced in the presence of the small contents of clay, while the elongation at break was reduced with increasing the clay content. The increase in tensile strength was attributed to the stronger interfacial adhesion between PS and the clay platelets. However, the enhancement of modulus was reasonably ascribed to the high resistance exerted by the clay platelets against the plastic deformation and the stretching resistance of the oriented polymer backbones in the galleries. The improvement of tensile strength in PS/MMT-3 compared to pure PS was ~47%, which is greater than the earlier reported value in the literature (~21%) for PS/MMT nanocomposite with 3wt% MMT prepared by melt blending. [64] Similarly, the enhancement of Young's modulus in PS/MMT-3 compared to pure PS was ~25%, which is much greater than the reported value (7.4% improvement for PS/MMT nanocomposite with 5wt% clay prepared by emulsion polymerization). [67] However, the elongations at break were reduced with increasing the clay content. Similar results were earlier reported. For example, the reduction of elongation at break in PS/MMT nanocomposite with 4.4wt% MMT prepared by melt blending was reported to ~26%. [63]

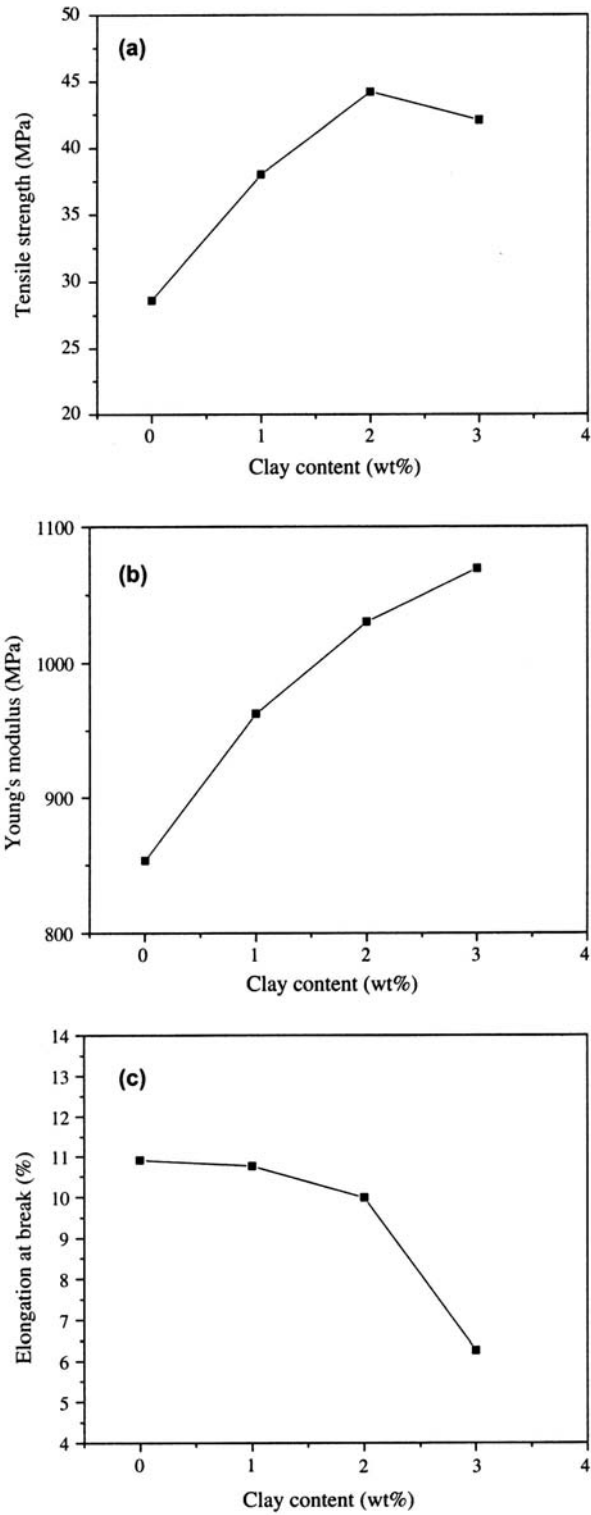


Figure 1-22. (a) Tensile strengths, (b) Young's modulus and (c) elongations at break of PS/MMT nanocomposites. [68]

#### 1.6.4 Gas barrier properties

Clays are believed to increase the barrier properties by creating a maze or “tortuous path” (Figure 1-23) that retards the progress of the gas molecules through the matrix resin. The direct benefit of the formation of such a path is clearly observed in polyimide/clay nanocomposites by dramatically improved barrier properties, with a simultaneous decrease in the thermal expansion coefficient. [78,79] The polyimide/layered silicate nanocomposites with a small fraction of OMLS exhibited reduction in the permeability of small gases, e.g. O<sub>2</sub>, H<sub>2</sub>O, He, CO<sub>2</sub>, and ethylacetate vapors. [80] For example, at 2 wt % clay loading, the permeability coefficient of water vapor was decreased ten-fold with synthetic mica relative to pristine polyimide. By comparing nanocomposites made with layered silicates of various aspect ratios, the permeability was seen to decrease with increasing aspect ratio.

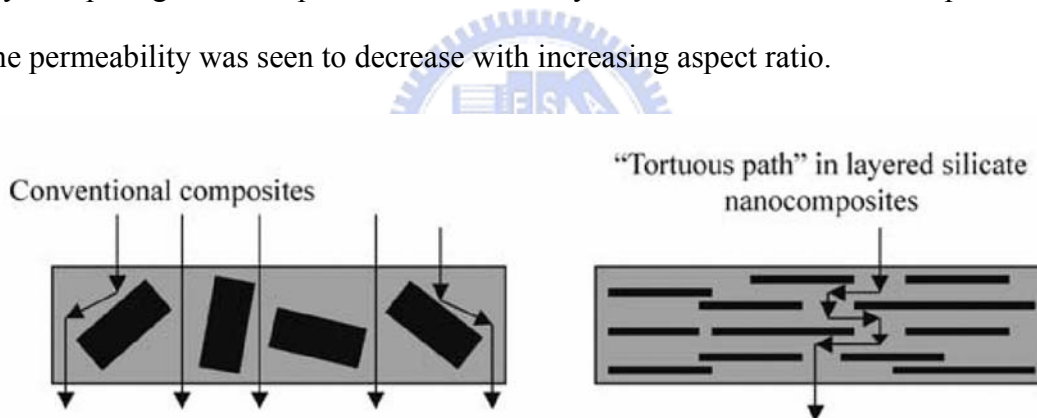


Figure 1-23 Formation of tortuous path in PLS nanocomposites.

Apparently, significant improvements in barrier properties are also achievable with nonplate-like nanoparticles. [81] Nano Material Inc. reports that a PVA/EVOH matrix composite with 7 nm silica and titania nanoparticles exhibits a gas permeability of  $1 \text{ cc m}^{-2} \text{ d}^{-1} \text{ atm}^{-1}$  and moisture permeability of less than  $1 \text{ g m}^{-2} \text{ d}^{-1}$ . Although this is achieved at very high loadings, the material is melt processable.

The absorption of water into composites is significant. For example, one of the limitations of Nylon is the reduction in mechanical properties that accompanies the

absorption of water. The addition of exfoliated montmorillonite increases the resistance to water permeation after 30 min from 2% to 1% at 5 wt. % of filler. [82] The mechanism of the reduction is attributed to the constrained region of the Nylon. If the constrained region is taken into account, the diffusion coefficient follows a rule of mixtures. Figure 1-24 shows the change in diffusion coefficient of water in Nylon in response to clay content.

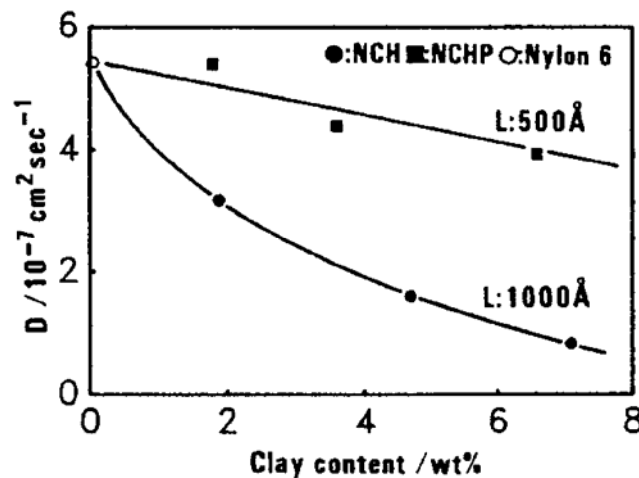


Figure 1-24 Dependence of diffusion coefficient of water on clay content for montmorillonite with a layer width of 100 nm, and saponite with a layer width of 50 nm. [82]

### 1.6.5 Electrical and Optical Properties

The electrical and optical properties of nanofilled polymers are exciting areas of research. This is particularly true because of the possibility of creating composites with unique combinations of functionalities, such as electrically conducting composites with good wear properties that are optically clear. Such properties can result because nanoparticles, with diameters distinctly below the Rayleigh scattering limit, still display their solid-state physical properties when embedded in transparent matrices.

Optical composites have been defined as composites consisting of optically

active nanoparticles embedded in a transparent host material, often a polymer. Optical composites take advantage of the optical properties of materials that are hard to grow in single-crystal form or that require protection from the environment and give them the ease of processing afforded many polymers. In addition, sometimes the material must be used at the nanoscale to achieve specific optical properties, and the matrix is used just to hold the particles together and provide processability. For example, high-grade optical composites, with properties otherwise obtainable only in optical glasses, become accessible through the use of polymer molding techniques.





## 1.7 Summary

The nanocomposite presented here is a composite material reinforced with silicate sheets. Silicate sheet is an ultrafine filler of nanometer size, which is almost equal to the size of the matrix polymer. Although the content of the filler is as little as several wt%, individual filler particles exist at a distance as close as tens of nanometers from each other because of their ultrafine size. One end of the polymer is strongly restrained to the silicate sheet by polar interaction. Thus, the nanocomposite has a microstructure that has never been seen in conventional composites. The characteristic properties of the nanocomposite are derived from this very structure. Considering the properties, the nanocomposite may be, in a sense, an embodiment of the ideal polymer composite, or a completely novel composite. Silicate sheet can be regarded as a rigid inorganic polymer. In this sense, the nanocomposite realized is a molecular composite in which a silicate sheet is used instead of an organic rod-like polymer.

## References

- [1] Blumstein, A. Bull. Chim. Soc. 1961, 899.
- [2] Usuki, A.; Kojima, Y.; Kawasumi, M.; Okada, A.; Fukushima, Y.; Kurauchi, T.; Kamigaito, O. J. Mater. Res. 1993, 8, 1179.
- [3] Lan, T.; Pinnavaia, T. J. Chem. Mater. 1994, 6, 2216.
- [4] Usuki, A.; Kato, M.; Okada, A.; Kurauchi, T. J. App. Polym. Sci. 1997, 63, 137.
- [5] Jeon, H. G.; Jung, H. T.; Lee, S. D.; Hudson, S. Polymer Bulletin 1998, 41, 107.
- [6] Giannelis, E. Adv. Mater. 1996, 8, 29.
- [7] Fisher, H.; Gielgens, L.; Koster, T. Nanocomposites from Polymers and Layered Minerals; TNO-TPD Report, 1998.
- [8] Carrado, K. A.; Langui, X. Microporous Mesoporous Mater. 1999, 27, 87.
- [9] Friedlander, H. Z.; Grink, C. R. J. Polym. Sci., Polym. Lett. 1964, 2, 475.
- [10] Blumstein, A. J. Polym. Sci., Part A. 1965, 3, 2653.
- [11] Kato, C.; Kuroda, K.; Takahara, H. Clay and Clay Minerals 1981, 29, 294.
- [12] Kelly, P.; Moet, A.; Qutubuddin, S. J. Mater. Sci. 1994, 29, 2274.
- [13] Akelah, A.; Kelly, P.; Qutubuddin, S.; Moet, A. Clay Minerals 1994, 29, 169.
- [14] Akelah, A.; Moet, A. J. Mater. Sci. 1996, 31, 3189.
- [15] Akelah, A.; Moet, A. Mater. Lett. 1993, 18, 97.
- [16] Giannelis, E. P.; Adv. Mater. 1996, 8, 29.
- [17] Vaia, R.; Ishii, H.; Giannelis, E. Chem. Mater. 1993, 5, 1694.
- [18] Doh, J. G.; Cho, I. Polymer Bulletin 1998, 41, 511.
- [19] Takekoshi, T.; Fouad, F.; Mercx, F. P. M.; De Moor, J. J. M. US patent 5,773,502. Issued to General Electric Co., 1998.
- [20] Okada, K. (Sekisui) Japan Patent 11-228748, 1999.
- [21] Zhu, J.; Alexander, B. M.; Frank, J. L.; Charles, A. W. Chem. Mater. 2001, 13, 3774
- [22] Dongyan, W.; Jin, Z.; Qiang, Y.; Charles, A. W. Chem. Mater. 2002, 14, 3837.

- [23] Dongyan, W.; Charles, A. W. *Polym. Deg. Stab.* 2003, 82, 309.
- [24] Fu, X.; Qutubuddin, S. *Polymer* 2001, 42, 807.
- [25] Lin, J. J.; Cheng, I. J.; Chou, C. C. *Macromol. Rapid Commun.* 2003, 24, 492.
- [26] Yei, D. R.; Kuo, S. W.; Fu, H. K.; Chang, F. C. *Polymer* 2005, 46, 741.
- [27] Yei, D. R.; Kuo, S. W.; Su, Y. C.; Chang, F. C. *Polymer* 2004, 45, 2633.
- [28] Tseng, C.R.; Wu, J.Y.; Lee, H.Y.; Chang, F.C. *Polymer* 2001; 42: 10063.
- [29] Tseng, C.R.; Lee, H.Y.; Chang, F.C. *J. Polym Sci Part B: Polym Phys* 2001; 39: 2097.
- [30] Chen, H. W.; Chiu, C. Y.; Chang, F.C. *J. Polym Sci Part B: Polym Phys* 2002; 40: 1342.
- [31] Tseng, C.R.; Wu, J.Y.; Lee, H.Y.; Chang, F.C. *J Appl Polym Sci* 2002; 85: 1370.
- [32] Tseng, C.R.; Wu, H.D.; Wu, J.Y.; Chang, F.C. *J Appl Polym Sci* 2002; 86: 2492.
- [33] Weimer, M. W.; Chen, H.; Giannelis, E. P.; Sogah, D. Y. *J. Am. Chem. Soc.* 1999, 121, 1615.
- [34] Zhou, Q.; Fan, X.; Xia, C.; Mays, J.; Advincula, R. *Chem. Mater.* 2001, 13, 2465.
- [35] Fan, X.; Zhou, Q.; Xia, C.; Crsitopholi, W.; Mays, J.; Advincula, R. C. *Langmuir* 2002, 18, 4511.
- [36] Fan, X.; Xia, C.; Advincula, R. C. *Langmuir* 2003, 19, 4381.
- [37] Meier, L.; Shelden, R.; Caseri, W.; Suter, U. *Macromolecules* 1994, 27, 1637.
- [38] Prucker, O.; Ruhe, J. *Macromolecules* 1998, 31, 592.
- [39] Prucker, O.; Ruhe, J. *Macromolecules* 1998, 31, 602.
- [40] Yano, K.; Usuki, A.; Okada, A.; Kuraychi, T.; Kamigaito, O. *Polym. Prepr.* 1991, 32, 65.
- [41] Kojima, Y.; Usuki, A.; Kawasumi, M.; Okada, A.; Kurauchi, T.; Kamigaito, O. *J. Polym. Sci., Part A: Polym. Chem.* 1993, 31, 983.

- [42] Liu, L.; Qi, A.; Zhu, X. *J. Appl. Poly. Sci.* 1999, 71, 1133.
- [43] Yano, K.; Usuki, A.; Okada, A.; Kuraychi, T.; Kamigaito, O. *J. Polym. Sci., Part A: PolymChem.* 1993, 31, 2493.
- [44] Yano, K.; Usuki, A.; Okada, A. *J. Polym. Sci., Part A: Polym. Chem.* 1997, 35, 2289.
- [45] Lan, T.; Kaviratna, P. D.; Pinnavaia, T. J. *Chem. Mater.* 1994, 6, 573.
- [46] Tyan, H.L.; Liu, Y.C.; Wei, K.H. *Polymer* 1999, 40, 4877.
- [47] Kawasumi, M.; Hasegawa, N.; Kato, M.; Usuki, A.; Okada, A. *Macromolecules* 1997, 30, 6333.
- [48] Kato, M.; Usuki, A.; Okada, A. *J. Appl. Polym. Sci.* 1997, 66, 1781.
- [49] Kuchta, F.D.; Lemstra, P. J.; Kellar, A.; Batenburg, L. F.; Fischer, H. R. *MRS Symp. Proc.* 1999, 576, 363.
- [50] Lee, D. C.; Lee, J. W. *J. Appl. Polym. Sci.* 1996, 61, 1117.
- [51] Okamoto, M.; Morita, S.; Taguchi, H.; Kim, Y.H.; Kotaka, T.; Tateyama, H. *Polymer* 2000, 41, 3887.
- [52] Chen, G.; Chen, X.; Lin, S.; Ye, W. *J. Mater. Sci. Lett.* 1999, 18, 1761.
- [53] Dietsche, F.; Thomann, Y.; Thomann, R.; Mulhaupt, R. *J. Appl. Polym. Sci.* 2000, 75, 396.
- [54] Hasegawa, N.; Okamoto, H.; Kawasumi, M.; Usuki, A. *J. Appl. Poly. Sci.* 1999, 74, 3359.
- [55] Lan, T.; Pinnavaia, T. J. *Chem. Mater.* 1994, 6, 2216.
- [56] Wang, Z.; Lan, T.; Pinnavaia, T. J. *Chem. Mater.* 1996, 8, 2200.
- [57] Massam, J.; Pinnavaia, T. J. *MRS Symp. Proc.* 1998, 20, 223.
- [58] C. Zeng, L. J. Lee, *Macromolecules* 2001, 34, 4098.
- [59] Gilman, J. W.; Jackson, C. L.; Morgan, A. B.; Harris, R.; Giannelis, E. P.; Phillips, S. H. *Chem. Mater.* 2000, 12, 1866.

- [60] T. Agag, T. Koga, T. Takeichi, *Polymer* 2001, 42, 3399.
- [61] J. Lee, E. Giannelis, *Polym. Prepr.* 1997, 38, 688.
- [62] S. D. Burnside, E. P. Giannelis, *Chem. Mater.* 1995, 7, 1597.
- [63] Hasegawa, N.; Okamoto, H.; Kawasumi, M.; Usuki, A. *J. Appl. Polym. Sci.* 1999, 74, 3359.
- [64] Park, C.I.; Choi, W.M.; Kim, M.K.; Park, O.O. *J. Polym. Sci. Part B: Polym. Phys.* 2004, 42, 1685.
- [65] Fu, X.; Qutubuddin, S. *Mater. Lett.* 2000, 42, 12.
- [66] Kim, Y.K.; Choi, Y.S.; Wang, K.H.; Chung, I. J. *Chem. Mater.* 2002, 14, 4990.
- [67] Noh, M.W.; Lee, D.C. *Polym. Bull.* 1999, 42, 619.
- [68] Uthirakumar, P.; Song, M.K.; Nah, C.; Lee, Y.S. *Euro. Polym. J.* 2005, 41, 211.
- [69] Aranda, P.; Ruiz-Hitzky, E. *App. Clay Sci.* 1999, 15, 119.
- [70] Chen, W.; Xu, Q.; Yuan, Z. *J. Mater. Sci. Lett.* 1999, 18, 711.
- [71] Vaia, R. A.; Vasudevan, S.; Krawwiec, W.; Scanlon, L. G.; Giannelis, E. P. *Adv. Mater.* 1995, 7, 154.
- [72] Kojima, Y.; Fukumori, K.; Usuki, A.; Kurauchi, T.; J. *Mater. Sci. Lett.* 1993, 12, 889.
- [73] Kresge, E. N.; Lohse, D. J. *US Patent* 1996, 5, 576, 372.
- [74] Laus, M.; Francescangeli, O.; Sandrolini, F. J. *Mater. Res.* 1997, 12, 3134.
- [75] Oriakhi, C. O.; Zhang, X.; Lerner, M. M. *Appl. Clay Sci.* 1999, 15, 109.
- [76] Huang, X.; Lewis, S.; Brittain, W. J.; Vaia, R. A. *Macromolecules* 2000, 33, 2000.
- [77] Wu, Q.; Xue, Z.; Qi, Z.; Wang, F. *Polymer* 2000, 41, 2029.
- [78] Yano, K.; Usuki, A.; Okada, A.; Kurauchi, T.; Kamigaito, O. *Synthesis and properties of polyimide–clay hybrid.* *Polym Prepr (Jpn)* 1991, 32(1), 65.
- [79] Yano, K.; Usuki, A.; Okada, A. *Synthesis and properties of polyimide–clay*

hybrid films. *J Polym Sci, Part A: Polym Chem* 1997, 35, 2289.

[80] Yano, K.; Usuki, A.; Okada, A.; Kurauchi, T.; Kamigaito, O. Synthesis and properties of polyimide–clay hybrid. *J Polym Sci, Part A: Polym Chem* 1993, 31, 2493.

[81] *Modern Plastics*, February, 1999.

[82] Kojima, Y.; Usuki, A.; Kawasumi, M.; Okada, A.; Kurauchi, T.; Kamigaito, O. J. *Appl. Polym. Sci.* 1993, 49, 1259.

[83] US Patent 4,739007 (19 Apr 1988).

[84] Lee, D. C.; Jan, L. W. *J. Appl. Polym. Sci.* 1996, 61, 1117.



## Chapter 2

### **Enhanced Thermal Properties of PS Nanocomposites formed from Inorganic POSS-Treated Montmorillonite**

#### **Abstract**

We have prepared polystyrene/clay nanocomposites using an emulsion polymerization technique. The nanocomposites were exfoliated at up to a 3 wt % content of pristine clay relative to the amount of polystyrene (PS). We used two different surfactants for the montmorillonite: the aminopropylisobutyl polyhedral oligomeric silsesquioxane (POSS) and the ammonium salt of cetylpyridinium chloride (CPC). Both surfactants can intercalate into the layers of the pristine clay dispersed in water prior to polymerization. Although the  $d$  spacing of the POSS-intercalated clay is relatively smaller than that of the CPC-intercalated clay, PS more easily intercalates and exfoliates the POSS-treated clay than the CPC-treated clay. IR spectroscopic analysis further confirms the intercalation of POSS within the clay layers. We used X-ray diffraction (XRD) and transmission electron microscopy (TEM) to characterize the structures of the nanocomposites. The nanocomposite prepared from the clay treated with the POSS containing surfactant is exfoliated, while an intercalated clay was obtained from the CPC-treated surfactant. The molecular weights of polystyrene (PS) obtained from the nanocomposite is slightly lower than the virgin PS formed under similar polymerization conditions. The value of  $T_g$  of the PS component in the nanocomposite is 8 °C higher than the virgin PS and its thermal decomposition temperature (21 °C) is also higher significantly. The presence of the POSS unit in the MMT enhances the thermal stability of the polystyrene.

## 2.1 Introduction

Nanoclay-filled polymeric systems offer the prospect of greatly improving many of the properties of their mother polymers. In the recent literature, there have been reports of nanoclay-filled polymeric systems that display significant improvements in tensile and thermal properties [1—9], heat distortion temperatures [1—6], and resistance to flammability [12] and reduced permeability to small molecules [5,10,11] and reduced solvent uptake [13]. A common observation emerging from these studies is that the magnitude of improvement depends strongly on the state of dispersion of the clay layers in the polymer matrix.

The nanocomposite typically comprises the organically modified clay and the mother polymer. Montmorillonite (MMT), which is an aluminosilicate mineral with sodium counterions present between the layers, is the most commonly used clay. The space between these clay layers is referred to as the clay gallery. To make this inorganic clay compatible with organic polymers, the sodium counterions are usually ion-exchanged with an organic ammonium or phosphonium salt to convert the material into hydrophobic ammonium- or phosphonium-treated clays. The nanocomposites may be prepared either by a blending process (either melt blending or solution blending) or by an in situ polymerization process in the presence of the organically modified clay.

In this paper, we describe the preparation of two types of nanocomposites formed from cetylpyridinium chloride (CPC)- and aminopropylisobutyl polyhedral oligomeric silsesquioxane (POSS)-treated clays (Scheme 2-1). The PS/clay nanocomposite formed using the CPC-treated clay exhibited no significant improvements in thermal properties [14—18] in our laboratory. Major reason of choice POSS molecules are typically stable up to 300 °C, which is higher than the



thermal degradation temperatures of most organic molecules. POSS consists of a rigid cubic silica core, having 0.53-nm side lengths, to which organic functional groups can be attached, at the vertices, for further reactions. POSS derivatives containing amine functional groups can play the role of surfactants for the treatment of clay; the thermal stability of the resulting nanocomposite is enhanced.

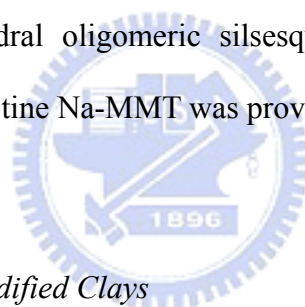
PS/clay nanocomposites were prepared through emulsion polymerization by suspending the surfactant-treated clay in styrene monomer. IR spectroscopic analysis confirmed the existence of POSS in the intercalated clay samples. We used both X-ray diffraction (XRD) and transmission electron microscopy (TEM) to characterize the clay structure. The properties of these PS/clay nanocomposites were characterized by thermogravimetric analysis (TGA), differential scanning calorimetry (DSC), and gel permeation chromatography (GPC).



## 2.2 Experimental

### 2.2.1 Materials

Most of chemicals used in this study, including monomeric styrene, chemically pure acetone, methanol, tetrahydrofuran, and potassium hydroxide (KOH) were acquired from the Aldrich Chemical Co., Inc. The styrene monomer was purified by removing the inhibitor with the aid of an inhibitor-removal column, which was also acquired from Aldrich. Sodium dodecyl sulfate (SDS) and hydrochloride acid were both obtained from Curtin Matheson Scientific, Inc. Potassium persulfate ( $K_2S_2O_8$ ) and aluminum sulfate [ $Al_2(SO_4)_3$ ] were acquired from Fisher Scientific Co., USA. Cetylpyridinium chloride (CPC) was obtained from Acros Organics, USA. Aminopropylisobutyl polyhedral oligomeric silsesquioxane (POSS) was obtained from Hybrid Plastics, Inc. Pristine Na-MMT was provided by Telekal Co., Taiwan.



### 2.2.2 Preparation of CPC-Modified Clays

The organically modified clay was obtained by combining sodium montmorillonite (5 g) and the desired quantity (1, 1.5, 2, or 2.5 g) of the ammonium salt (CPC), as previously described [19].

### 2.2.3 Preparation of POSS-Modified Clays

The prewashed clay (1 g) and water (50 mL) were placed into a 100-mL two-neck round-bottom flask and stirred continuously for 4 h. POSS (0.4 g) in THF (1 mL) was placed into another flask and then 10 % hydrochloric acid (1 mL) was added and then stirring for 1 h. This POSS solution was then added into the suspended clay and the mixture was stirred overnight. The mixture was filtered, washed several times

with deionized water, and then dried overnight in a vacuum oven at room temperature.

#### *2.2.4 Preparation of Polystyrene/Clay Nanocomposites*

Emulsion polymerization was performed as follows. A suspension of clay (0.3 g) in deionized water (40 mL) was stirred for 4 h at room temperature. A solution of surfactant (CPC or POSS; 0.12 g) was added and the mixture was stirred for 4h. KOH (0.02 g) and SDS (0.4 g) were added into the solution and the temperature was raised to 50 °C. Styrene monomer (10 g) and  $K_2S_2O_8$  (0.05g) were added slowly to the flask. Polymerization was performed at 50 °C for 8 h. After cooling, 2.5 % aqueous aluminum sulfate (10 mL) was added to the polymerized emulsion, followed by dilute hydrochloric acid (10 mL), with stirring. Finally, acetone was added to break down the emulsion completely. The polymer was washed several times with methanol and distilled water and then dried overnight in a vacuum oven at 80 °C. Similar procedures were employed to prepare virgin polystyrene.

#### *2.2.5 Instrumentations*

IR spectroscopy was performed on a Nicolet Avatar 320 FTIR Spectrophotometer; 32 scans were collected at a spectral resolution of  $1\text{ cm}^{-1}$ . Infrared spectra of the organic-modified clay were obtained using the conventional KBr pellet method. X-Ray diffraction spectra were collected on an M18XHF-SPA X-ray diffraction instrument (MacScience Co., Japan), using Co  $K\alpha$  radiation; Bragg's law ( $\lambda = 2d\sin\theta$ ) was used to compute the spacing. Transmission electron microscopy (TEM) images of the composites were obtained at 100 kV using a Hitachi H-7500 Electron Microscope. The sample was ultramicrotomed at room temperature using a glass knife on a Leica Ultracut UCT Microtome to give 100 nm-thick sections. The

contrast between the layered silicates and the polymer phase is sufficient for imaging and, therefore, no heavy metal staining was required prior to imaging. Thermogravimetric analyses (TGA) were performed on a TA Instruments Thermal Analyzer under a 40 mL/min flow of nitrogen gas at a scan rate of 20 °C /min from 30 to 800 °C. A Du-Pont (DSC-9000) differential scanning calorimeter (DSC) was used to measure the glass transition temperature ( $T_g$ ) of the PS/clay. The sample was preheated at a scan rate of 20 °C /min from 30 to 200 °C and then cooled quickly to 30 °C from the melt of the first scan. The second scan rate was 20 °C /min from 30 to 200 °C and the value of  $T_g$  was taken as the midpoint of the heat capacity transition between the upper and lower points of deviation from the extrapolated liquid and glass lines. Molecular weights and molecular weight distributions were characterized by GPC using a Waters 510 HPLC—equipped with a 410 Differential Refractometer, a UV detector, and three Ultrastyrigel columns (100, 500, and  $10^3$  Å) connected in series in order of increasing pore size—using THF as an eluent at a flow rate of 0.4 mL/min. The molecular weight calibration curve was obtained using polystyrene standards.

## 2.3 Results and Discussion

This study focused on comparing nanocomposites prepared using two different surfactant-modified clays. The CPC surfactant is an ammonium salt that contains a long aliphatic chain. The POSS surfactant is an ammonium salt that features a cube-like cage structure containing seven isobutyl groups located at the corner positions. Scheme 2-1 displays the structures of these two ammonium salts, CPC and POSS, used to prepare the modified clays. Conventional surfactants, such as CPC, are unstable at high temperatures. Thus, we expected that nanocomposites prepared from the POSS surfactant would possess better thermal stabilities relative to those formed using the CPC surfactant.

### 2.3.1 X-Ray Diffractions.

We used X-ray diffraction (XRD) to characterize the layered structures of the modified clays and polymer/clay nanocomposites, since changes in  $2\theta$  indicate changes in the gallery distance of the clay. Figure 2-1 displays X-ray diffraction patterns of organic-modified clays containing different CPC/clay ratios. The basal space indicates the interlayer spacing of the silicate layers which is calculated from the peak position using the Bragg equation. The pristine clay has this peak at  $6.94^\circ$ , which corresponds to a basal space of 1.26 nm. The insertion of the CPC surfactant between the galleries of the clay increases the  $d$  spacing as the CPC/clay ratio increases. When the CPC/clay ratio is greater than 0.4, the  $d$  spacing remains constant, which implies that oversaturation of the surfactant has occurred. This result indicates that the CPC surfactant becomes successfully intercalated into the galleries of the clay nanoparticles.

Figure 2-2 displays the XRD results of the POSS-intercalated clay. The pure POSS surfactant has characteristic diffraction peaks at 7.9° and 8.8° that arise from aggregation of the POSS. When the POSS surfactant is inserted between the galleries of the clay, the  $d$  spacing is increased from 1.26 nm for the pristine clay to 1.61 nm for the POSS surfactant-intercalated clay, which indicates that the POSS surfactant has indeed been intercalated successfully into the galleries of the clay. This  $d$  spacing is relatively smaller than that of the CPC-treated clay, but it does not affect the clay intercalation or exfoliation within the PS matrix. The POSS is known to interact with PS to promote intercalation and exfoliation [20]. This result agrees well with the TEM result that indicated that the degree of clay exfoliation of the POSS-treated nanocomposite is even greater than that of the CPC-treated material. The POSS surfactant-intercalated clay (POSS/Clay) exhibits only one diffraction peak; no peak was detected to arise from the aggregation of POSS. The POSS surfactant-intercalated clay is presented schematically in Scheme 2-2. The interlamellar distance indicated in the figure is calculated by the expression:  $\Delta d = d \text{ spacing} - \text{thickness of one platelet} (\sim 1.0 \text{ nm})$ . In the case of the clay intercalated with POSS surfactant, the distance between two adjacent clay plates is 0.71 nm which is close to the particle size of the POSS. The R group (isobutyl group) of the POSS experiences van der Waals interactions with the styrene monomer, and thus allows the styrene monomer can polymerize within the galleries of the clay.

The formation of a true polymer/clay nanocomposite requires the insertion of the polymer between the layers of the clay. There are two terms used to describe the general classes of nanocomposites: intercalation and exfoliation (also called delamination). In the case of intercalation, polymer chains are inserted between galleries of the clay, and the spacing between the galleries is increased. On the other hand, in the case of exfoliation, these individual silicate layers are distributed

randomly such that they no longer interact with the cations. Characterizing the formation of a nanocomposite requires measurement of the  $d$  spacing by XRD and the use of TEM to determine the actual distribution of platelets within the polymer matrix. The formation of an exfoliated structure usually results in the complete loss of registry between the clay layers so that no peak can be observed by XRD. The most likely occurrence is the formation of a mixture of exfoliated and intercalated structures; this phenomenon requires detection by TEM.

Figure 2-3 presents the XRD results for CPC/Clay/PS and POSS/Clay/PS nanocomposites. No peak is detected for the nanocomposites from both the CPC- and POSS-treated clays, which suggests that they have exfoliated structure. TEM is still required, however, to observe the true structure and distribution of the silica platelets. There is an angle detecting limit for the XRD detector which is unable to detect the diffraction angle less than  $3.5^\circ$ .



### 2.3.2 TEM Measurements on the Nanocomposites.

Figure 2-4 displays TEM images of two nanocomposites prepared from the CPC- and POSS-modified clays. The layers of platelets observed for these CPC-treated nanocomposites are, in fact, an intercalated structure. For the POSS-treated nanocomposite, each clay layers is isolated and evenly distributed within the PS matrix, which implies that a full exfoliation is formed that is consistent with the XRD data.

### 2.3.3 Infrared Spectroscopy.

IR analysis further confirms the existence of the POSS in the intercalated clay sample. Figure 2-5 presents the IR spectra of pure POSS, pure clay, and the POSS-treated clay. The pure clay exhibits a strong absorbance at  $1040\text{ cm}^{-1}$  for the Si—O—Si bond in montmorillonite silicate. The pure POSS surfactant exhibits characteristic absorption peaks for its C—H bonds at  $2950\text{--}2800\text{ cm}^{-1}$ , the Si—C bonds at  $1230\text{ cm}^{-1}$ , and the Si—O—Si bonds of the cage structure at  $1109\text{ cm}^{-1}$ . The POSS-treated clay possesses all of the characteristic peaks of pure POSS and pure clay, which is an indication that the POSS surfactant is intercalated into the host galleries of the clay. This result is consistent with XRD data.

### 2.3.4 Analyzing Glass Transition Temperatures.

Figure 2-6 displays the DSC thermograms for the virgin PS and surfactant-modified clay nanocomposites. The  $T_g$  of the virgin PS is  $100\text{ }^\circ\text{C}$  while the values of  $T_g$  for the CPC/clay and POSS/clay nanocomposites are  $102$  and  $108\text{ }^\circ\text{C}$ , respectively. The presence of the clay layer tends to retard PS chain movement near its value of  $T_g$ . The better-dispersed clay nanocomposite (POSS/clay) retards chain movement more effectively than does the CPC/clay-modified nanocomposite.

### 2.3.5 Molecular Weights of the Nanocomposites.

Table 2-2 lists the molecular weights of PS in nanocomposites under similar emulsion polymerization conditions. The virgin PS has higher average molecular weights ( $M_n$  and  $M_w$ ) and a lower polydispersity index (PDI) than the two nanocomposites. It has been reported [21] that clay may act as additional micelles that



are responsible for the observed lower molecular weight.

### 2.3.6 Characterization by TGA.

Figure 2-7 displays the TGA traces of pure clay, clay treated with the POSS, and clay treated with the CPC. As expected, the inorganic montmorillonite silicate possesses exceptionally high thermal stability. The total weight loss of the pristine clay is only 5.7% up to 800 °C, which corresponds to three different types of water present in the montmorillonite clay [22]. In contrast, the surfactant-intercalated clays are more easily decomposed. Both CPC- and POSS-modified clays begin to decompose at much lower temperatures than the pure clay. The modified clays possessing identical component weight ratio (surfactant/clay = 0.4) give different temperatures of the 5% weight loss. The POSS-modified clay decomposes at a higher temperature of 386 °C while the CPC-modified clay decomposes at 278 °C. The POSS-intercalated clay is relatively more thermally stable than the CPC-intercalated clay. Thermal decompositions and removal of surfactants are responsible for the observed weight losses of these intercalated clays. This result also agrees well with the IR result that suggested that the clay indeed contains the organic surfactant.

Figure 2-8 presents TGA thermograms of nanocomposites and polystyrene. Both of the surfactant-modified PS nanocomposites display higher decomposition temperatures than the virgin PS. The onset of thermal decomposition for the nanocomposites is shifted to higher temperatures. The POSS-intercalated clay nanocomposite is the most thermally stable one among these three samples. The nanocomposite prepared from clay/POSS displays a 21 °C increase in the decomposition temperature for 5% weight loss relative to virgin PS; the clay/CPC

nanocomposite is 18 °C higher. Table 2-1 summarizes the TGA results for the nanocomposites. The highest temperature of 50% weight loss is observed for the POSS-intercalated clay nanocomposite. In the case of the CPC-intercalated clay nanocomposite, the temperature of 50% weight loss is actually the same as that for the virgin polystyrene. Therefore, the nanocomposite prepared from CPC-modified clay exhibits no improvement over the virgin PS, but, in the contrast, the nanocomposite prepared with POSS-modified clay has an improved thermal stability.



## 2.4 Conclusions.

We have prepared polystyrene/clay nanocomposites that have (a) an exfoliated structure when derived from POSS treatment and (b) an intercalated forms when treated with CPC. The intercalation of surfactants into montmorillonite clay nanoparticles was confirmed by XRD and FTIR spectroscopy. Results of XRD indicated that the  $d$  spacing increased from 1.26 nm for pristine clay to 1.61 nm for the POSS-intercalated clay. TGA of the nanocomposites suggests that the onset of thermal degradation occurs at a higher temperature for the nanocomposite formed from POSS than for either the virgin PS or the nanocomposite derived from CPC treatment. It appears that the presence of the POSS in the clay enhances the thermal stability of polystyrene. Surfactant-modified clays give PS having lower molecular weights ( $M_n$  and  $M_w$ ) and a higher MW distribution (polydispersity index, PDI) relative to the virgin PS formed under similar emulsion polymerization conditions. The glass transition temperatures of the nanocomposites incorporating CPC or POSS are higher than that of the virgin PS.

## References

- [1] Okada A, Kawasumi M, Usuki A, Kojima Y, Kurauchi T, Kamigaito O. *Mater Res Soc Symp Proc* 1990; 171: 45.
- [2] Okada A, Kawasumi M, Kurauchi T, Kamigaito O. *Polym Prepr* 1987; 28: 447.
- [3] Kojima Y, Usuki A, Kawasumi M, Okada A, Kurauchi T, Kamigaito O. *J Polym Sci Part A: Polym Chem* 1993; 31: 983.
- [4] Usuki A, Kojima Y, Kawasumi M, Okada A, Fukushima T, Kurauchi T, Kamigaito O. *J Mater Res* 1993; 8: 1179.
- [5] Yano K, Usuki A, Okada A, Kurauchi T, Kamigaito O. *J Polym Sci Part A: Polym Chem* 1993; 31: 2493.
- [6] Okada A, Usuki A. *Mater Sci Eng* 1995; 3: 109.
- [7] Lan T, Pinnavaia T. *J Chem Mater* 1994; 6: 2216.
- [8] Lan T, Pinnavaia T. *J Chem Mater* 1994; 6: 573.
- [9] Lan T, Kaviratna PD, Pinnavaia T. *J Chem Mater* 1995; 7: 2144.
- [10] Messersmith P, Giannelis EP. *J Polym Sci Part A: Polym Chem* 1995; 33: 1047.
- [11] Messersmith P, Giannelis EP. *Chem Mater* 1994; 6: 1719.
- [12] Gilman JW, Jackson CL, Morgan A, Harris R, Manias E, Giannelis EP, Wuthenow M, Hilton D, Phillips SA. *Chem Mater* 2000; 12: 1866.
- [13] Burnside SD, Giannelis EP. *Chem Mater* 1995; 7: 1597.
- [14] Tseng CR, Wu JY, Lee HY, Chang FC. *Polymer* 2001; 42: 10063.
- [15] Tseng CR, Lee HY, Chang FC. *J. Polym Sci Part B: Polym Phys* 2001; 39: 2097.
- [16] Wu HD, Tseng CR, Chang FC. *Macromolecules* 2001; 34: 2992.
- [17] Tseng CR, Wu JY, Lee HY, Chang FC. *J Appl Polym Sci* 2002; 85: 1370.
- [18] Tseng CR, Wu HD, Wu JY, Chang FC. *J Appl Polym Sci* 2002; 86: 2492.
- [19] Jin Z, Alexander BM, Frank JL, Charles AW. *Chem Mater* 2001; 13: 3774.

- [20] Wenhua Z, Bruce XF, Seo Y, Eric S, Hsiao B, Patrick TM, Yang NL, Dayi X, Harald A, Miriam R, Jonathan S. *Macromolecules* 2002; 35: 8029.
- [21] Dongyan W, Jin Z, Qiang Y, Charles AW. *Chem Mater* 2002; 14: 3837.
- [22] Xie W, Gao Z, Pan W, Hunter D, Vaia RA, Singh A. *PMSE Prepr* 2000; 82: 284.



Table 2-1. Results of TGA and DSC for Polystyrene Nanocomposites

Sample	$T_g$ , °C <sup>a</sup>	$T_{0.05}$ , °C <sup>b</sup>	$T_{0.5}$ , °C <sup>c</sup>	Char at 600 °C, %
PS	100	390	424	0
CPC/Clay/PS	102	408	424	2.9
POSS/Clay/PS	108	411	446	2.8

<sup>a</sup>Glass transition temperature ( $T_g$ ). <sup>b</sup>5% degradation temperature ( $T_{0.05}$ ). <sup>c</sup>50% degradation temperature ( $T_{0.5}$ ).

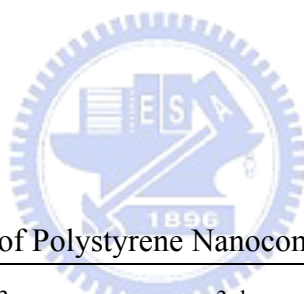
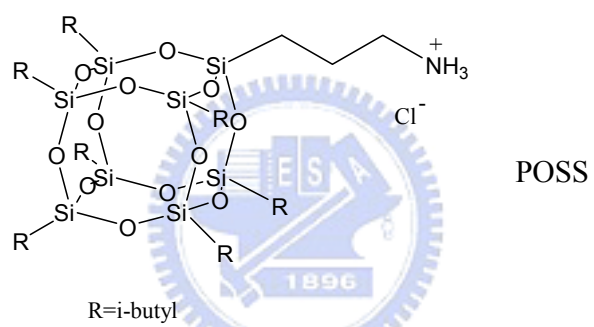
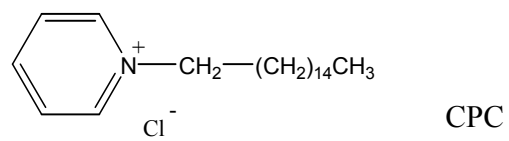


Table 2-2. Molecular Weights of Polystyrene Nanocomposites

Sample	$M_n$ ( $\times 10^3$ ) <sup>a</sup>	$M_w$ ( $\times 10^3$ ) <sup>b</sup>	PDI ( $M_w/M_n$ ) <sup>c</sup>
PS	26.1	31.8	1.22
CPC/Clay/PS	22.5	30.8	1.37
POSS/Clay/PS	21.9	31.1	1.42

<sup>a</sup>Number-average molecular weights ( $M_n$ ) and <sup>b</sup>weight-average molecular weights ( $M_w$ ) were determined by GPC. <sup>c</sup>Polydispersity index,  $M_w/M_n$ .



Scheme 2-1. Chemical structures of the surfactants used to prepare the modified clays.





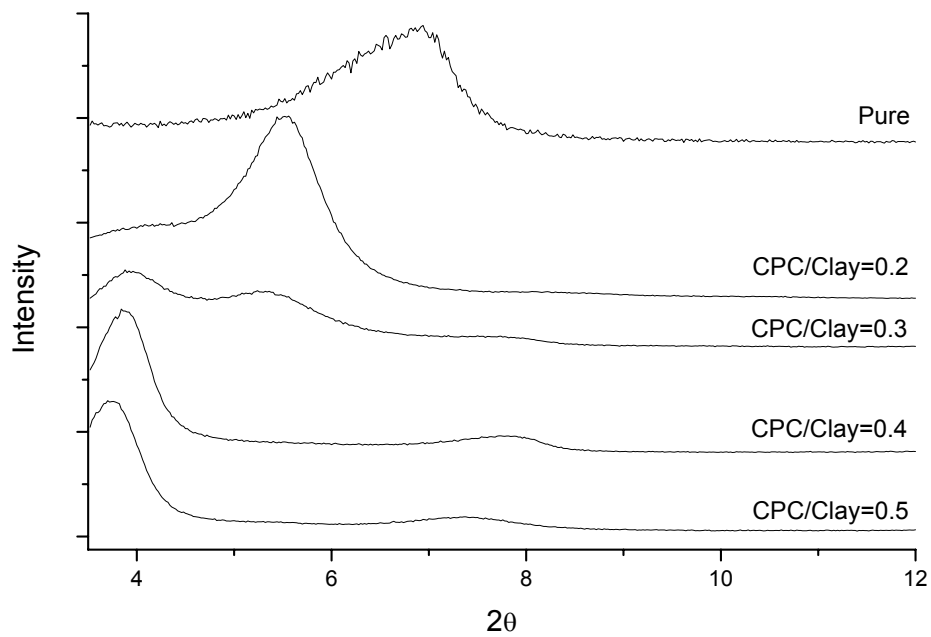


Figure 2-1. XRD spectra of materials featuring the various ratios of the organic ammonium salt.

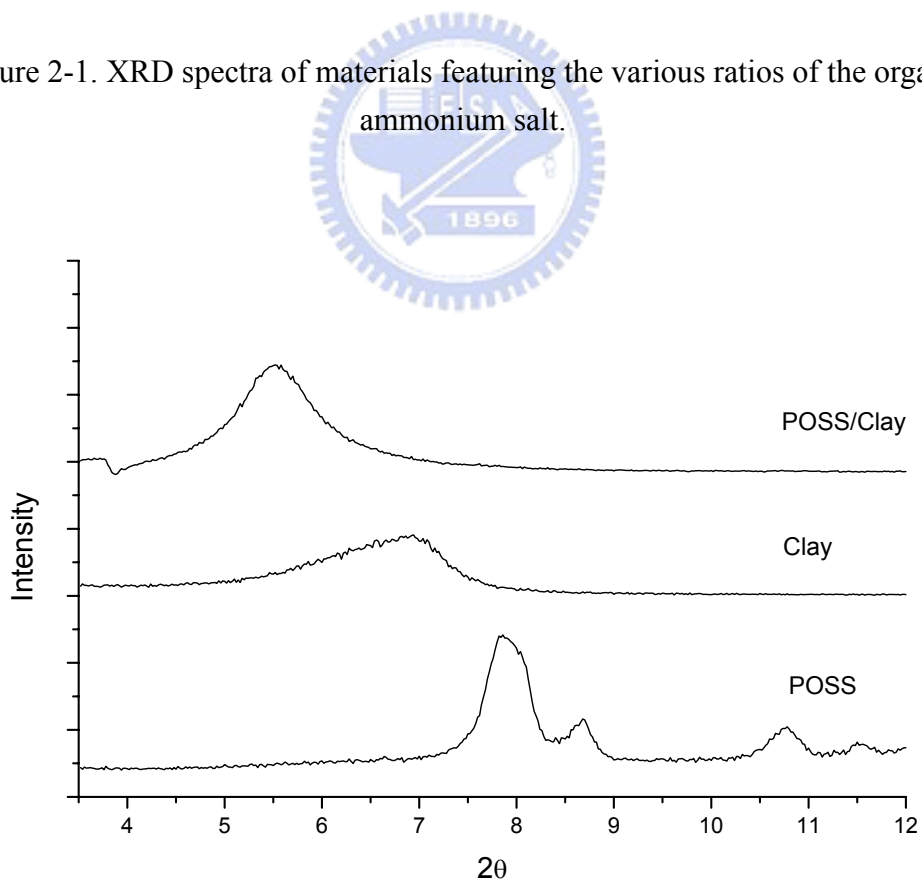


Figure 2-2. X-Ray powder diffraction patterns of pure POSS, pure clay, and intercalated clay.

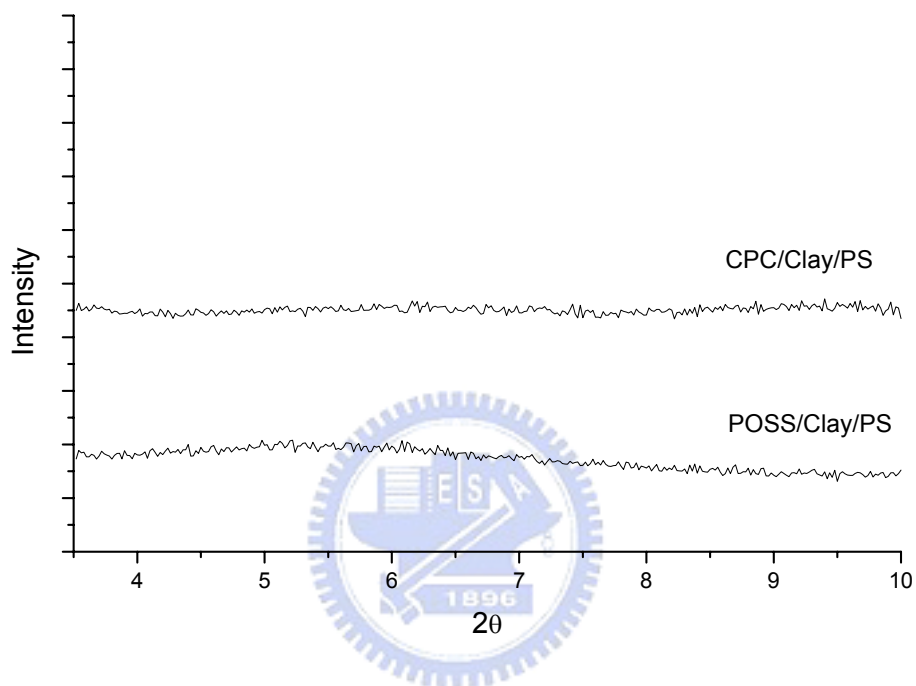


Figure 2-3. XRD spectra of the two surfactant-containing nanocomposites indicating the degree of exfoliation.

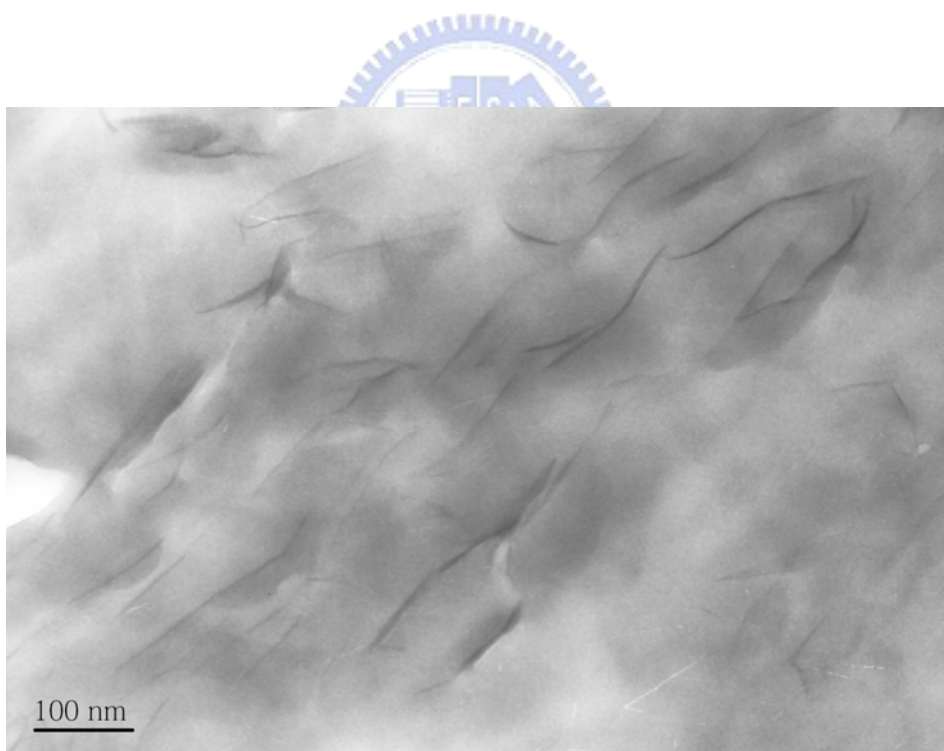
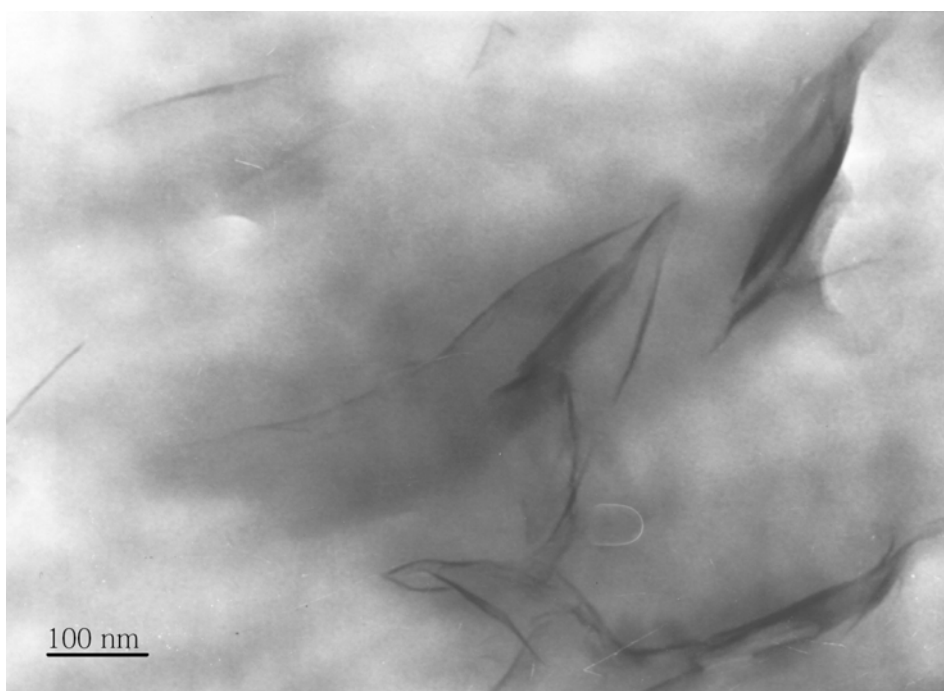


Figure 2-4. TEM micrographs of (a, top) the CPC-treated nanocomposite and (b, bottom) the POSS-treated nanocomposite.

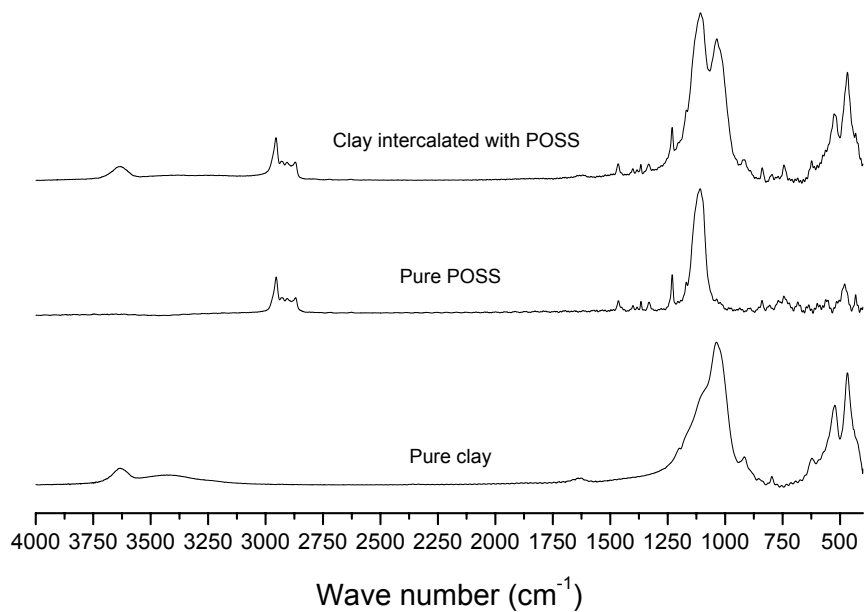


Figure 2-5. IR spectra of pure clay, pure POSS, and intercalated clay.

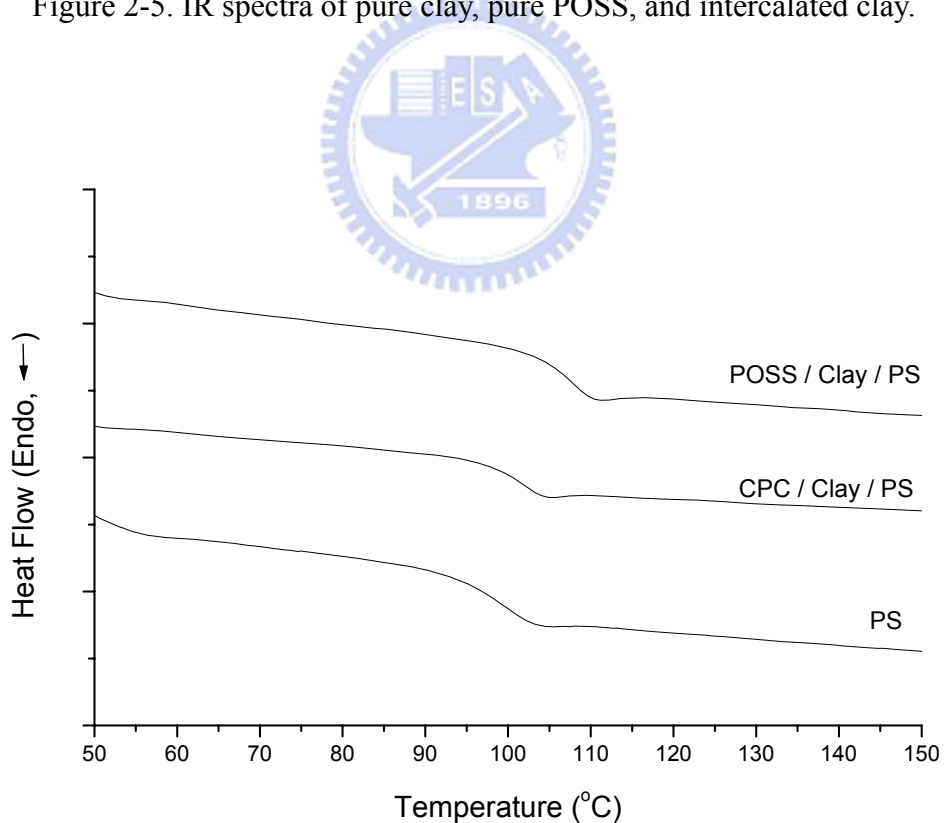


Figure 2-6. DSC curves for determining the glass transition temperature of the nanocomposites.

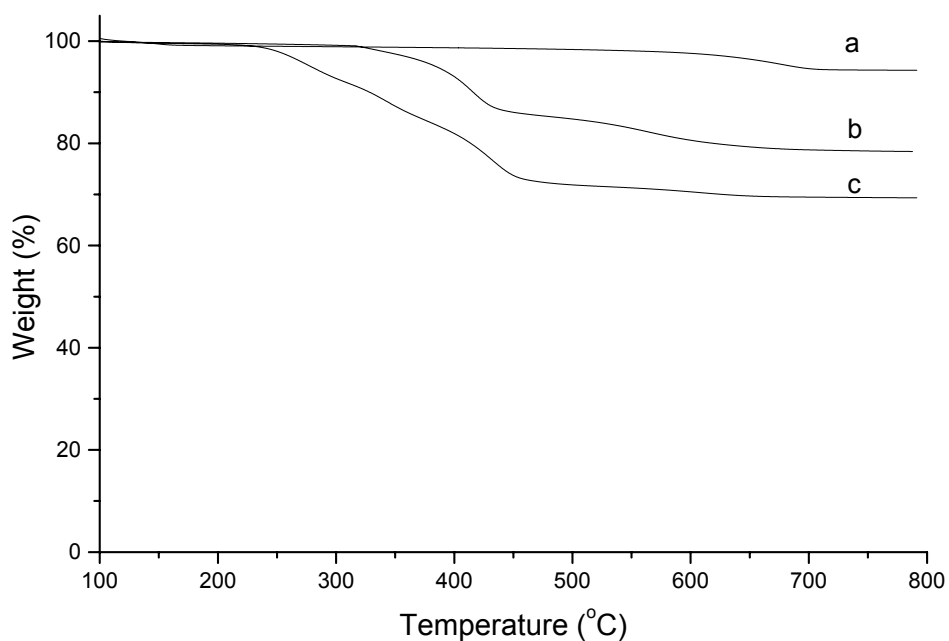


Figure 2-7. TGA traces of (a) pure clay, (b) clay intercalated with POSS, and (c) clay intercalated with CPC.

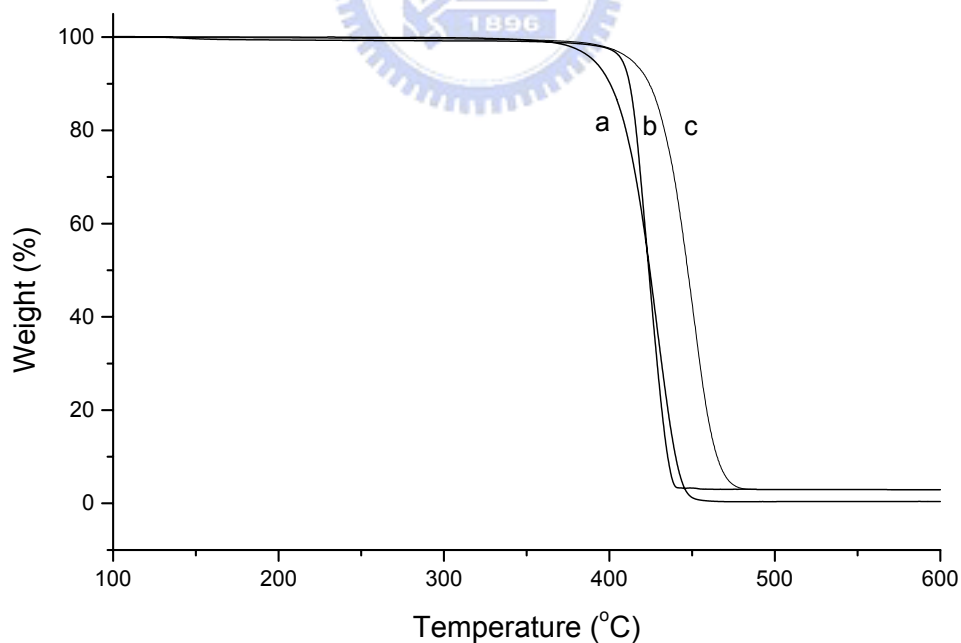


Figure 2-8. TGA curves for the nanocomposites under a nitrogen atmosphere: (a) pure PS, (b) the nanocomposite formed with CPC, and (c) the nanocomposite formed with POSS.

## Chapter 3

### **Thermal Properties of Exfoliated Polystyrene Nanocomposites formed from Rigid Intercalation Agents-Treated Montmorillonite**

#### **Abstract**

We synthesized intercalation agent APB and prepared polystyrene/clay nanocomposites using an emulsion polymerization technique. We used two different intercalation agents to treat clay: the phosphonium salt (APP) and the ammonium salt (APB). Both intercalation agents can intercalate into the layers of the pristine clay dispersed in water. We expected that the intercalation agent APB containing rigid adamantane group also has high thermal stability besides phosphonium group. We used X-ray diffraction (XRD) and transmission electron microscopy (TEM) to characterize the structures of the nanocomposites. The nanocomposites prepared from the APB- and APP-treated clay have exfoliated structures. The molecular weights of polystyrene (PS) obtained from the nanocomposite is slightly lower than the virgin PS formed under similar polymerization conditions. The coefficient of thermal expansion (CTE) was obtained from thermomechanical analysis. A 44~55 % decrease of CTE is observed for APB- and APP-intercalated clay nanocomposites relative to the pure PS. The value of  $T_g$  of the PS component in the nanocomposite is higher than the virgin PS and its thermal decomposition temperature is also higher significantly. It appears that the presence of the clay enhances the thermal stability of polystyrene.

### 3.1 Introduction

Polystyrene (PS) is one of the most mass-productive and commercialized polymers, and copolymers are being produced by various methods such as solution polymerization and emulsion polymerization. Hence, PS/clay nanocomposites may have huge the applicability, so many people have been focusing on the PS/clay nanocomposites with various methods. The clay in nanocomposites has been intercalated by in situ polymerization [1–6] and melts intercalation [7] of PS using organically modified silicate, and recently exfoliated by a few researchers. [8–11] On the polymer-clay nanocomposites, number of papers that show higher thermal stability and a reduced rate of heat release in the cone calorimeter. [12–17] Barrier properties could include both the thermal barrier, which protects the polymer from fire, and the mass transport barrier, which makes it difficult for degradation products to leave the polymer.

The nanocomposite typically comprises the organically modified clay and the mother polymer. Montmorillonite (MMT), which is an aluminosilicate mineral with sodium counterions present between the layers, is the most commonly used clay. The space between these clay layers is referred to as the clay gallery. To make this inorganic clay compatible with organic polymers, the sodium counterions are usually ion-exchanged with an organic ammonium or phosphonium salt to convert the material into hydrophobic ammonium- or phosphonium-treated clays. The nanocomposites may be prepared either by a blending process (either melt blending or solution blending) or by an in situ polymerization process in the presence of the organically modified clay.

In this paper, we describe the preparation of two new organically modified clays and the preparation of nanocomposites of these clays by emulsion polymerization. An

organic ammonium salt (APB) and a phosphonium salt (APP) were shown in scheme 3-1. We synthesized intercalation agent of APB and compared thermal stability with APP. In general, intercalation agent usually is the linear aliphatic chain, but it is not good for thermal stability. [18 – 22] Some literatures report that they used phosphonium cation as intercalation agent to enhance thermal stability. [23, 24] The APB contains the rigid group of adamantane and be expected to enhance thermal stability as good as phosphonium cation. We used the APP not only contains phosphonium cation to keep from inflammation, but also has a double bond to participate in polymerization.

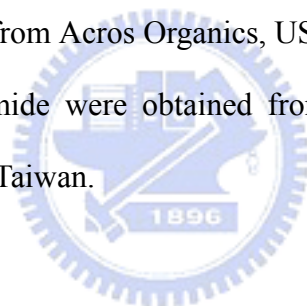
PS/clay nanocomposites were prepared through emulsion polymerization by suspending the organic-treated clay in styrene monomer. We used both X-ray diffraction (XRD) and transmission electron microscopy (TEM) to characterize the clay structure. The thermal properties of these PS/clay nanocomposites were characterized by thermogravimetric analysis (TGA) and differential scanning calorimetry (DSC). Coefficient of thermal expansion was obtained using thermomechanical analyzer (TMA). The molecular weight was obtained by gel permeation chromatography (GPC).



## 3.2 Experimental

### 3.2.1 Materials

Most of chemicals used in this study, including monomeric styrene, chemically pure acetone, methanol, tetrahydrofuran, potassium iodide (KI), and potassium hydroxide (KOH) were acquired from the Aldrich Chemical Co., Inc. The styrene monomer was purified by removing the inhibitor with the aid of an inhibitor-removal column, which was also acquired from Aldrich. Both Sodium dodecyl sulfate (SDS) and hydrochloride acid were obtained from Curtin Matheson Scientific, Inc. Potassium persulfate ( $K_2S_2O_8$ ) and aluminum sulfate [ $Al_2(SO_4)_3$ ] were acquired from Fisher Scientific Co., USA. Allyl-triphenyl-phosphonium chloride (APP), chloroform, and hydrazine were obtained from Acros Organics, USA. Both 4-(1-adamantyl)phenol and n-(4-bromobutyl)phthalimide were obtained from TCI, Inc. Pristine Na-MMT was provided by Telekal Co., Taiwan.



### 3.2.2 Synthesis of Intercalation Agent of 4-(4-adamantyl phenoxy)-1-butanamine (APB)

APB that contains a rigid group of adamantane was prepared according to the pathway shown in Scheme 3-2. First, 4-(4-adamantylphenoxy)butyl phthalimide (1) was prepared by the reaction between 4-(1-adamantyl)phenol (0.8 g, 3.5mmol) and N-(4-bromobutyl)phthalimide (1.19 g, 4.2 mmol) dissolved in 50 ml of acetonitrile. Both potassium hydroxide (KOH, 0.5 g) and potassium iodide (KI, 0.006g) were added with magnetic stirring to obtain a homogeneously system and its contents were heated to 70 °C for 24 h. Removal of the solvent in a rotary evaporator at 50 °C gave a residue that was dissolved in ether and washed several times with distilled water.

Then the ether solution was dried with anhydrous sodium sulfate, followed by evaporation of ether under vacuum to afford yellow product (1).

Second, A mixture of **1** (0.438 g, 1.02 mmol), hydrazine monohydrate (0.3 g, 6 mmol), chloroform/methanol (7:3, 10 ml) was heated overnight at 55~60 °C. After cooling to RT, the solid by-product was filtered off. The filtrate was diluted with CHCl<sub>3</sub> (100 ml), washed with water (2 x 100 ml), dried over MgSO<sub>4</sub>, and concentrated. The residue was dissolved in ether (10 ml) and CH<sub>2</sub>Cl<sub>2</sub> (5 ml) to which was added a solution of methanesulfonic acid (0.1 g, 1.04 mmol) in ether (30 ml). The resulting mixture was concentrated to 10 ml and placed at -20 °C overnight. The solid was collected by filtration to afford pale yellow product (2).

### 3.2.3 Preparation of Modified Clays

The prewashed clay (1 g) and water (50 mL) were placed into a 100-mL two-neck round-bottom flask and stirred continuously for 4 h. The intercalation agents (APP and APB) in water (10 mL) was placed into another flask and then 10 % hydrochloric acid (1 mL) was added and then stirring for 1 h. This intercalation agent solution was then added into the suspended clay and the mixture was stirred overnight. The mixture was filtered, washed several times with deionized water, and then dried overnight in a vacuum oven at room temperature.

### 3.2.4 Preparation of Polystyrene/Clay Nanocomposites

Emulsion polymerization was performed as follows. A suspension of clay (0.3 g) in deionized water (40 ml) was stirred for 4 h at room temperature. A aqueous solution of surfactant (APP or APB; 0.12 g) was added and the mixture was stirred for 4h.

KOH (0.02 g) and SDS (0.4 g) were added into the solution and the temperature was raised to 50 °C. Styrene monomer (10 g) and K<sub>2</sub>S<sub>2</sub>O<sub>8</sub> (0.05g) were added slowly to the flask. Polymerization was performed at 50 °C for 8 h. After cooling, 2.5 % aqueous aluminum sulfate (10 mL) was added to the polymerized emulsion, followed by dilute hydrochloric acid (10 mL), with stirring. Finally, acetone was added to break down the emulsion completely. The polymer was washed several times with methanol and distilled water and then dried overnight in a vacuum oven at 80 °C. Similar procedures were employed to prepare virgin polystyrene.

### 3.2.5 Instrumentations

X-Ray diffraction spectra were collected on an M18XHF-SPA X-ray diffraction instrument (MacScience Co., Japan), using Co K $\alpha$  radiation; Bragg's law ( $\lambda = 2d\sin\theta$ ) was used to compute the spacing. Transmission electron microscopy (TEM) images of the composites were obtained at 100 kV using a Hitachi H-7500 Electron Microscope. The sample was ultramicrotomed at room temperature using a diamond knife on a Leica Ultracut UCT Microtome to give 70 nm-thick sections. The contrast between the layered silicates and the polymer phase is sufficient for imaging and, therefore, no heavy metal staining was required prior to imaging. Thermogravimetric analyses (TGA) were performed on a TA Instruments Thermal Analyzer under a 40 mL/min flow of nitrogen gas at a scan rate of 20 °C /min from 30 to 800 °C. A Du-Pont (DSC-9000) differential scanning calorimeter (DSC) was used to measure the glass transition temperature ( $T_g$ ) of the PS/clay nanocomposites. Molecular weights and molecular weight distributions were characterized by GPC using a Waters 510 HPLC using THF as an eluent at a flow rate of 0.4 mL/min. Coefficient of thermal expansion was obtained using a TA 2940 thermomechanical analyzer (TMA). The force applied

was 0.005 N and it was heated at a rate of 10 °C/min from room temperature to 140 °C.



### 3.3 Results and Discussion

This study focused on comparing nanocomposites prepared using two different intercalation agents modified clays. The intercalation agent of the APB is an ammonium salt that contains a rigid group of the adamantane. The intercalation agent of the APP is a phosphonium salt that features a double bond polymerizing with monomer styrene. Scheme 3-1 displays the structures of these two intercalation agents, APB and APP, used to prepare the modified clays. Conventional surfactants containing the linear aliphatic chain are unstable at high temperatures. [25,26] Thus, we expected that the intercalation agent APB containing rigid adamantane group also has high thermal stability besides phosphonium group.

#### 3.3.1 Preparation of 4-(4-adamantylphenoxy)-1-butanamine (APB)

APB was prepared according to Scheme 3-2. The  $^1\text{H}$  NMR spectrum shown in Figure 3-1 established the structure of the APB. The aromatic protons appeared as doublet at 7.1 and 6.7 ppm. The two triplets at 3.8 and 2.9 ppm are typical corresponding to the protons of  $-\text{O}-\text{CH}_2-$  and  $-\text{CH}_2-\text{N}$  in butylamine group, respectively. The protons of adamantane (**e**) showed a multiplet at 1.8 ppm. The protons of **f** and **h** (Figure 3-1) overlap at 1.6 ppm. The protons of **g** and **i** also overlap at 1.5 ppm.

#### 3.3.2 X-Ray Diffractions.

We used X-ray diffraction (XRD) to characterize the layered structures of the modified clays and polymer/clay nanocomposites, since changes in  $2\theta$  indicate changes in the gallery distance of the clay. Figure 3-2 displays X-ray diffraction

patterns of intercalation agents-treated clays. The basal space indicates the interlayer spacing of the silicate layers which is calculated from the peak position using the Bragg's equation. The pristine clay has this peak at  $6.14^\circ$ , which corresponds to a basal space of  $14.3 \text{ \AA}$ . The insertion of the APP intercalation agent between the galleries of the clay increases the  $d$  spacing from  $14.3$  to  $18.5 \text{ \AA}$ . This result indicates that the intercalation agent of APP becomes successfully intercalated into the galleries of the clay nanoparticles. Furthermore, the APB intercalation agent also is inserted between the galleries of the clay, and the  $d$  spacing is increased from  $14.3 \text{ \AA}$  for the pristine clay to  $20.6 \text{ \AA}$  for the APB-intercalated clay, which indicates that the APB has indeed been intercalated into the galleries of the clay.

The formation of a true polymer/clay nanocomposite requires the insertion of the polymer between the layers of the clay. There are two terms used to describe the general classes of nanocomposites: intercalation and exfoliation (also called delamination). In the case of intercalation, polymer chains are inserted between galleries of the clay, and the spacing between the galleries is increased. On the other hand, in the case of exfoliation, these individual silicate layers are distributed randomly such that they no longer interact with the cations. Characterizing the formation of a nanocomposite requires measurement of the  $d$  spacing by XRD and the use of TEM to determine the actual distribution of platelets within the polymer matrix. The formation of an exfoliated structure usually results in the complete loss of registry between the clay layers so that no peak can be observed by XRD. The most likely occurrence is the formation of a mixture of exfoliated and intercalated structures; this phenomenon requires detection by TEM.

Figure 3-3 presents the XRD results for APP-Clay/PS and APB-Clay/PS nanocomposites. No peak is detected for the nanocomposites from both the APP- and APB-treated clays, which suggests that they have exfoliated structure. It was still

necessary to observe the true structures and distributions of the silica platelets through the use of TEM.

### *3.3.3 TEM Measurements on the Nanocomposites.*

Figure 3-4 and 3-5 show TEM images at two magnifications of nanocomposites prepared from the APP- and APB-modified clays. These images indicate the dispersion of the clay within the polymer. In Figure 3-4, the layers of platelets observed for these APP-modified nanocomposites are, in fact, an exfoliated structure. Figure 3-5 shows an image of the APB-modified nanocomposite: each clay layers is isolated and evenly distributed within the PS matrix, which implies that a full exfoliation has occurred; this conclusion is consistent with the XRD data.



### *3.3.4 Analyzing Glass Transition Temperatures.*

Figure 3-6 displays the DSC thermograms for the virgin PS and organic-modified clay nanocomposites. Table 3-1 summarizes the results of DSC measurements. The glass transition temperature ( $T_g$ ) of the virgin PS is 100 °C while the values of  $T_g$  for the APP-clay and APB-clay nanocomposites are 107 and 109 °C, respectively. The presence of the clay layer tends to retard movement of the PS chain and, thus, it results in a higher value of  $T_g$ .

### *3.3.5 Molecular Weights of the Nanocomposites.*

Table 3-2 lists the molecular weights of PS in nanocomposites under similar emulsion polymerization conditions. The virgin PS has higher average molecular weights ( $M_n$  and  $M_w$ ) and a lower polydispersity index (PDI) than the two

nanocomposites. It has been reported [27] that clay may act as additional micelles that are responsible for the observed lower molecular weight.

### 3.3.6 Coefficient of Thermal Expansion.

The coefficient of thermal expansion (CTE) was obtained from thermomechanical analysis. Figure 3-7 showed CTE values of pure PS and nanocomposites. A 44~55 % decrease of CTE is observed for APB- and APP-intercalated clay nanocomposites relative to the pure PS. The results indicate that polymer adding silica layer can reduce CTE and provide good dimensional stability for the nanocomposites.

### 3.3.7 Characterization by TGA.

Figure 3-8 shows TGA traces of pure APP and APB under nitrogen atmosphere. The pure APB decomposes at a higher temperature of 308 °C while pure APP decomposes at 288 °C. The pure APB is relatively more thermally stable than pure APP. In other words, intercalation agent containing rigid adamantane is also a thermally stable group besides phosphonium group.

Figure 3-9 presents TGA thermograms of nanocomposites and pure polystyrene. Both of the intercalation agent-treated clay nanocomposites display higher decomposition temperatures than the virgin PS. The onset of thermal decomposition for the nanocomposites is shifted to higher temperatures. Table 1 summarizes the TGA results for the nanocomposites. The nanocomposite prepared from APP-intercalated clay displays a 24 °C increase in the decomposition temperature for 5% weight loss relative to virgin PS; the APB-intercalated clay nanocomposite is



5 °C higher. In the case of the APP-intercalated clay nanocomposite, the temperature of 50% weight loss is actually the same as that for APB-intercalated clay nanocomposite. Both nanocomposites containing silica layer will obviously have a larger char yield. So both adamantane and phosphonium group all can enhance thermal stability of the nanocomposites.



### 3.4 Conclusions.

In this study, we successfully synthesized intercalation agent of APB and prepared PS/clay nanocomposites with a fully exfoliated structure. The intercalation of APB and APP into clay nanoparticles was confirmed by XRD. Results of XRD indicated that the  $d$  spacing increased from 14.3 Å for pristine clay to 20.6 Å for the APB-intercalated clay. TGA of the nanocomposites suggests that the onset of thermal degradation occurs at a higher temperature for the nanocomposite than for the virgin PS. It appears that the presence of the clay enhances the thermal stability of polystyrene. Results of TGA indicated that intercalation agent containing rigid adamantane also has high thermal stability besides phosphonium group. Intercalation agents-treated clays give PS having lower molecular weights ( $M_n$  and  $M_w$ ) and a higher MW distribution (polydispersity index, PDI) relative to the virgin PS formed under similar emulsion polymerization conditions. The glass transition temperatures of the nanocomposites incorporating APB or APP are higher than that of the virgin PS. The polymer adding silica layer can reduce CTE and provide good dimensional stability for the nanocomposites.

## References

- [1] Kojima Y, Usuki A, Kawasumi M, Okada A, Kurauchi T, Kamigaito O. *J Polym Sci Part A: Polym Chem* 1993; 31: 983.
- [2] Usuki A, Koiwai A, Kojima Y, Kawasumi M, Okada A, Kurauchi T, Kamigaito O. *J Appl Polym Sci* 1995; 55: 119.
- [3] Noh MW, Lee DC. *Polym Bull* 1999; 42: 619.
- [4] Doh JG, Cho I. *Polym Bull* 1998; 41: 511.
- [5] Okamoto M, Morita S, Taguchi H, Kim YH, Kotaka T, Tateyama H. *Polymer* 2000; 41: 3887.
- [6] Zeng C, Lee LJ. *Macromolecules* 2001; 34: 4098.
- [7] Lim YT, Park OO. *Macromol Rapid Commun* 2000; 21: 231.
- [8] Fu X, Qutubuddin S. *Mater Lett* 2000; 42: 12.
- [9] Fu X, Qutubuddin S. *Polymer* 2001; 42: 807.
- [10] Hoffmann B, Dietrich C, Thomann R, Friedrich C, Mulhaupt R. *Macromol Rapid Commun* 2000; 21: 57.
- [11] Weimer MW, Chen H, Giannelis EP, Sogah DY. *J Am Chem Soc* 1999; 121: 1615.
- [12] Gilman JW, Kashiwagi T, Giannelis EP, Manias E, Lomakin S, Lichtenham JD, Jones P. In *Fire Retardancy of Polymers: The Use of Intumescence*; Le Bras M, Camino G, Bourbigot S, Delobel R. Eds; Royal Society of Chemistry: London 1998; pp 201-221
- [13] Gilman JW, Kashiwagi T, Nyden M, Brown JET, Jackson CL, Lomakin S, Giannelis EP, Manias E. In *Chemistry and Technology of Polymer Additives*; Al-Malaika S, Golovoy A, Wilkie CA, Eds; Blackwell Scientific 1999; PP 249-265.

- [14] Zhu J, Wilkie CA. *Polym Int* 2000; 49: 1158.
- [15] Zhu J, Morgan AB, Lamelas FJ, Wilkie CA. *Chem Mater* in press.
- [16] Doh JD, Cho I. *Polym Bull* 1998; 41: 511.
- [17] Gilman JW, Kashiagi T. In *Polymer-Clay Nanocomposites*; Pinnavaia TJ, Beall GW, Eds; John Wiley & Sons: New York 2000; pp 193-206.
- [18] Tseng CR, Wu JY, Lee HY, Chang FC. *Polymer* 2001; 42: 10063.
- [19] Tseng CR, Lee HY, Chang FC. *J. Polym Sci Part B: Polym Phys* 2001; 39: 2097.
- [20] Wu HD, Tseng CR, Chang FC. *Macromolecules* 2001; 34: 2992.
- [21] Tseng CR, Wu JY, Lee HY, Chang FC. *J Appl Polym Sci* 2002; 85: 1370.
- [22] Tseng CR, Wu HD, Wu JY, Chang FC. *J Appl Polym Sci* 2002; 86: 2492.
- [23] Jin Z, Alexander BM, Frank JL, Charles AW. *Chem Mater* 2001; 13: 3774.
- [24] Jin Z, Fawn MU, Alexander BM, Charles AW. *Chem Mater* 2001; 13: 4649.
- [25] Yei DR, Kuo SW, Su YC, Chang FC. *Polymer* 2004; 45: 2633.
- [26] Yei DR, Kuo SW, Fu HK, Chang FC. *Polymer* 2005; 46: 741.
- [27] Dongyan W, Jin Z, Qiang Y, Charles AW. *Chem Mater* 2002; 14: 3837.

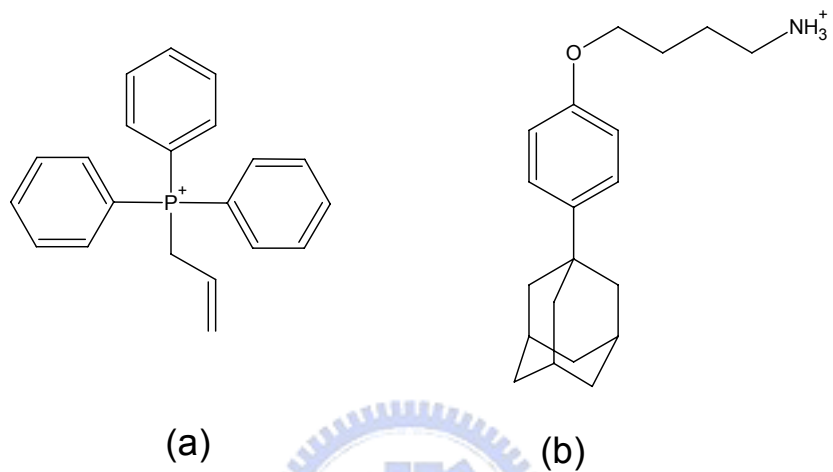
Table 3-1. Results of TGA and DSC for Polystyrene Nanocomposites.

Sample	Clay wt %	$T_g$ (°C)	Weight loss temperature (°C)		Char yield (%)
			5 wt %	50 wt %	
PS	0	100	390	424	0
APB/Clay/PS	3	109	395	452	3.2
APP/Clay/PS	3	107	414	453	3.2

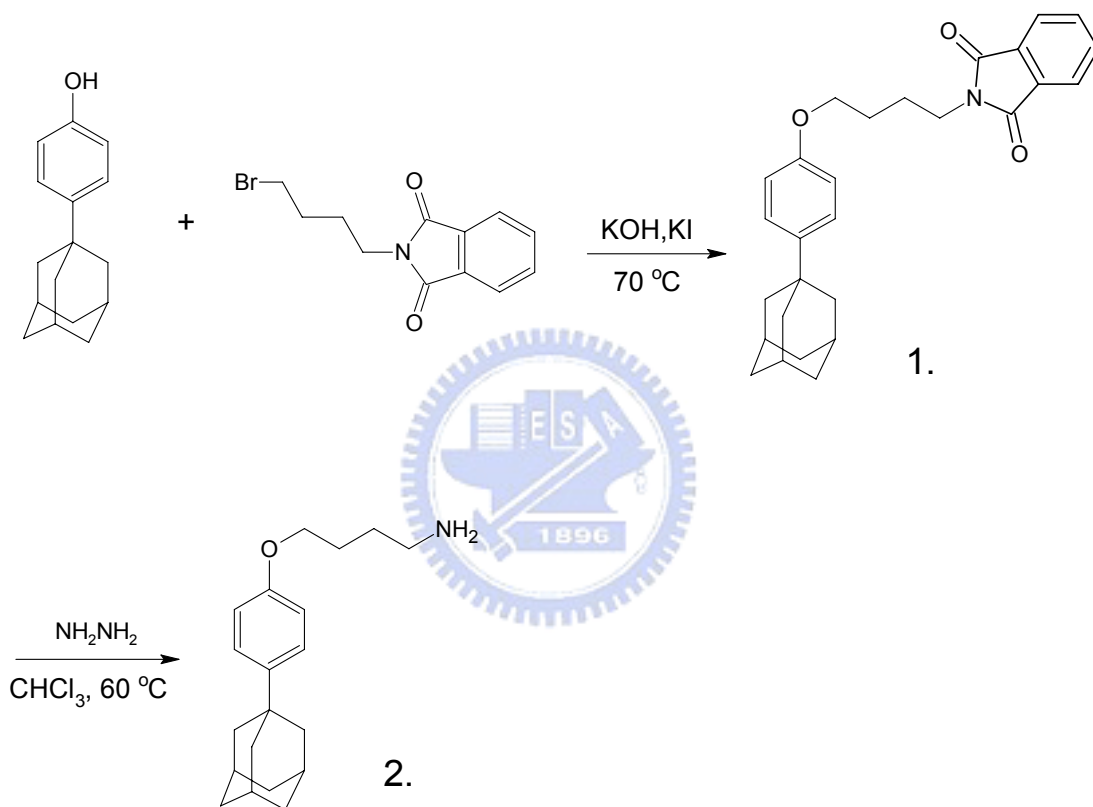
Table 3-2. Molecular Weights of Polystyrene Nanocomposites.

Sample	$M_n$ ( $\times 10^4$ ) <sup>a</sup>	$M_w$ ( $\times 10^4$ ) <sup>b</sup>	PDI ( $M_w/M_n$ ) <sup>c</sup>
PS	44.1	53.4	1.21
APB/Clay/PS	39.6	51.9	1.31
APP/Clay/PS	41.1	51.0	1.24

<sup>a</sup>Number-average molecular weights ( $M_n$ ) and <sup>b</sup>weight-average molecular weights ( $M_w$ ) were determined by GPC. <sup>c</sup>Polydispersity index,  $M_w/M_n$ .



Scheme 3-1. Structures of Intercalation Agent (a) APP (b) APB.



Scheme 3-2. Preparation of Intercalation Agent (APB).

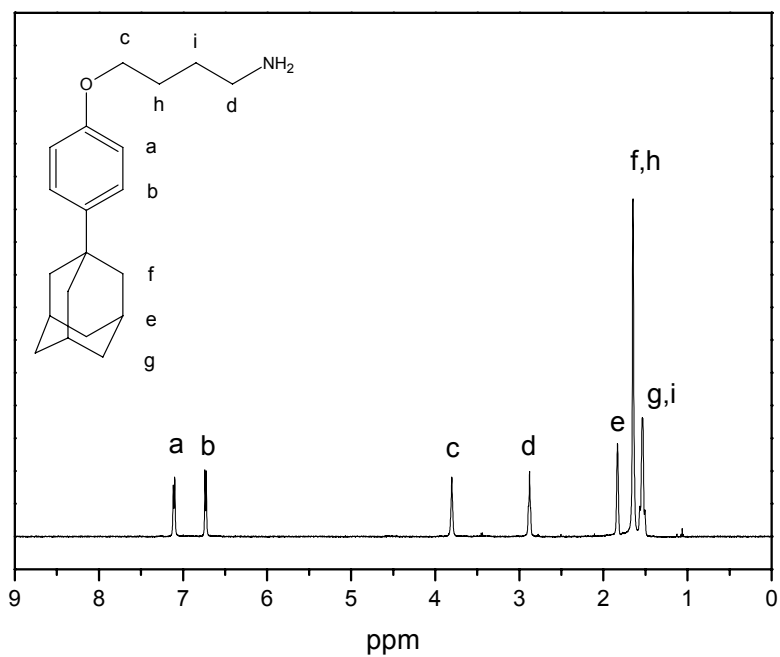


Figure 3-1. Proton NMR spectra of intercalation agent (APB)

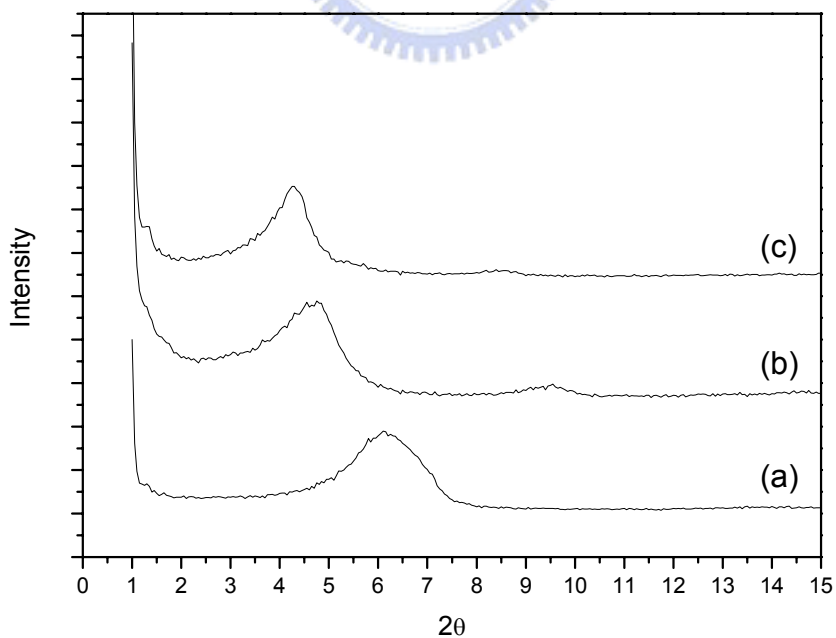


Figure 3-2. X-ray diffraction patterns of (a) pure clay, (b) the APP-intercalated clay, (c) the APB-intercalated clay.



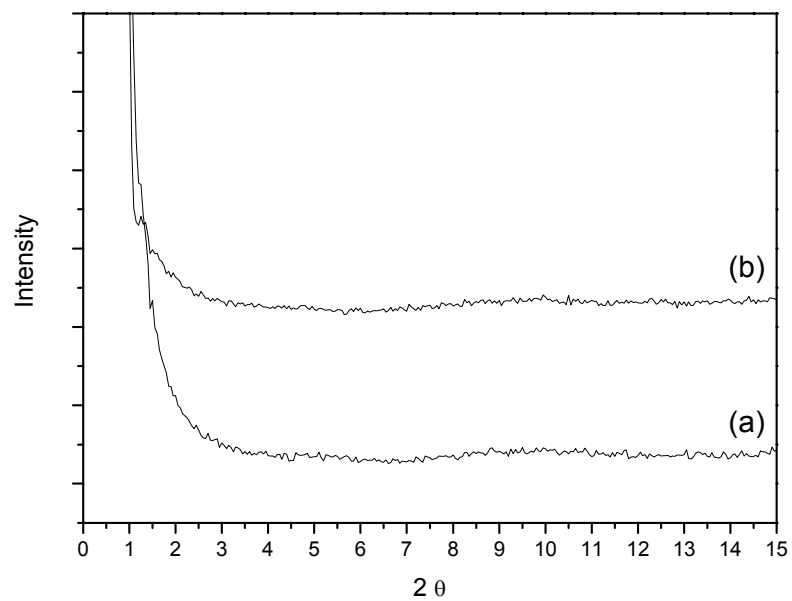
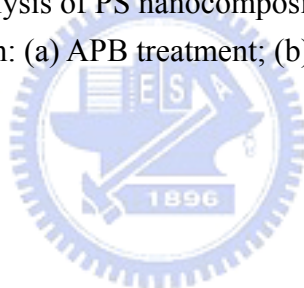


Figure 3-3. WAXD analysis of PS nanocomposites prepared by emulsion polymerization: (a) APB treatment; (b) APP treatment.



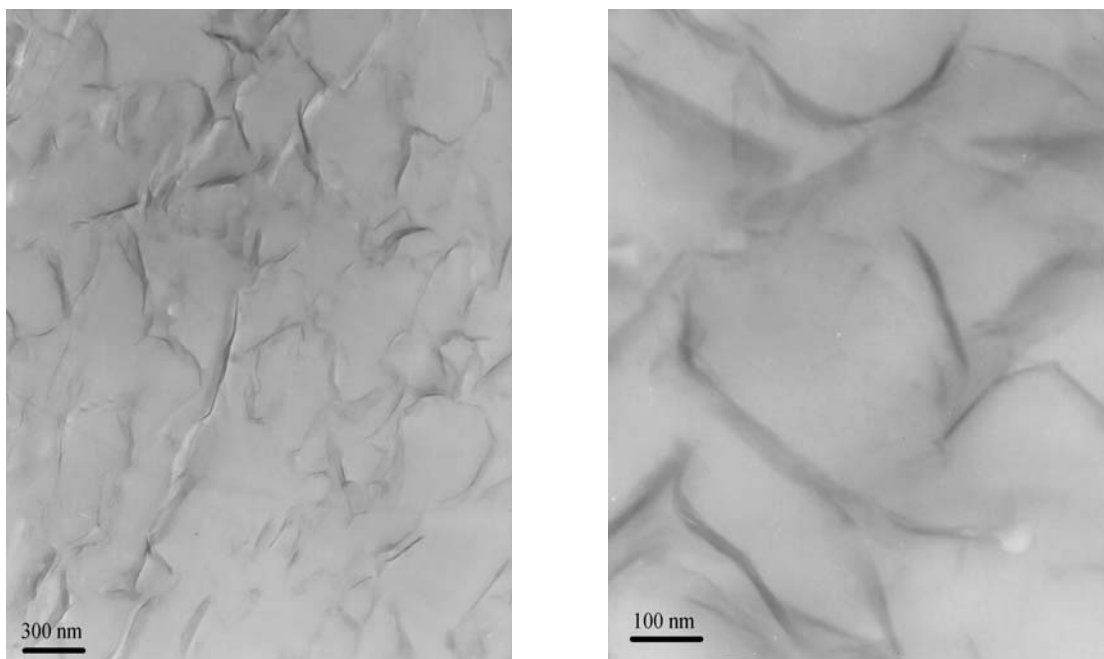


Figure 3-4. TEM images of the APP-treated nanocomposite at low (left) and high (right) magnifications.

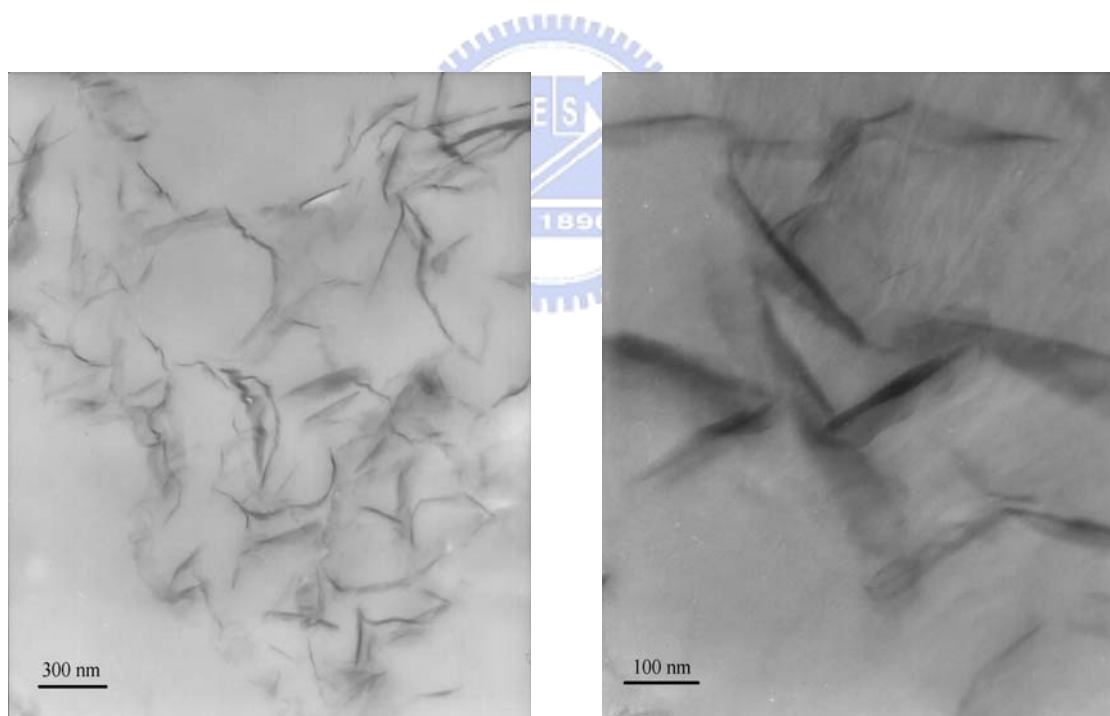


Figure 3-5. TEM images of APB-treated nanocomposite at low (left) and high (right) magnifications.

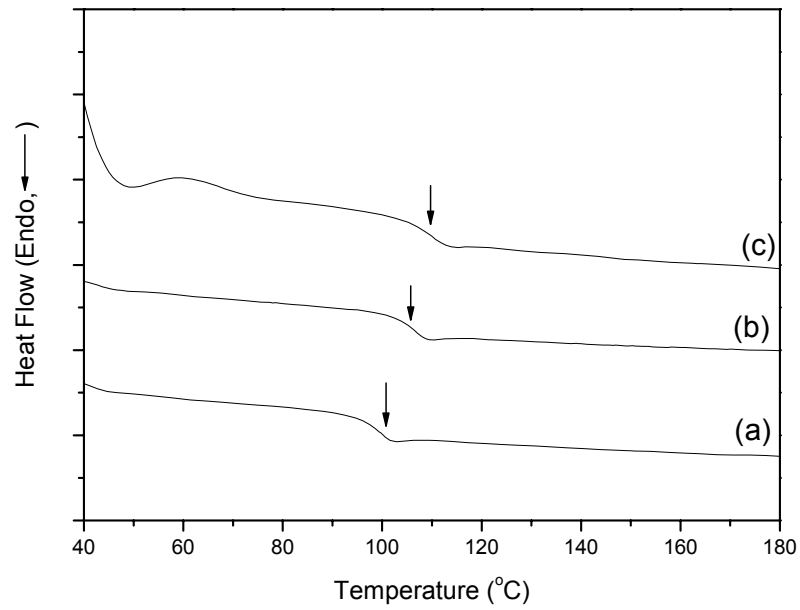


Figure 3-6. DSC curves for determining the glass transition temperature of (a) PS, (b) the nanocomposite formed using APP, and (c) the nanocomposite formed using APB.

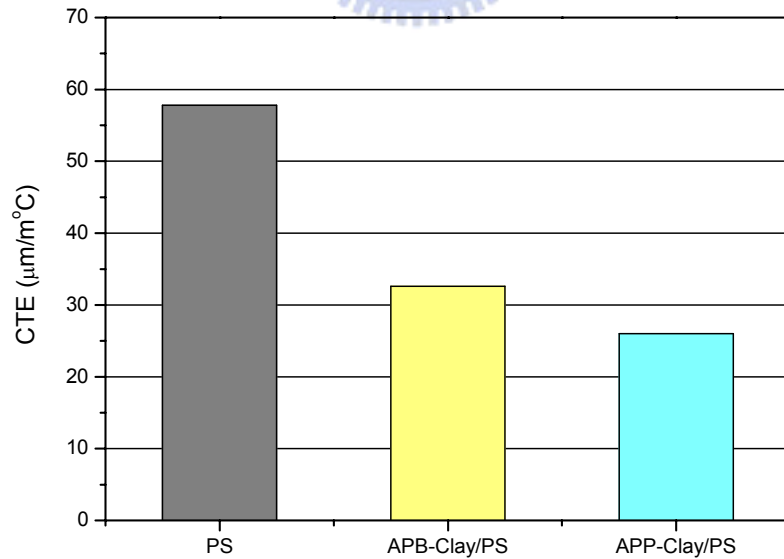


Figure 3-7. Coefficient of thermal expansion of nanocomposites.

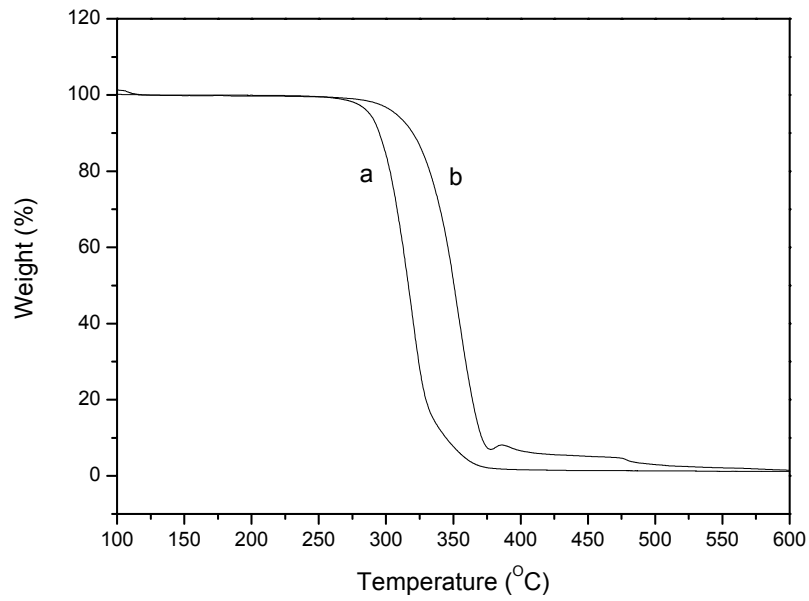


Figure 3-8. TGA curves of (a) pure APP (b) pure APB.

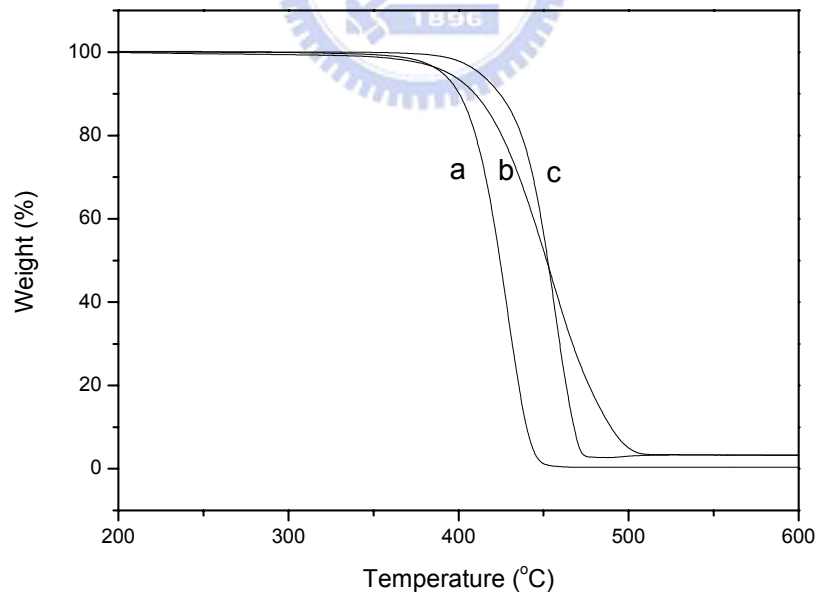


Figure 3-9. TGA curves of the nanocomposites recorded under nitrogen atmospheres: (a) pure PS, (b) the nanocomposite formed using APB, and (c) the nanocomposite formed using APP.

## Chapter 4

### Enhanced Thermal Properties of PS Nanocomposites formed from Montmorillonite Treated with a Surfactant/Cyclodextrin Inclusion Complex

#### Abstract

We have prepared polystyrene/clay nanocomposites using an emulsion polymerization technique. The nanocomposites were exfoliated at 3wt% content of pristine clay relative to the amount of polystyrene (PS). We employed two surfactants for the montmorillonite: cetylpyridinium chloride (CPC) and the CPC/ $\alpha$ -CD inclusion complex. Prior to polymerization, each surfactant intercalates into the layers of the pristine clay dispersed in water. The inclusion complex was characterized by X-ray diffraction,  $^{13}\text{C}$  CP/MAS NMR spectra, and  $^1\text{H}$  NMR spectroscopy, and TGA. X-Ray powder patterns of the CPC/ $\alpha$ -CD complex indicate that the  $\alpha$ -CDs units form channels. The  $^{13}\text{C}$  CP/MAS NMR spectrum of the complex suggests that a CPC chain is included in the channel formed by the  $\alpha$ -CDs. The  $^1\text{H}$  NMR spectra of the complexes indicate that the stoichiometry of the complexes is 1:2 (i.e., one CPC molecule and two  $\alpha$ -CD units). The TGA reveals that the inclusion complex has higher thermal stability relative to the virgin CPC. We employed both X-ray diffraction (XRD) and transmission electron microscopy (TEM) to characterize the structures of the nanocomposites. The value of  $T_g$  of the PS component in the nanocomposite is 6 °C higher than that of the virgin PS and its thermal decomposition temperature is 33 °C higher. The CPC/ $\alpha$ -CD-treated clay is more effective than is virgin CPC-treated clay at enhancing the thermal stability of polystyrene.

## 4.1 Introduction

A number of extensive investigations into the intercalation of organic alkylammonium cations into montmorillonite clay have been reported. [1-3] Most of these intercalating agents have been low-molecular-weight alkylammonium salts, amino acids, and diamine salts. [4-6] Typically, intercalation results in a widening of the clay basal spacing to within the range 19-40 Å, which correlates linearly with the molecular size of the intercalating agent. [3,4,7] These intercalated smectic clays may be exfoliated by using a polymer to form nanocomposites. [8] Nanocomposites offer the prospect of vastly improved properties relative to their mother polymers. There have been reports that suggest that nanoclay-filled polymeric systems display significant improvements in their tensile and thermal properties, [9-17] heat distortion temperatures, [9-14] resistance to flammability, [20] reduced permeability to small molecules, [13,18,19] and reduced solvent uptake. [21] A common observation emerging from these studies is that the magnitude of improvement depends strongly on the state of dispersion of the clay layers in the polymer matrix.

To date, cyclodextrins (CDs) have never been reported as surfactants for intercalating in clay. CDs comprise a series of  $\alpha$ -1,4-linked cyclic oligosaccharides consisting of six ( $\alpha$ -CD), seven ( $\beta$ -CD), eight ( $\gamma$ -CD), or more glucose units; their shapes resemble hollow truncated cones, The cavities of CDs are hydrophobic because they contain no hydroxyl groups; thus, CDs have the ability to include hydrophobic molecules within their cavities. Since the discovery of CDs, a large number of their inclusion complexes with various low-molecular-weight compounds have been prepared and characterized. [22] In this study, we have examined whether including a surfactant within CD channels improves its thermal stability.

In this paper, we describe the preparation of two types of nanocomposites

formed from clays treated with either cetylpyridinium chloride (CPC) or the CPC/ $\alpha$ -CD inclusion complex. The PS/clay nanocomposite formed using the CPC-treated clay exhibited no significant improvements in its thermal properties. [23–27] We found that CPC, a linear aliphatic surfactant, is able to form a crystalline complex with cyclodextrin. Including CPC within CD channels improves the thermal stability of the virgin CPC.

We prepared PS/clay nanocomposites through emulsion polymerization by suspending the surfactant-treated clay in styrene monomer. The formation of a complex between  $\alpha$ -CD and CPC was studied quantitatively; we confirmed the stoichiometry of the inclusion complex from the  $^1\text{H}$  NMR spectrum. X-Ray powder patterns of the CPC/ $\alpha$ -CD complex indicated that the guest surfactant chain resides within the channels provided by the orderly stacked  $\alpha$ -cyclodextrin molecules. We used solid-state  $^{13}\text{C}$  NMR spectroscopy to measure the structure of the CPC chain within its the inclusion complex with  $\alpha$ -CD, and both X-ray diffraction (XRD) and transmission electron microscopy (TEM) to characterize the structure of the clay. The properties of these PS/clay nanocomposites were characterized by thermogravimetric analysis (TGA) and differential scanning calorimetry (DSC).

## 4.2 Experimental

### 4.2.1 Materials

Most of chemicals used in this study, including monomeric styrene, acetone, methanol, tetrahydrofuran, and potassium hydroxide (KOH) were acquired from the Aldrich Chemical Co., Inc. The styrene monomer was purified by removing the inhibitor with the aid of an inhibitor-removal column, which was also acquired from Aldrich. Sodium dodecyl sulfate (SDS) and hydrochloric acid were both obtained from Curtin Matheson Scientific, Inc. Potassium persulfate ( $K_2S_2O_8$ ) and aluminum sulfate [ $Al_2(SO_4)_3$ ] were acquired from Fisher Scientific Co. (USA). Cetylpyridinium chloride (CPC) was obtained from Acros Organics, (USA).  $\alpha$ -Cyclodextrin was obtained from Tokyo Kasei Kogyo co. (Japan); pristine Na-MMT was provided by Telekal Co. (Taiwan).



### 4.2.2 Preparation of Inclusion Complex.

CPC (5.59 mmol) in water (80 mL) was mixed at room temperature with a saturated solution of  $\alpha$ -CD (16.8 mmol) in water (80 mL). The mixture was stirred at 70 °C for 8 h and then it was left to stand at room temperature overnight. The mixture became turbid and the complex was obtained as a white crystalline precipitate. The precipitated product was collected by centrifugation and dried in a vacuum oven at 70 °C. The complex was then washed several times with water to remove any uncomplexed  $\alpha$ -CD and CPC. Finally, the powder was dried in a vacuum oven at 60 °C for 24 h.



#### *4.2.3 Preparation of Surfactant-Modified Clays.*

A suspension of pre-washed sodium montmorillonite (Na-MMT, 5 g) in distilled water (250 mL) was stirred overnight in a 500-mL, two-neck, round-bottom flask. The surfactant (CPC or CPC/ $\alpha$ -CD inclusion complex; 2 g), which was dissolved in 10 mL of 1N HCl solution, was then added dropwise at room temperature to the stirred aqueous solution. After stirring the mixture for 3 h, the white precipitate was filtered, washed with water until no chloride ion could be detected by an aqueous AgNO<sub>3</sub> solution, and then dried overnight in a vacuum oven at room temperature.

#### *4.2.4 Preparation of Polystyrene/Clay Nanocomposites.*

Emulsion polymerization was performed as follows. A suspension of clay (0.3 g) in deionized water (40 mL) was stirred for 4 h at room temperature. A solution of surfactant (CPC or CPC/ $\alpha$ -CD inclusion complex; 0.12 g) was added and the mixture was stirred for 4 h. KOH (0.02 g) and SDS (0.4 g) were added into the solution and the temperature was raised to 50 °C. Styrene monomer (10 g) and K<sub>2</sub>S<sub>2</sub>O<sub>8</sub> (0.05 g) were added slowly to the flask. Polymerization was performed at 50 °C for 8 h. After cooling, 2.5% aqueous aluminum sulfate (10 mL) was added to the polymerized emulsion, followed by dilute hydrochloric acid (10 mL), with stirring. Finally, acetone was added to break the emulsion down completely. The polymer was washed several times with methanol and distilled water and then dried overnight in a vacuum oven at 80 °C. A similar procedure was employed to prepare the virgin polystyrene.

#### 4.2.5 Instrumentations

X-Ray diffraction spectra were collected on an M18XHF-SPA X-ray diffraction instrument (MacScience Co., Japan), using Co K $\alpha$  radiation. Bragg's law ( $\lambda = 2d\sin\theta$ ) was used to compute the spacing. Transmission electron microscopy (TEM) images of the composites were obtained at 100 kV using a Hitachi H-7500 Electron Microscope. The sample was ultramicrotomed at room temperature using a diamond knife on a Leica Ultracut UCT Microtome to give 70-nm-thick sections. The contrast between the layered silicates and the polymer phase was sufficient for imaging and, therefore, no heavy metal staining was required prior to imaging.  $^1\text{H}$  NMR spectra of the complex were recorded at 500 MHz on a Varian 500 NMR Spectrometer (USA). Chemical shifts of the complex were referenced to the signal for DMSO at  $\delta=2.50$  ppm.  $^{13}\text{C}$  CP/MAS NMR spectra were measured on a Bruker DSX400WB NMR spectrometer (Germany) using a sample spinning rate of 5.4 kHz at room temperature. The spectra were acquired using a 3.9- $\mu\text{s}$  proton 90° pulse, a 3-ms contact time, and a 3-s repetition time. Thermogravimetric analyses (TGA) were performed on a TA Instruments Thermal Analyzer under a flow of nitrogen gas (40 mL/min) at a scan rate of 20 °C/min from 30 to 800 °C. A Du-Pont (DSC-9000) differential scanning calorimeter (DSC) was used to measure the glass transition temperature ( $T_g$ ) of the PS/clay nanocomposites. The sample was preheated at a scan rate of 20 °C/min from 30 to 200 °C and then cooled quickly to 30 °C from the melt of the first scan. The second scan rate was 20 °C/min from 30 to 200 °C and the value of  $T_g$  was taken as the midpoint of the heat capacity transition.

### 4.3 Results and Discussion

In this study, we focused on comparing nanocomposites prepared using two surfactant-modified clays. The CPC surfactant is an ammonium salt containing a long aliphatic chain that can be include within the cavity of  $\alpha$ -CD to form an inclusion complex. Two surfactant, CPC and CPC/ $\alpha$ -CD inclusion complex, are used to prepare the modified clays. Conventional surfactants, such as CPC, are thermally unstable at high temperatures. Thus, we expected that nanocomposites prepared from the CPC/ $\alpha$ -CD surfactant would possess greater thermal stabilities relative to those formed using the conventional CPC surfactant alone.

#### 4.3.1 X-Ray Diffraction.

We employed X-ray diffraction (XRD) to characterize the layered structures of the modified clays and polymer/clay nanocomposites. Changes in the value of  $2\theta$  reflect changes in the gallery distance of the clay. In addition, X-ray diffraction can also be used to detect whether the CPC units are included within the cavities of  $\alpha$ -CD units. Figure 4-1 displays the X-ray diffraction patterns of pure  $\alpha$ -CD, the inclusion complex, and its intercalated clay. The most prominent peak for the CPC/ $\alpha$ -CD inclusion complex appears at  $19.7^\circ$  ( $2\theta$ ), which indicates that the inclusion complex is indeed formed from CPC units included within the CD channels. [28] We also observe that the CPC/ $\alpha$ -CD inclusion complex pattern is similar to that of the PEO/ $\alpha$ -CD inclusion complex. [29] This finding provides strong evidence that the CPC/ $\alpha$ -CD inclusion complex had a channel-type structure. Furthermore, the XRD pattern of the clay intercalated by the inclusion complex indicates a diffraction peak at  $19.7^\circ$ , which implies that the inclusion complex remains present in the gallery of the clay. Scheme 4-1 displays clay intercalated by CPC/ $\alpha$ -CD inclusion complexes. We

calculated the interlamellar distance indicated in this figure by using the following expression:  $\Delta d = d \text{ spacing} - \text{thickness of one platelet (ca. } 10 \text{ \AA)}$ . In the case of the clay intercalated with the inclusion complex, the distance between two adjacent clay plates is 42.2 Å which is a value close to that expected for two layers of CPC.

Figure 4-2 displays the XRD results of the surfactant-intercalated clay. The pristine clay exhibits a peak at  $6.14^\circ$ , which corresponds to a basal space of 1.43 nm. The insertion of the CPC surfactant between the galleries of the clay increases the  $d$  spacing from 1.43 to 2.27 nm. This result indicates that the CPC surfactant is intercalated successfully into the galleries of the clay nanoparticles. Furthermore, the  $d$  spacing of the clay intercalated by the inclusion complex is increased to 5.12 nm; i.e., the  $d$  spacing caused by the inclusion complex is substantially higher than that caused by CPC alone. We believe that this finding can be explained by considering that the linear aliphatic chain within the CPC/ $\alpha$ -CD can not bend within the galleries of the clay and, therefore, the  $d$  spacing of clay intercalated by the CPC/ $\alpha$ -CD inclusion complex is significantly higher than that formed using pure CPC.

Figure 4-3 presents the XRD patterns for polymer/clay nanocomposites. We detected no peak for the nanocomposites prepared from the CPC- and CPC/ $\alpha$ -CD-treated clays, which implies that they all possess exfoliated structures. Because there is a limit to the angle of detection when using XRD, it is impossible to detect diffraction angle below  $1^\circ$ . Thus, it was still necessary to observe the true structures and distributions of the silica platelets through the use of TEM.

#### 4.3.2 TEM Characterization.

Figures 4-4 and 4-5 display TEM images at two magnifications of the nanocomposites prepared from the CPC- and CPC/ $\alpha$ -CD-treated clays. These images

indicate the dispersion of the clay layers within the polymer. In Figure 4-4, we observe that the clay platelets of the CPC-treated nanocomposite are mainly exfoliated, but in certain regions they are more concentrated and intercalated. Figure 4-5 displays an image of the CPC/ $\alpha$ -CD-treated nanocomposite: essentially all of the clay layers are isolated and evenly distributed within the PS matrix, which implies that a full exfoliation has occurred; this conclusion is consistent with the finding of the XRD data.

#### 4.3.3 Stoichiometry of the complex.

We isolated the complex by centrifugation, washed it with water to remove and uncomplexed CD and CPC, and dried the sample in a vacuum oven at 70°C. We used  $^1\text{H}$  NMR spectroscopy to investigate the stoichiometry of this complex. Figure 4-6 present the  $^1\text{H}$  NMR spectrum of the inclusion complex formed between  $\alpha$ -CD and CPC in DMSO. By comparing the value of the integrals of selected peaks of  $\alpha$ -CD (C1H) and CPC (the ethyl group, a), we obtained an  $\alpha$ -CD/CPC ratio of 2. The estimated length of the alkyl tail of the CPC unit is roughly equal to the length of two  $\alpha$ -CD molecules, so the theoretically predicted result agrees well with the experimental result.

#### 4.3.4 Solid state $^{13}\text{C}$ NMR spectroscopic analysis.

Solid state  $^{13}\text{C}$  NMR spectroscopy [e.g.,  $^{13}\text{C}$  cross-polarization magic angle spinning (CP/MAS) NMR spectroscopy] provided additional information concerning the structure of the  $\alpha$ -CD complex. Figure 4-7 displays the  $^{13}\text{C}$  CP/MAS NMR spectra of  $\alpha$ -CD, the CPC/ $\alpha$ -CD complex, and the clay intercalated by the inclusion complex.

The resonances of the C(1) and C(4) nuclei of the pure  $\alpha$ -CD result in multiple lines because of asymmetric glucopyranosyl conformations. In contrast, the signals of the C(1) and C(4) nuclei of the CPC/ $\alpha$ -CD complex appear as sharp singlets, which implies that the  $\alpha$ -CD unit adopts a symmetric cyclic conformation upon complexation. The solid state  $^{13}\text{C}$  NMR spectra provide evidence that  $\alpha$ -CD forms a channel-type complex with CPC. The signals of the clay intercalated by the inclusion complexes also appear as sharp singlets, which indicate that the inclusion complexes of the intercalated clay exist within the gallery of the clay. The peaks recorded from the intercalated clay are, however, relatively broad when compared with the other signals. Inserting the inclusion complex within the gallery of the clay decreases the spin-spin relaxation time ( $T_2$ ) and, thus, results in a greater width at half-height.

#### 4.3.5 Glass Transition Temperatures.

Figure 4-8 shows the DSC thermograms for virgin PS and surfactant-modified clay nanocomposites. Table 1 summarizes the results of DSC measurements. The glass transition temperature ( $T_g$ ) of the virgin PS is 100 °C and the values of  $T_g$  of the CPC/clay and inclusion complex/clay nanocomposites are 102 and 106 °C, respectively. The presence of the clay layers tends to retard movement of the PS chain and, thus, it results in a higher value of  $T_g$ . The better-dispersed clay nanocomposite (i.e., that of the inclusion complex-intercalated clay) retards chain movement more effectively than that of the CPC/clay-modified nanocomposite.

#### 4.3.6 Characterization by TGA.

Figure 4-9 displays TGA traces of pure CPC and the CPC/ $\alpha$ -CD inclusion complex. The CPC/ $\alpha$ -CD inclusion complex decomposes at a higher temperature (284 °C) than the pure CPC (220 °C). Thus, the formation of an inclusion complex between CPC and  $\alpha$ -CD improves the thermal stability of the CPC surfactant. The mechanism for the enhancement in thermal property is that the presence of the  $\alpha$ -CD is able to protect the CPC from earlier decomposition.

Figure 4-10 presents TGA thermograms of the nanocomposites and pure polystyrene. The two surfactant-modified PS nanocomposites display higher decomposition temperatures than does the virgin PS with the CPC/ $\alpha$ -CD-intercalated clay nanocomposite being the most thermally stable among the three samples. The nanocomposite prepared from the CPC/ $\alpha$ -CD-intercalated clay exhibits a 5% weight loss temperature that is 33 °C higher than that of the virgin PS. TEM micrograph of the CPC-intercalated clay nanocomposite is a mixture of intercalated and exfoliated structures. The 5% weight loss temperature of the CPC-intercalated clay nanocomposite is 18 °C higher than the virgin PS. Table 1 summarizes the TGA results for these nanocomposites. The nanocomposite containing  $\alpha$ -CD will obviously have a larger char yield. It will be more meaningful to prove that the weight loss of PS itself is improved by the presence of  $\alpha$ -CD. We also observed that the highest temperature for 50% weight loss occurred for the CPC/ $\alpha$ -CD-intercalated clay nanocomposite. Because the CPC-intercalated clay nanocomposite possesses a 50% weight loss temperature that is the same as that of virgin polystyrene, it is clear that this nanocomposite offers no substantial improvements over the virgin PS. In contrast, the nanocomposite prepared from the CPC/ $\alpha$ -CD-modified clay displays improved thermal stability.

#### 4.4 Conclusions.

We have prepared polystyrene/clay nanocomposites that have (a) a mainly exfoliated structures with some portions intercalated when treated with CPC and (b) a fully exfoliated structure when treated with CPC/ $\alpha$ -CD. We confirmed the existence of an inclusion complex between CPC and  $\alpha$ -CD by XRD and  $^{13}\text{C}$  CP/MAS NMR spectroscopic analyses. The  $^1\text{H}$  NMR spectra of the complexes demonstrate that the stoichiometry of the complexes is 1:2 (one CPC molecule to two  $\alpha$ -CD units). TGA revealed that the inclusion complex possesses increased thermal stability relative to that of the virgin CPC. We used XRD to confirm that intercalation of surfactants occurred into the montmorillonite clay nanoparticles. Our XRD data indicated that the  $d$  spacing after treatment with the inclusion complex was higher than that after treatment with the pure CPC surfactant. The results of TGA indicated that the onset of thermal degradation occurred at a higher temperature for the nanocomposite formed from CPC/ $\alpha$ -CD than it did for either the virgin PS or the nanocomposite derived after treatment with CPC. Thus, it appears that the presence of the CPC/ $\alpha$ -CD complex in the clay enhanced the thermal stability of polystyrene. The glass transition temperatures of the nanocomposites were slightly higher than that of the virgin PS.



## References

- [1] Pinnavaia TJ. *Science* 1983; 220: 365.
- [2] Zanetti M, Lomakin S, Camino G. *Macromol Mater Eng* 2000; 279: 1.
- [3] Giannelis EP. *Appl Organomet Chem* 1998; 12: 675.
- [4] Theng BK, G. *Formation and properties of clay-polymer complexes*; Elsevier: New York, 1979.
- [5] Alexandre M, Dubois P. *Mater Sci Eng* 2000; 28: 1.
- [6] LeBaron PC, Wang Z, Pinnavaia TJ. *Appl Clay Sci* 1999; 15: 11.
- [7] Vaia RA, Ishii H, Giannelis EP. *Chem Mater* 1993; 5: 1694.
- [8] Usuki A, Kojima Y, Kawasumi M, Okada A, Fukushima Y, Kurauchi T, Kamigaito O. *J Mater Res* 1993; 8: 1179.
- [9] Okada A, Kawasumi M, Usuki A, Kojima Y, Kurauchi T, Kamigaito O, *Mater Res Soc Symp Proc* 1990; 171: 45.
- [10] Okada A, Kawasumi M, Kurauchi T, Kamigaito O. *Polym Prepr* 1987; 28: 447.
- [11] Kojima Y, Usuki A, Kawasumi M, Okada A, Kurauchi T, Kamigaito O. *J Polym Sci Part A: Polym Chem* 1993; 31: 983.
- [12] Usuki A, Kojima Y, Kawasumi M, Okada A, Fukushima T, Kurauchi T, Kamigaito O. *J Mater Res* 1993; 8: 1179.
- [13] Yano K, Usuki A, Okada A, Kurauchi T, Kamigaito O. *J Polym Sci Part A: Polym Chem* 1993; 31: 2493.
- [14] Okada A, Usuki A. *Mater Sci Eng* 1995; 3: 109.
- [15] Lan T, Pinnavaia T. *J Chem Mater* 1994; 6: 2216.
- [16] Lan T, Pinnavaia TJ. *Chem Mater* 1994; 6: 573.
- [17] Lan T, Kaviratna PD, Pinnavaia TJ. *Chem Mater* 1995; 7: 2144.
- [18] Messersmith P, Giannelis EP. *J Polym Sci Part A: Polym Chem* 1995; 33: 1047.
- [19] Messersmith P, Giannelis EP. *Chem Mater* 1994; 6: 1719.

- [20] Gilman JW, Jackson CL, Morgan A, Harris R, Manias E, Giannelis EP, Wuthenow M, Hilton D, Phillips SA. *Chem Mater* 2000; 12: 1866.
- [21] Burnside SD, Giannelis EP. *Chem Mater* 1995; 7: 1597.
- [22] Bender ML, Komiyama M. *Cyclodextrin Chemistry*, Springer-Verlag: Berlin, 1978.
- [23] Tseng CR, Wu JY, Lee HY, Chang FC. *Polymer* 2001; 42: 10063.
- [24] Tseng CR, Lee HY, Chang FC. *J Polym Sci Part B: Polym Phys* 2001; 39: 2097.
- [25] Wu HD, Tseng CR, Chang FC. *Macromolecules* 2001; 34: 2992.
- [26] Tseng CR, Wu JY, Lee HY, Chang FC. *J Appl Polym Sci* 2002; 85: 1370.
- [27] Tseng CR, Wu HD, Wu JY, Chang FC. *J Appl Polym Sci* 2002; 86: 2492.
- [28] Cristian CR, Constantin L, Alan ET. *Macromolecules* 2001; 34: 1318.
- [29] Hua J, Goh SH, Valiyaveetil S. *Macromolecules* 2002; 35: 1399.

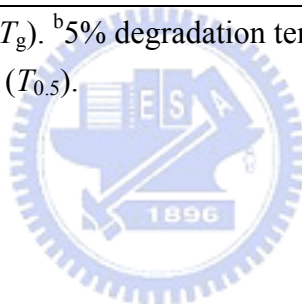


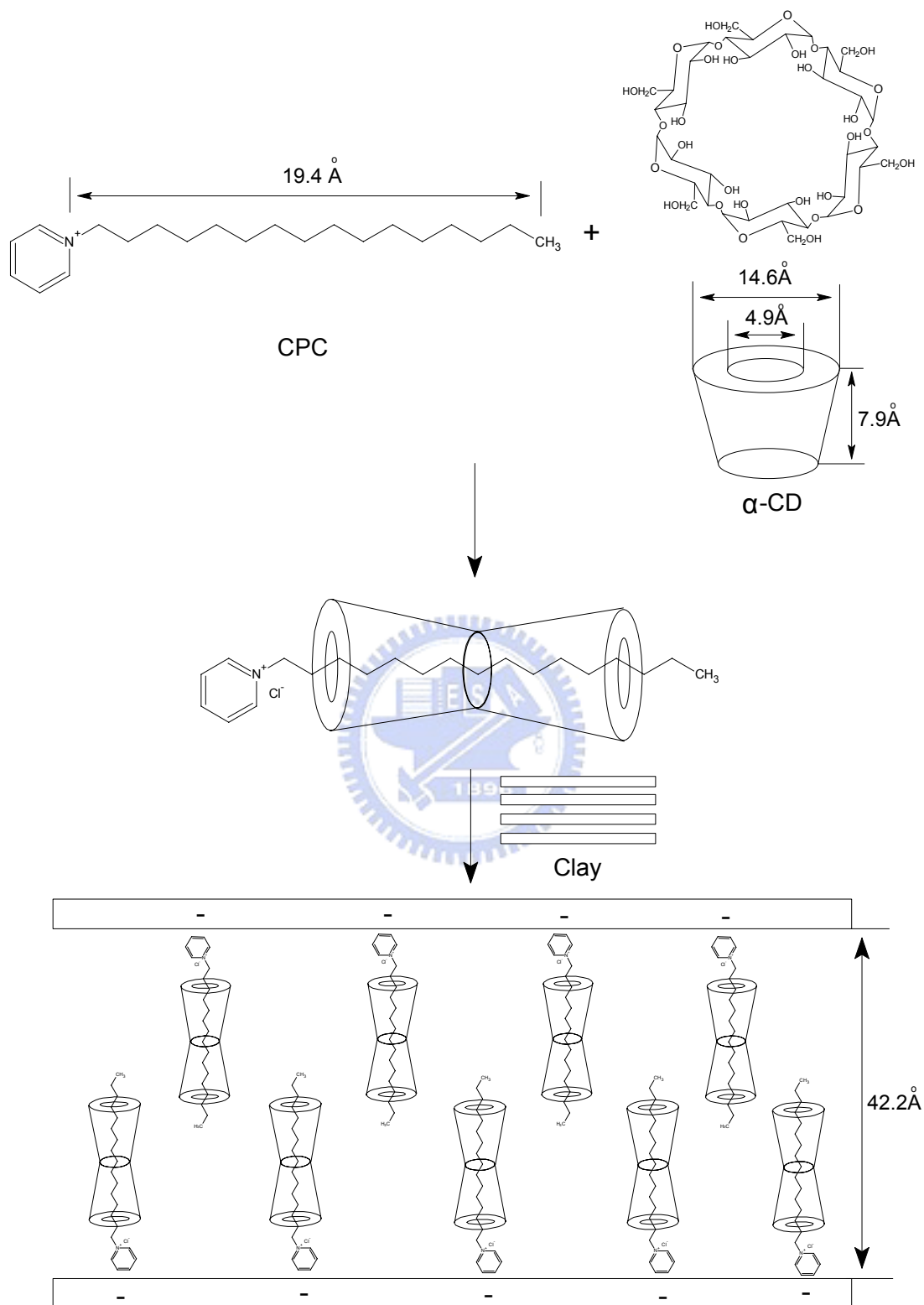
Table 4-1. Results of TGA and DSC Data for the Polystyrene Nanocomposites.

Sample	Clay content, %	$T_g$ , °C <sup>a</sup>	$T_{0.05}$ , °C <sup>b</sup>	$T_{0.5}$ , °C <sup>c</sup>	Char at 600 °C, %
PS	0	100	390	424	0
CPC/Clay/PS	3	102	408	424	2.9
$\alpha$ -CD/CPC/Clay/PS	3	106	423	452	5.8

<sup>a</sup>Glass transition temperature ( $T_g$ ). <sup>b</sup>5% degradation temperature ( $T_{0.05}$ ).

<sup>c</sup>50% degradation temperature ( $T_{0.5}$ ).





Scheme 4-1. Schematic representation of clay intercalated by the CPC/ $\alpha$ -CD inclusion complexes.

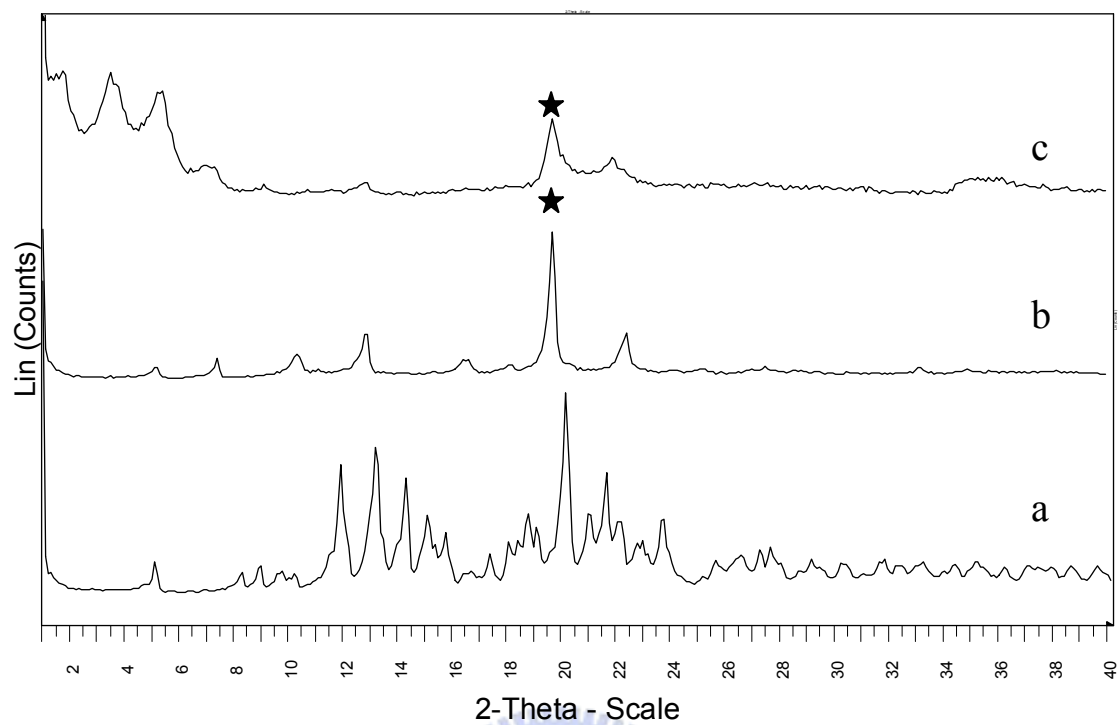


Figure 4-1. X-Ray diffraction patterns of (a)  $\alpha$ -CD, (b) the CPC/ $\alpha$ -CD inclusion complex, and (c) clay intercalated by the CPC/ $\alpha$ -CD inclusion complex.

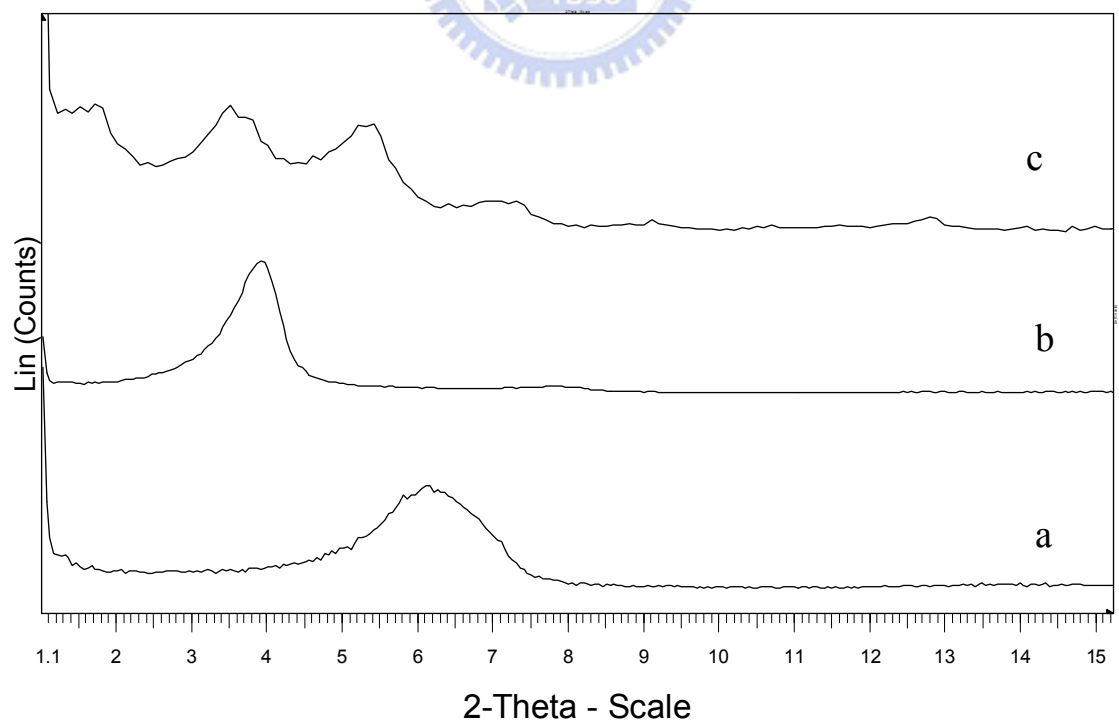


Figure 4-2. X-Ray diffraction patterns of (a) pure clay, (b) the CPC-intercalated clay, and (c) the CPC/ $\alpha$ -CD intercalated clay.

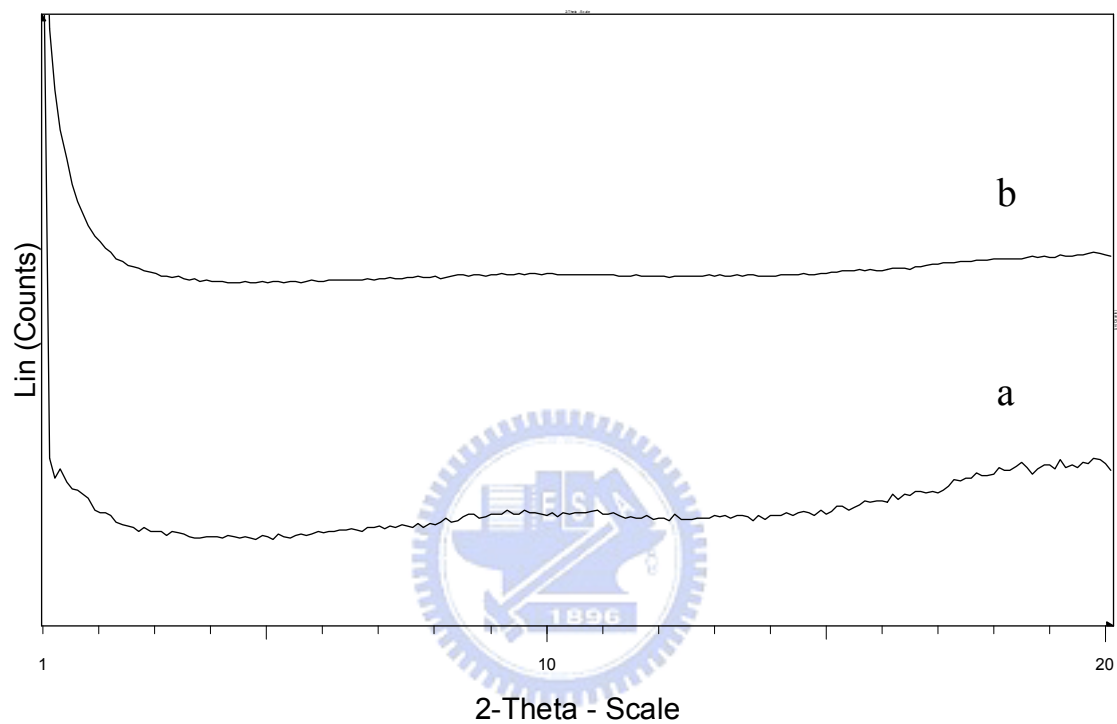


Figure 4-3. WAXD analysis of PS nanocomposites prepared by emulsion polymerization: (a) CPC treatment; (b) CPC/ $\alpha$ -CD treatment.

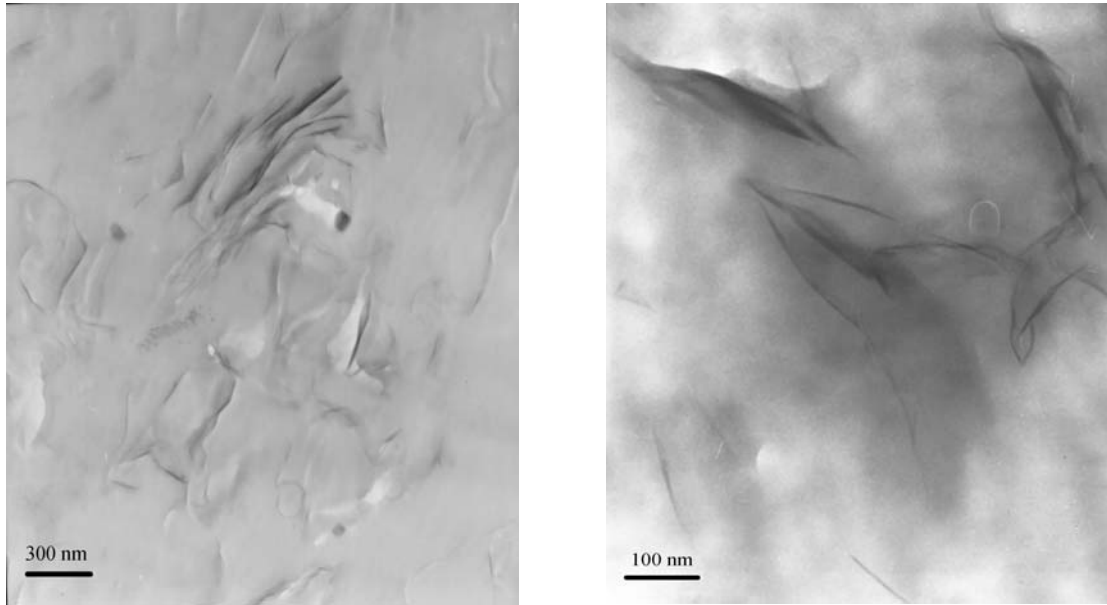


Figure 4-4. TEM images of the CPC-treated nanocomposite at low (left) and high (right) magnifications.

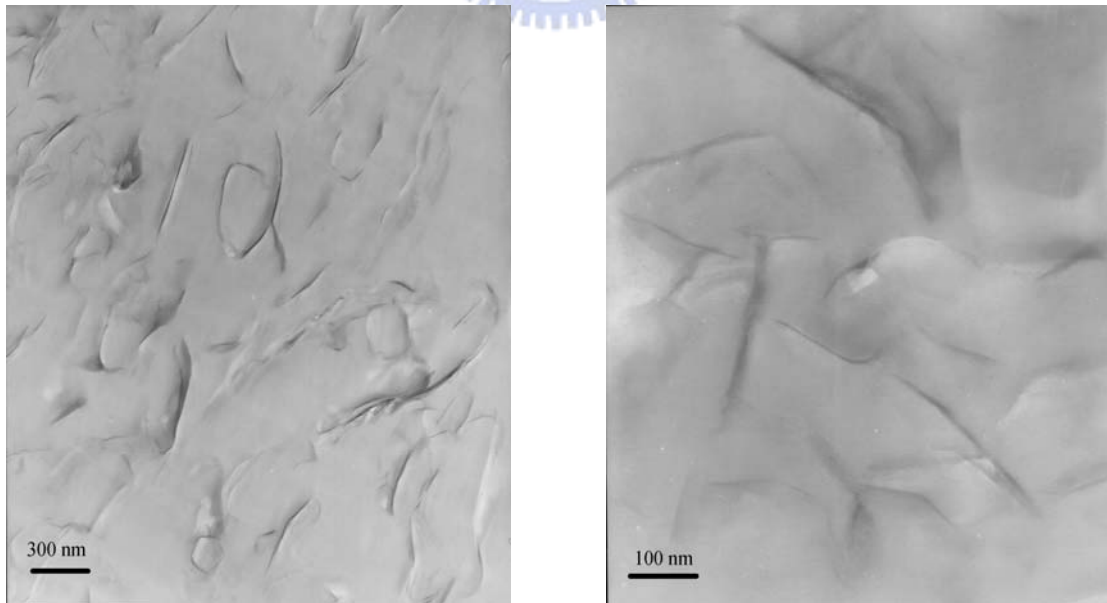


Figure 4-5. TEM images of CPC/ $\alpha$ -CD-treated nanocomposite at low (left) and high (right) magnifications.

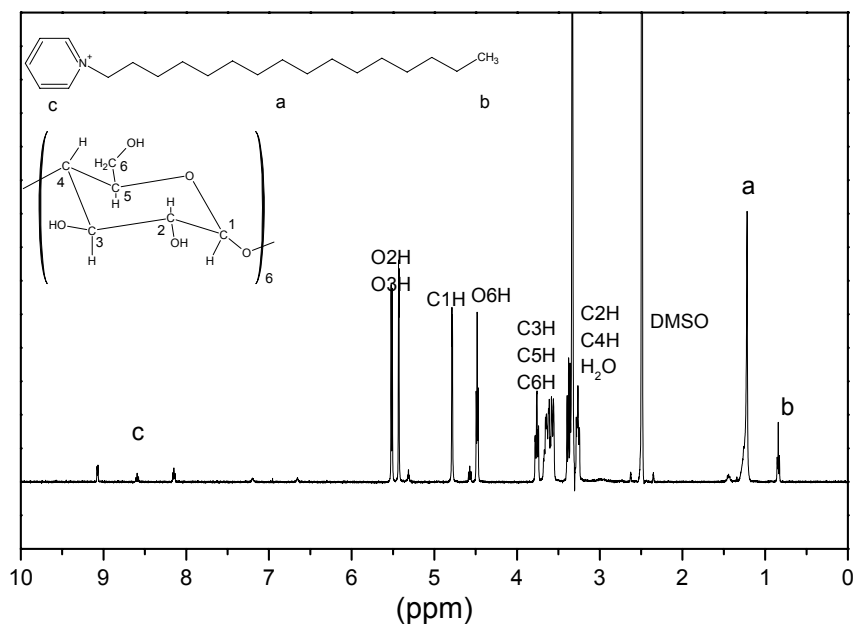


Figure 4-6.  $^1\text{H}$  NMR spectrum (500 MHz) of the CPC/ $\alpha$ -CD complex in  $\text{DMSO-}d_6$ .

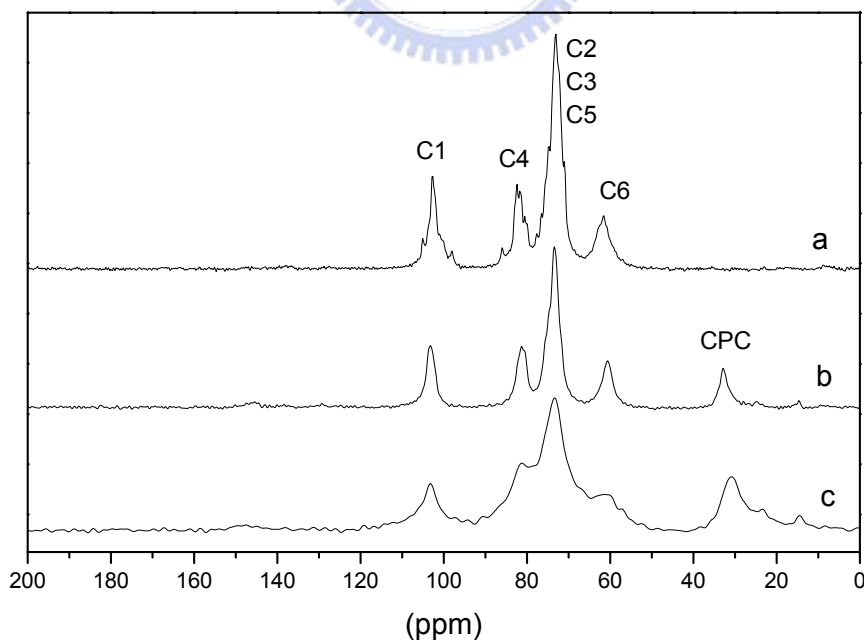


Figure 4-7.  $^{13}\text{C}$  CP/MAS NMR spectra of (a)  $\alpha$ -CD, (b) CPC/ $\alpha$ -CD, and (c) CPC/ $\alpha$ -CD intercalated clay.



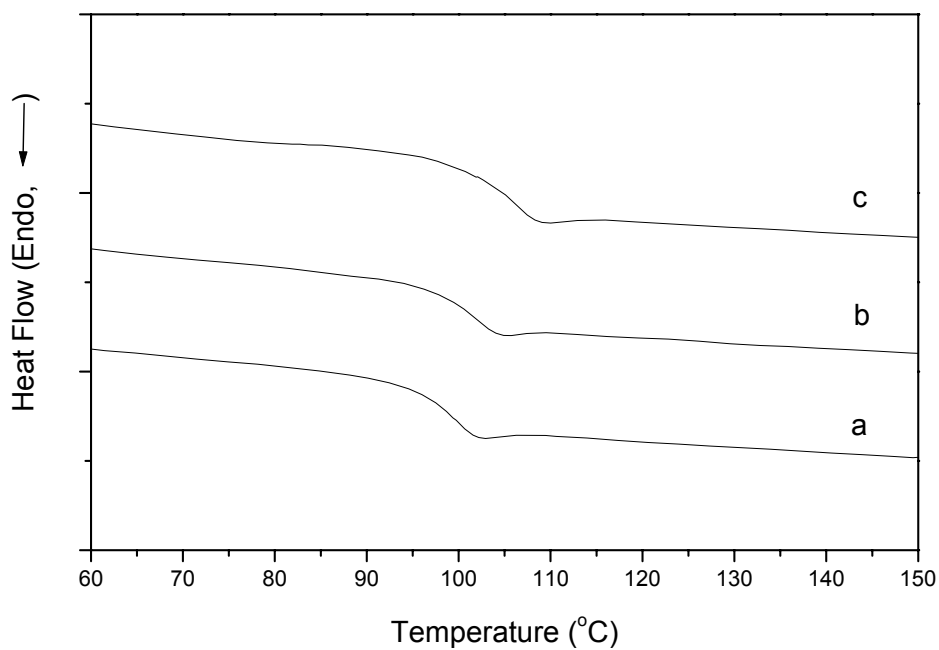


Figure 4-8. DSC curves for determining the glass transition temperature of (a) PS, (b) the nanocomposite formed using CPC, and (c) the nanocomposite formed using CPC/ $\alpha$ -CD.

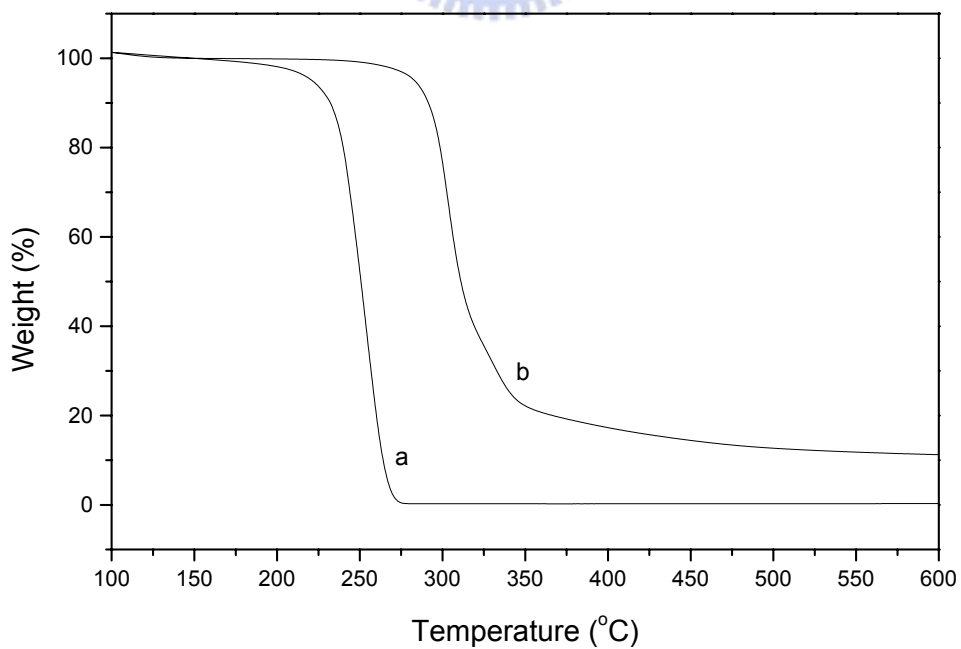


Figure 4-9. TGA curves of (a) pure CPC and (b) the CPC/ $\alpha$ -CD inclusion complex.

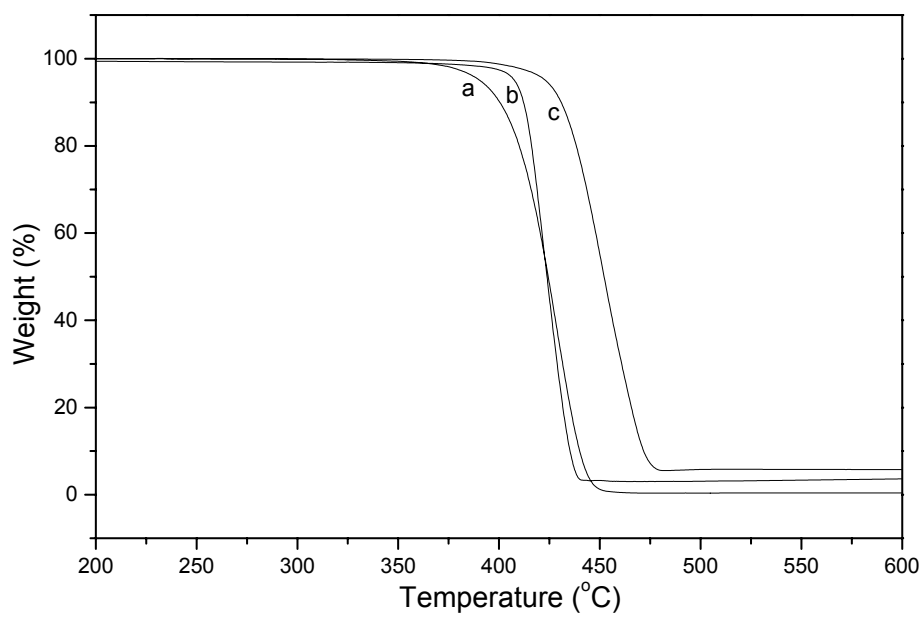
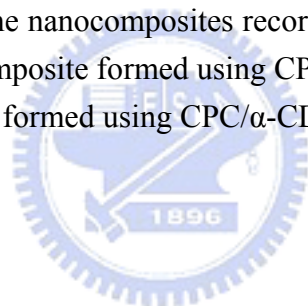


Figure 4-10. TGA curves of the nanocomposites recorded under nitrogen atmospheres: (a) pure PS, (b) the nanocomposite formed using CPC, and (c) the nanocomposite formed using CPC/ $\alpha$ -CD.



## Chapter 5

### Synthesis of a Novel Benzoxazine Monomer-Intercalated Montmorillonite and the Curing Kinetics of Polybenzoxazine/Clay Hybrid Nanocomposites

#### Abstract

Polybenzoxazine, which has a structure similar to that of phenolic resin, is formed through the thermal self-curing of benzoxazine, i.e., through a heterocyclic ring opening reaction that requires no catalyst and releases no condensation byproducts. We have used the solvent blending method to prepare polybenzoxazine/clay nanocomposites possessing various clay contents. We synthesized a monofunctional benzoxazine monomer (MBM) and then treated the clay with this intercalation agent. The results of XRD analysis indicated that MBM intercalated into the galleries of the clay; the nanocomposite possessed an exfoliated structure at a 3% clay content. To better understand the curing kinetics of the polybenzoxazine/clay nanocomposites, we performed dynamic and isothermal differential scanning calorimetry (DSC) measurements. We describe the thermodynamics of the curing process using all three of the Kissinger, Ozawa, and Kamal models. The Kissinger and Ozawa methods gave fairly close results for the calculated activation energies, which decreased upon increasing the clay content. The Kamal method—based on an autocatalytic model—suggested a total reaction order of between 2.4 and 2.8. The glass transition temperature ( $T_g$ ) decreased upon increasing the clay content. TGA indicated that the nanocomposites have higher decomposition temperatures than does the pristine polybenzoxazine; this finding suggests an enhancement in their thermal stability.

## 5.1 Introduction

Polybenzoxazine (PBZ) is a newly developed thermosetting resin that has a number of interesting properties. It is a novel type of phenolic resin that was developed to overcome the shortcomings of the traditional novolac and resole polymers. Although PBZ possesses the excellent properties commonly associated with the traditional phenolic resins—such as heat, electrical, and flame resistance—it also displays a number of unique characteristics, including excellent dimensional stability (resulting from the ring-opening polymerization mode), improved toughness, a stable dielectric constant, and low moisture absorption. In addition, PBZ derivatives can be synthesized from inexpensive raw materials, can be cured without requiring strong acid or base catalysis, and do not release any by-products during polymerization; thus, they are considered to be attractive candidates for many applications [1–7].

Polymer/clay nanocomposites, in which the layered silicates of the clay become dispersed in the polymeric matrix, are a new class of composite materials. As a result of the dispersion of the clay on the nanoscale, such nanocomposites often exhibit outstanding improvements in their properties—include increased modulus, strength, thermal stability, and solvent resistance and decreased gas permeability and flammability [8-25]—relative to those of conventional fiber or filler-filled composites. The layered silicate that is most widely used for the preparation of polymer/clay nanocomposites is montmorillonite (MMT).

MMT is a multilayer silicate mineral that naturally possesses inorganic cations within its galleries to balance the charge of the oxide layers in a hydrophilic environment. The ion exchange of these cations with organic ammonium ions affords hydrophobic environment within the galleries of the organically modified MMT (OMMT) [15]. The organophilic galleries of OMMT enhance the compatibility of the

clay with polymers [15], improve the dispersion of the silicate layers into the matrix [12], and assist the penetration of monomers or polymers into the galleries [22]. In addition, the organic ammonium cations can provide functional groups that react or interact with the monomer or polymer units to improve the interfacial strength between the reinforcement and the polymer matrix [18]. The degree of dispersion of clay nanolayers and the resulting morphology of the nanocomposite depend on a number of factors, including the mixing method (melt or solvent), temperature, and time, the choice of solvent, and its concentration, the steric size of the monomer or polymer, the choice of intercalation agent, and the yield of the ion exchange process.

In this study, we synthesized a monofunctional benzoxazine monomer (MBM) that behaves as an intercalation agent and used it subsequently to prepare PBZ/clay hybrid nanocomposites. We expected that this intercalation agent would undergo ring opening polymerization with benzoxazine matrix to promote the formation of an exfoliated nanocomposite structure. Scheme 5-1 displays the structures of the benzoxazine monomer and polybenzoxazine. To study the kinetics of the development process, we performed isothermal and dynamic differential scanning calorimetry (DSC) experiments. We have used two dynamic kinetic models and one isothermal model to study the kinetics of the curing of the PBZ/clay nanocomposites. We used both X-ray diffraction (XRD) and transmission electron microscopy (TEM) to characterize the structure of the clay, and characterized the thermal properties of the PBZ/clay nanocomposites through thermogravimetric analysis (TGA).

## 5.2 Experimental

### 5.2.1 Materials

Bis(3-phenyl-3,4-dihydro-2*H*-1,3-benzoxazinyl) isopropane (B-a), a polybenzoxazine precursor, was supplied by Shikoku Chemicals Co. Phenol was purchased from SHOWA Chemical Co., Japan. Formalin and *N,N*-dimethyl-1,3-propanediamine were obtained from Acros Organics, USA. Tetrahydrofuran and dioxane were purchased from Aldrich Chemical Co., USA. Pristine Na-MMT was provided by Telekal Co., Taiwan.

### 5.2.2 Synthesis of monofunctional benzoxazine monomer (MBM)

MBM was synthesized according to the procedure presented in Scheme 5-2. Formalin (37%, 16.23 g, 200 mmol) and dioxane (100 mL) were mixed in a 500-mL flask that was cooled in an ice bath. *N,N*-Dimethyl-1,3-propanediamine (10.2 g, 100 mmol) in dioxane (100 mL) was added portionwise to this solution. The solution was then stirred for 30 min while maintaining the temperature below 5 °C. Thereafter, a solution of phenol (9.41 g, 100 mmol) in dioxane (100 mL) was added. The solution was heated under reflux at 110 °C for 4 h. Removal of the solvent in a rotary evaporator at 50 °C gave a viscous residue that was dissolved in ether (200 mL) and washed several times with 3 N sodium hydroxide solution and then with distilled water. The ether solution was dried (anhydrous sodium sulfate); evaporation of the solvent under vacuum afforded a pale-yellow viscous fluid.

### 5.2.3 Preparation of MBM-Modified Clays

Pre-washed clay (1 g) and water (50 mL) were placed into a 100-mL, two-neck, round-bottom flask and stirred continuously for 4 h. In a separate flask, 10% hydrochloric acid (5 mL) was added to a solution of MBM (0.4 g) in THF (5 mL); this mixture was stirred for 1 h before being added to the suspended clay and then stirred overnight. The mixture was filtered, washed several times with deionized water, and then dried overnight in a vacuum oven at room temperature.

### 5.2.4 Preparation of polybenzoxazine/Clay nanocomposites

Benzoxazine (B-a) and the MBM-modified clay were blended together at various weight ratios. An example of the solvent method is presented here for the preparation of a sample possessing a 3% inclusion of MBM-modified clay: MBM-modified clay (0.3 g) was dispersed in THF (20 mL) at room temperature for 2 h. B-a (9.7 g) was added to the MBM-modified clay suspension and then the sample was stirred at room temperature overnight to form a well-dispersed mixture. The THF was evaporated under vacuum. The prepared samples were used for isothermal and dynamic curing experiments employing DSC. Subsequently, the samples were cured at 130, 160, 180 and 200 °C for 2 h each in an oven under an atmosphere of air to obtain the PBZ/clay nanocomposites.

### 5.2.5 Isothermal Curing

The samples were placed in the Al cell at room temperature and then heated quickly to a preset temperature for each isothermal experiment. The instrument achieved a stable state ca. 60 s after reaching the setting temperature; the data were

recorded immediately. When the DSC exothermic peak reached the baseline level, the isothermal curing process was complete and the heat of reaction was measured by integrating the area of the exothermic peak. These isothermal curing curves were used to evaluate the kinetic parameters of the curing reaction.

### 5.2.6 *Dynamic Curing*

The non-isothermal experiments were performed at heating rates of 2.5, 5, 10, and 20 °C/min over the temperature range from 30 to 320 °C; the area of exothermic peak was integrated. We assumed that the total recorded heat of the reaction represented the total heat evolved for the complete curing process at the different curing rates.



### 5.2.7 *Instrumentation*

X-Ray diffraction spectra were collected on an M18XHF-SPA X-ray diffraction instrument (MacScience Co., Japan), using Co K $\alpha$  radiation; Bragg's law ( $\lambda = 2d\sin\theta$ ) was used to compute the spacing. Transmission electron microscopy (TEM) images of the composites were obtained at 100 kV using a Hitachi H-7500 electron microscope. The sample was ultra-microtomed at room temperature using a diamond knife on a Leica Ultracut UCT microtome to provide 80 nm-thick sections. The contrast between the layered silicates and the polymer phase was sufficient for imaging and, therefore, no heavy metal staining was required prior to imaging. Thermogravimetric analyses (TGA) were performed using a TA Instruments thermal analyzer under a 40 mL/min flow of nitrogen gas at a scan rate of 20 °C/min over the temperature range from 30 to 800 °C. A Du Pont (DSC-9000) differential scanning calorimeter (DSC) was used to



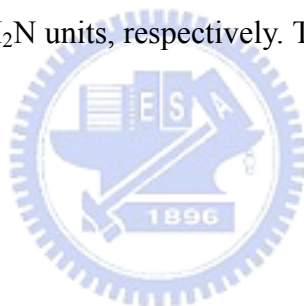
measure both the glass transition temperature ( $T_g$ ) of the PBZ/clay nanocomposite and the kinetic parameters of the curing reaction.



## 5.3 Results and Discussion

### 5.3.1 Preparation of Monofunctional Benzoxazine Monomer (MBM)

MBM was prepared according to the procedure presented in Scheme 5-2. Initially, dimethyl-1,3-propanediamine was reacted with formalin and phenol in dioxane. The crude product was dissolved in ether and washed with aqueous NaOH to remove any phenolic oligomers; evaporation of the solvent afforded MBM as a viscous yellow product. We used  $^1\text{H}$  NMR spectroscopy to confirm the chemical structure of MBM (Figure 5-1). The three multiplets at 1.75, 2.33 and 2.75 ppm are typical for the  $\text{CH}_2$  protons of the allyl group. We assign the peak at 2.23 ppm to the  $\text{N}(\text{CH}_3)_2$  protons. The characteristic protons of oxazine ring, at 3.95 and 4.83 ppm, are assigned to  $\text{ArCH}_2\text{N}$  and  $\text{OCH}_2\text{N}$  units, respectively. The aromatic protons appear as a multiplet at 6.73–7.23 ppm.



### 5.3.2 X-Ray Diffractions

We employed X-ray diffraction (XRD) to characterize the layered structures of the modified clays and PBZ/clay nanocomposites; changes in the value of  $2\theta$  reflect changes in the gallery distance of the clay. Figure 5-2 displays the XRD results of the MBM-intercalated clay. The pristine clay sample exhibits a peak at  $6.14^\circ$ , which corresponds to a basal space of 1.43 nm. The insertion of the MBM between the galleries of the clay increased the  $d$  spacing from 1.43 to 1.84 nm. This result indicates that the MBM was intercalated successfully into the galleries of the clay nanoparticles. Scheme 5-3 displays the clay intercalated by the MBM. We calculated the interlamellar distance, which is indicated in this Scheme, by using the expression:  $\Delta d = d \text{ spacing} - \text{thickness of one platelet (ca. } 9 \text{ \AA)}$ . For the clay intercalated with the

MBM, the distance between two adjacent clay plates was 9.4 Å; this value is close to the size of one MBM molecule.

Figure 5-3 presents the XRD patterns for the nanocomposites formed when varying the clay contents. We detected no peak for nanocomposite containing 3% clay content; this observation implies that this sample possesses an exfoliated structure. We did observe, however, a peak at ca.  $2\theta = 3.5^\circ$  for each of the samples containing 6, 10, and 15% clay content. These data suggest the presence of the intercalated structure, but these measurements alone were not conclusive for determining the true structures and distributions of the silica platelets; thus, we turned our attention to TEM measurements.

### 5.3.3 TEM Measurements of the Nanocomposites

Figure 5-4 displays TEM images of the 3 and 6% clay nanocomposites. These images indicate the dispersion of the clay layers within the polymer. The dark lines represent the clay layers that were positioned perpendicular to the sample's surface. For the 3% clay nanocomposite (Figure 5-4a), each clay layer was isolated and distributed evenly within the PBZ matrix; this situation implies that full exfoliation had occurred and is consistent with the results of the XRD analysis. The platelet layers we observe for the 6% clay nanocomposite are a mixture of fully exfoliated and intercalated structures.

### 5.3.4 Investigating the Curing Behavior of PBZ/Clay Nanocomposites Using DSC

DSC is an attractive technique because it can provide detailed information regarding the cure mechanism and the preferred temperature during the formation of

three-dimensional networks in materials. In addition, the apparatus is simple to use, data are obtained quickly, and only small quantities of samples are required. DSC is employed widely to elucidate the key parameters of the curing process, such as the extent and rate of chemical conversion and the glass transition temperature, from both isothermal and dynamic DSC experiments.

Figure 5-5 presents the dynamic exothermal curves, obtained at a heating rate 20 °C/min, of the samples possessing the various clay contents. We observed a single exothermic peak for each curing system, but the sharp exothermic peak for the pure PBZ system occurred at a relatively higher temperature. For the PBZ/clay systems, the exothermic peak was smooth and broad, and it shifted to a lower temperature upon increasing the clay content. These results suggest that the curing reaction in the pure PBZ system was delayed to a higher temperature.

Figure 5-6 presents the DSC exothermic curves of pure PBZ recorded at heating rates 2.5, 5, 10, and 20 °C/min. We observe that the curing temperature (i.e., the peak exotherm temperature,  $T_p$ ) increased upon increasing in the heating rate. We investigated these exotherms using the dynamic kinetic method to obtain the activation energy ( $E_a$ ) and other related parameters. Figure 5-7 displays the reaction rates of pure PBZ as a function of the curing time for different curing temperatures. We cured all of the samples without adding any catalyst and observed only a single exothermic peak in each DSC curve. In other words, this heterocyclic ring opening curing reaction involves a single exothermic chemical process. As expected, We found that a higher curing temperature increased the curing rate and decreased the curing time.

Figure 5-8 provides a plot of the conversion ( $\alpha$ ) as a function of the isothermal curing time for the samples containing various clay contents. When we increased the clay content from 0 to 15%, the conversion decreased from 0.67 to 0.43. In other

words, a higher clay content tends to retard the ring opening polymerization of benzoxazine as a result of the clay providing a steric barrier. Figure 5-9 displays plots of the reaction rate as a function of the conversion at various curing temperatures. The maximum reaction rates occurred at conversions between 17% (180 °C) and 23% (220 °C). These conversions are fairly close to those found typically for autocatalyzed reactions: the maximum reaction rate is usually obtained between 20 and 40% conversion. [26-28]

### 5.3.5 Kinetic Analysis

Kinetic analyses are performed most commonly [29] using three kinetic models: the Kissinger [30] and Osawa [31] methods are suitable for dynamic kinetic analyses, while the Kamal [32] method is suitable for isothermal kinetic analyses (autocatalytic model).

The extent of reaction,  $\alpha$ , is proportional to the heat generated during the reaction. The reaction rate is a function of conversion, which can be expressed by the general law provided in equation (1):

$$\frac{d\alpha}{dt} = k(T)f(\alpha) \quad (1)$$

where  $t$  is the time,  $k(T)$  is the rate constant, and  $f(\alpha)$  is a function of the dependence of conversion. By integrating the above equation, a new equation can be obtained:

$$g(\alpha) = \int_0^\alpha \frac{d\alpha}{f(\alpha)} = k(T)t \quad (2)$$

where  $g(\alpha)$  is the integrated form of the conversion-dependent function.

### 5.3.5.1 Dynamic Kinetic Method

The non-isothermal process can be modeled using both the single and multiple heating rate methods. The multiple heating rate method was proposed by Kissinger and Ozawa. We used these two methods in this study – rather than the other non-isothermal methods – because they do not require prior knowledge of the reaction mechanism to quantify the kinetic parameters.

#### (a) Kissinger Method

This approach assumes that, for thermoset curing, the extent of the reaction at the peak exotherm is constant and independent of the heating rate. The value of  $E_a$  can be obtained as follows:

$$-\frac{E_a}{R} = \frac{d[\ln(\beta/T_p^2)]}{d(1/T_p)} \quad (3)$$

where  $\beta$  is a heating rate,  $T_p$  is the maximum exothermic temperature, and  $R$  is the universal gas constant. Plotting  $\ln(\beta/T_p^2)$  against  $1/T_p$  provides the activation energy without requiring a specific assumption of the conversion-dependent function. We calculated the slope as indicated in Figure 5-10. Table 5-1 lists all of the values of  $E_a$ ; the activation energy is calculated to decrease upon increasing the clay content. In other words, a higher clay content can decrease the activation energy and promote the ring opening polymerization.

#### (b) Ozawa Method

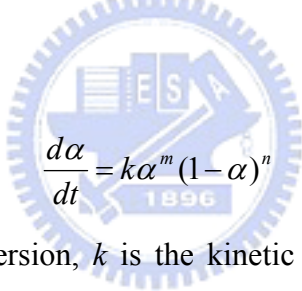
The Ozawa method is another approach that is used widely for dynamic kinetic analysis without requiring any assumptions to be made regarding the conversion-dependence function. Its general expression may be represented by equation (4):

$$E_a = \frac{-R}{1.052} \frac{\Delta \ln \beta}{\Delta(1/T_p)} \quad (4)$$

Figure 5-10 provides plots of  $\ln \beta$  as a function of  $(1/T_p)$ , from which we can obtain the values of the slope to calculate the activation energy. Table 5-1 also provides all of these values of  $E_a$ ; it indicates that the results obtained when using the Ozawa method are close to those provided by the Kissinger method.

### 5.3.5.2 Isothermal Kinetic Analysis (Autocatalytic Model)

The autocatalytic model is a phenomenological approach that was developed by Kamal. If a system is autocatalytic, the reaction rate can be described by the general expression:



$$\frac{d\alpha}{dt} = k\alpha^m(1-\alpha)^n \quad (5)$$

where  $\alpha$  is the reaction conversion,  $k$  is the kinetic rate constant,  $m$  and  $n$  are the kinetic exponents of the reaction, and  $(m+n)$  is the overall reaction order.

In practice, however, the curing reaction will cease when the reaction conversion reaches its maximum value ( $\alpha_{\max}$ ). In this case, equation (5) must be corrected into the form of equation (6). [33-35]

$$\frac{d\alpha}{dt} = k\alpha^m(\alpha_{\max} - \alpha)^n \quad (6)$$

(when  $\alpha = \alpha_{\max} \rightarrow \frac{d\alpha}{dt} = 0$ )

where  $\alpha_{\max}$  is based on different curing temperatures. Equation (7) and (8) are obtained after rearranging equation (6) and taking its natural logarithm. Using the iteration method allows the approximate values of  $m$ ,  $n$ , and  $k$  to be calculated according to equations (7) and (8). When  $|n_{i+1} - n_i| < 0.01$ , the iteration is stopped

and the values of  $m$ ,  $n$ , and  $k$  are obtained; Table 5-2 lists the results. The values of  $(m+n)$  exist within the range between 2.4 and 2.8. The rate constants increase upon increasing the curing temperature.

$$\ln\left(\frac{(d\alpha/dt)}{(\alpha_{\max} - \alpha)^n}\right) = \ln k + m \ln \alpha \quad (7)$$

$$\ln\left(\frac{(d\alpha/dt)}{k\alpha^m}\right) = n \ln(\alpha_{\max} - \alpha) \quad (8)$$

In addition, the rate constant,  $k$ , may be described by the Arrhenius expression: [33]

$$k = Ae^{-E_a/RT} \quad (9)$$

where  $A$  is Arrhenius factor,  $E_a$  is the activation energy,  $R$  is the universal gas constant, and  $T$  is the absolute temperature. Taking the natural logarithm of equation (9), we obtain equation (10). Plotting  $\ln k$  as a function of  $1/T$  for the different isothermal curing temperatures allows us to obtain the kinetic data, which are presented in Table 5-2. The activation energies of the PBZ/clay nanocomposites are smaller than that of pure PBZ.

$$\ln k = \ln A - E_a / RT \quad (10)$$

Comparing the results of the three kinetic models, we find that the values of the activation energies are quite close. Hence, it is possible to calculate the activation energy and kinetic parameters in this system—including the values of  $m$ ,  $n$ , and  $k$ —by using any one of the Kissinger, Osawa, or Kamal methods.

### 5.3.6 Analyzing Glass Transition Temperatures.

Figure 5-11 displays the DSC thermograms of pure PBZ and the PBZ/clay nanocomposites; Table 5-3 lists the data. The glass transition temperature,  $T_g$ , decreases upon increasing the clay content. The main reason for this phenomenon is



that the conversion of PBZ decreases upon increasing the clay content. Figure 5-8 indicated that reaching a high value for the conversion was difficult at a high clay content. In other words, the value of  $T_g$  is lower when the conversion is low.

### *5.3.7 Thermal Stability of PBZ/Clay Nanocomposites.*

We performed thermogravimetric analyses (TGA) of the MBM-clay based nanocomposites to monitor the effect that dispersion of the clay nanolayer in the PBZ matrix has on the thermal properties. Figure 5-12 displays the TGA traces of pure PBZ and the PBZ/clay nanocomposites. The PBZ/clay nanocomposites displayed higher decomposition temperatures than did pure PBZ; i.e., the thermal stability of the nanocomposites was improved by the presence of dispersed clay nanolayers, which act as barriers to minimize the permeability of the volatile degradation products from the material. [36] Table 5-3 summarizes the TGA results for these nanocomposites. From the temperatures of the 5 and 50% weight losses, the TGA results of the PBZ/clay samples indicate a clear trend of improved thermal stability upon increasing the clay content. The PBZ/clay nanocomposites obviously have greater char yield, which increases upon increasing the clay content, as expected. The increase in char yield suggests the reduction of the polymer's flammability. [37]

## 5.4 Conclusions

In this study, we successfully synthesized the intercalation agent MBM and prepared PBZ/clay hybrid nanocomposites. The sample had a fully exfoliated structure at a 3% clay content. The MBM intercalating agent, which contains a benzoxazine functional group that can undergo ring opening polymerization within the galleries of the clay, promotes the exfoliated structure of nanocomposite. DSC traces indicated that the onset of the ring opening of the benzoxazine unit in the presence of clay to form PBZ/clay nanocomposites occurred at relatively lower temperatures relative to that of the pristine benzoxazine; this finding suggests that the clay surface has a catalytic effect on the ring opening polymerization. Both the Kissinger and Ozawa methods of calculating the activation energy gave fairly consistent results; the activation energy decreased upon increasing the clay content as a result of a lower conversion. The Kamal method—based on an autocatalytic model—suggested that the total order of the reaction was between 2.4 and 2.8. The glass transition temperature ( $T_g$ ) is decreased upon increasing the clay content. TGA traces indicated that the nanocomposites have higher thermal stabilities relative to that of the pristine PBZ. The char yields increased upon increasing the clay content.

## References

- [1] Riess G, Schwob JM, Guth G, Roche M, Laude B. In: Culbertson BM, McGrath JE. Editors. *Advances in polymer science synthesis*. New York: Plenum. 1985.
- [2] Ning X, Ishida H, *J Polym Sci. Part A: Polym Chem* 1994; 32: 1121.
- [3] Dunkers J, Ishida H. *Spectrochim Acta* 1995; 51: 855.
- [4] Ishida H, Allen D. *Polymer* 1996; 37: 4487.
- [5] Shen BS, Ishida H. *J Appl Sci* 1996; 61: 1595.
- [6] Ishida H, Allen DJ. *J Polym Sci. Part B: Polym Phys* 1996; 34: 1019.
- [7] Takeichi T, Komiya I, Takayama Y. *Kyoka Purasutikkusu* 1997; 43: 109 in Japanese.
- [8] Usuki A, Kawasumi M, Kijima Y, Okada A, Kamigaito O. *J Mater Res* 1993; 8: 1174.
- [9] Kojima Y, Usuki A, Kawasumi M, Okada A, Kurauchi T, Kamigaito O. *J Polym Sci, Part A: Polym Chem* 1993; 31: 1755.
- [10] Yano K, Usuki A, Okada A, Kurauchi T. *J Polym Sci, Part A: Polym Chem* 1993; 31: 2493.
- [11] Usuki A, Koiwai A, Kojima Y, Kawasumi M, Okada A, Kurauchi T, Kamigaito O. *J Appl Polym Sci* 1995; 55: 1193.
- [12] Kawasumi M, Hasegawa N, Kato M, Kojima Y, Usuki A, Okada A. *Macromolecules* 1997; 30: 6333.
- [13] Moet A, Akelah A. *Mater Lett* 1993; 18: 97.
- [14] Moet A, Akelah A, Salahuddin N, Hiltner A, Baer E. *Mater Res Symp Proc* 1994; 351: 163.
- [15] Akelah A. In: Prasad PN, Mark JE, Tung JF, editor. *Polymers and others advanced materials: emerging technologies and business opportunities*. New

York: Plenum, 1995.

- [16] Giannelis EP. *Adv Mater* 1996; 8: 29.
- [17] Giannelis EP. *Annu Tech Conf Soc Plast Engng* 1996; 54: 2998.
- [18] Giannelis EP. In: Mann S, editor. *Biomimetic materials chemistry*. New York: VCH, 1996.
- [19] Giannelis EP. *Appl Organomet Chem* 1998; 12: 675.
- [20] Lan T, Pinnavaia TJ. *Chem Mater* 1994; 6: 2216.
- [21] Wang MS, Pinnavaia TJ. *Chem Mater* 1994; 6: 468.
- [22] LeBaron PC, Wang Z, Pinnavaia TJ. *Appl Clay Sci* 1999; 15: 11.
- [23] Yang Y, Zhu Z, Yin J, Wang X, Qi Z. *Polymer* 1999; 40: 4407.
- [24] Agag T, Koga T, Takeichi T. *Polymer* 2001; 42: 3399.
- [25] Agag T, Takeichi T. *Polymer* 2000; 41: 7083.
- [26] Horie K, Mita I, Kambe H. *J Polym Sci Polym Chem Edu* 1970; 8: 2839.
- [27] Prime RB. In “*Thermal Characterization of Polymeric Materials*” (Ed. E.A. Turi) Academic Press, New York 1981; 425~653.
- [28] Nam JD, Seferis JC. *J Appl Polym Sci* 1993; 50: 1555.
- [29] Barral L, Cano J, Lopez I, Bueno L, Nogueira P, Abad MJ, Ramirez C. *J Polym Sci Polym Phys* 2000; 38: 351.
- [30] Kissinger HE. *Anal Chem* 1957; 29: 1702.
- [31] Ozawa T. *J Therm Anal* 1970; 2: 301.
- [32] Kamal MR. *Polym Eng Sci* 1974; 27: 782.
- [33] Fischer M, Tran CD. *Anal Chem* 1999; 71: 953.
- [34] Cole RC. *Macromolecules* 1991; 24: 3093.
- [35] Cole KC, Hechler JJ, Nobel D. *Macromolecules* 1991; 24: 3098.
- [36] Frischer HR, Gielgens LH, Koster TPM. *Acta Polym* 1999; 50: 122.
- [37] Gilman JW, VanderHart DL, Kashiwagi T. In *Fire and Polymer*, Nelson GL. Ed.

ACS Symposium Series, American Chemical Society: Washington, DC, 1995;  
p161.



Table 5-1. Activation energies obtained using the Kissinger and Ozawa methods for PBZ/clay nanocomposites.

Sample	Clay Content (wt%)	$E_a$	
		Kissinger (KJmol <sup>-1</sup> )	Ozawa (KJmol <sup>-1</sup> )
PBZ	0	112	117
PBZ/clay	3	107	111
PBZ/clay	6	106	110
PBZ/clay	10	104	104
PBZ/clay	15	90	93



Table 5-2. Results obtained from isothermal experiments on the PBZ/clay nanocomposites.

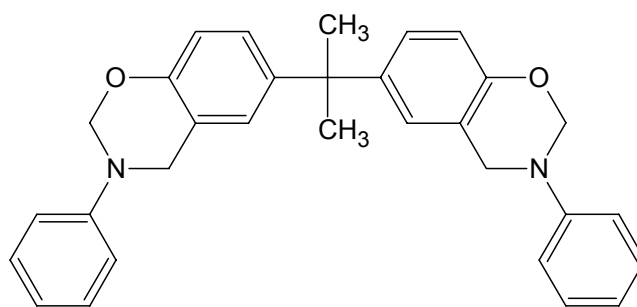
Sample	Clay Content (wt%)	Curing Temp. (°C)	Rate const. $k$ (min <sup>-1</sup> )	$E_a$ (KJ/mol)	$m$	$n$	$m + n$
PBZ	0	180	0.35	110	0.9	1.9	2.8
		190	0.54				
		200	0.98				
		210	2.14				
		220	2.62				
PBZ/clay	3	180	0.29	104	0.6	2.0	2.6
		190	0.43				
		200	0.62				
		210	0.98				
		220	1.87				
PBZ/clay	6	180	0.39	100	0.8	1.7	2.5
		190	0.42				
		200	0.56				
		210	1.13				
		220	1.55				
PBZ/clay	10	180	0.37	105	0.5	2.1	2.6
		190	0.35				
		200	0.61				
		210	1.15				
		220	2.82				
PBZ/clay	15	180	0.14	106	0.2	2.2	2.4
		190	0.41				
		200	0.88				
		210	1.71				
		220	5.41				

Table 5-3. TGA and DSC data for PBZ/clay nanocomposites.

Sample	clay wt%	T <sub>g</sub> (°C)	Weight loss temperature (°C)		Char yield (%)
			5 wt%	50 wt%	
PBZ	0	185	315	450	32
PBZ/clay	3	172	317	464	31
PBZ/clay	6	169	323	497	37
PBZ/clay	10	166	331	523	42
PBZ/clay	15	151	297	734	49

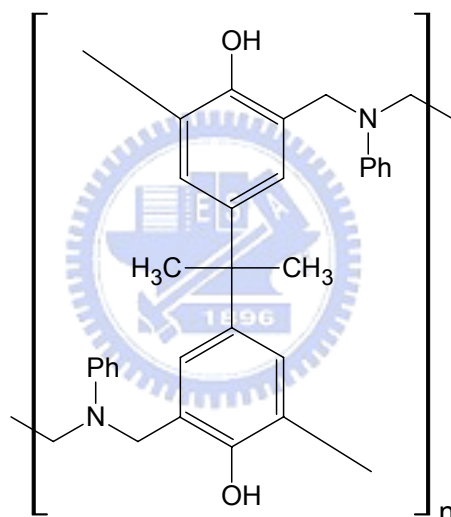






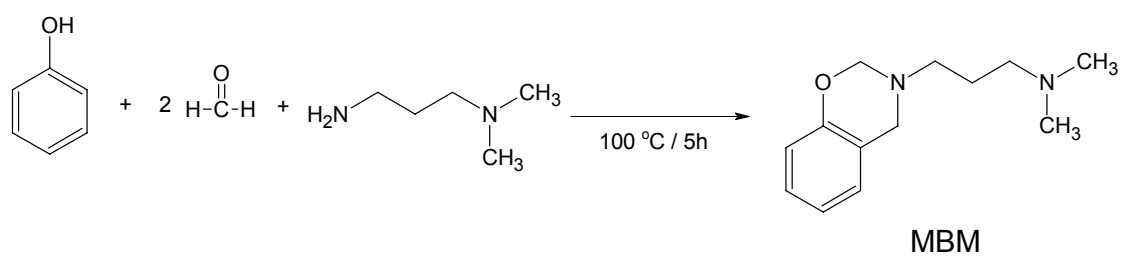
B-a

Thermal treatment



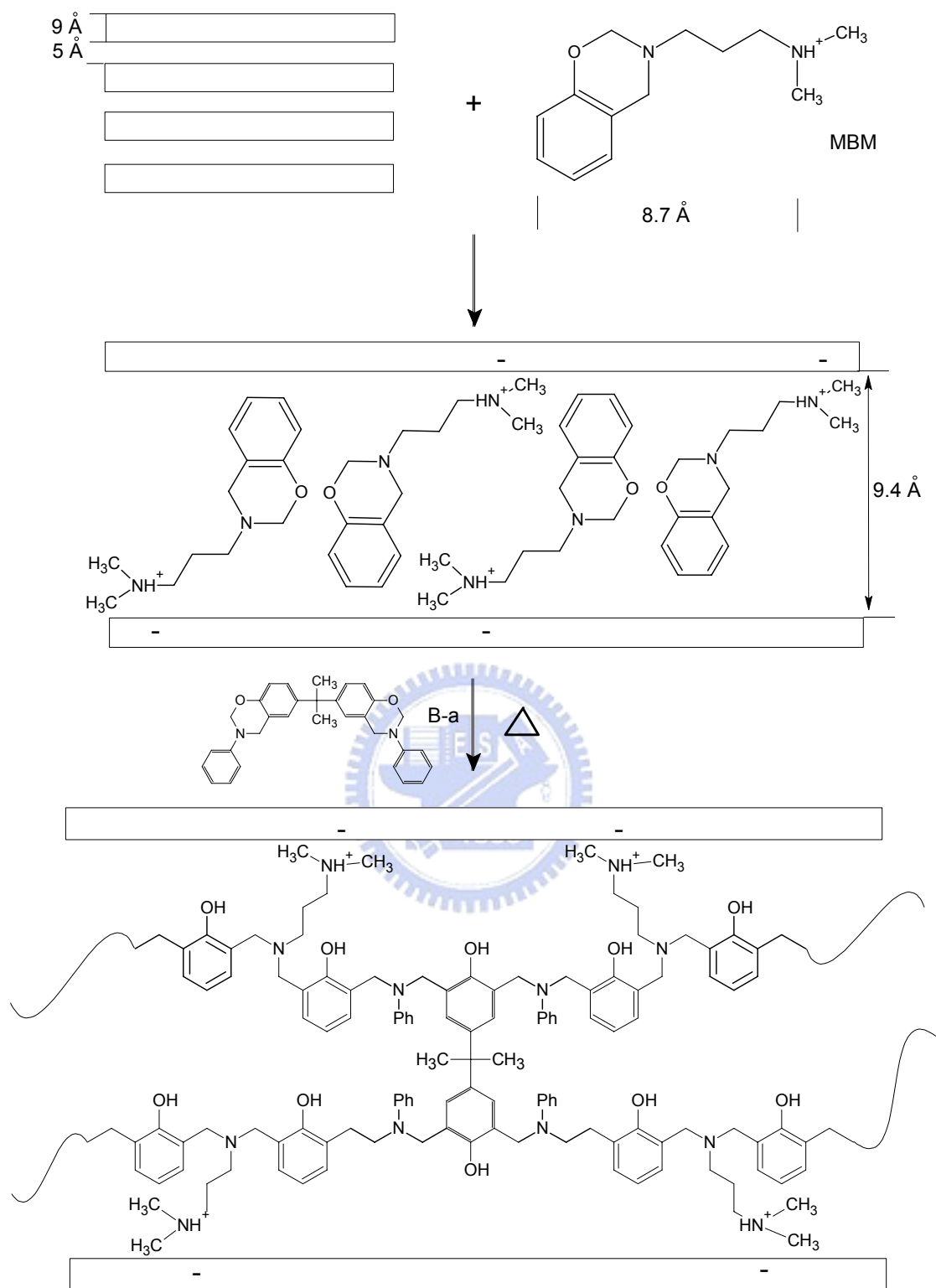
Polybenzoxazine (PBZ)

Scheme 5-1. Preparation of polybenzoxazine (PBZ).



Scheme 5-2. Preparation of the monofunctional benzoxazine monomer (MBM).





Scheme 5-3. Schematic illustration of clay intercalated by the MBM and polybenzoxaine.

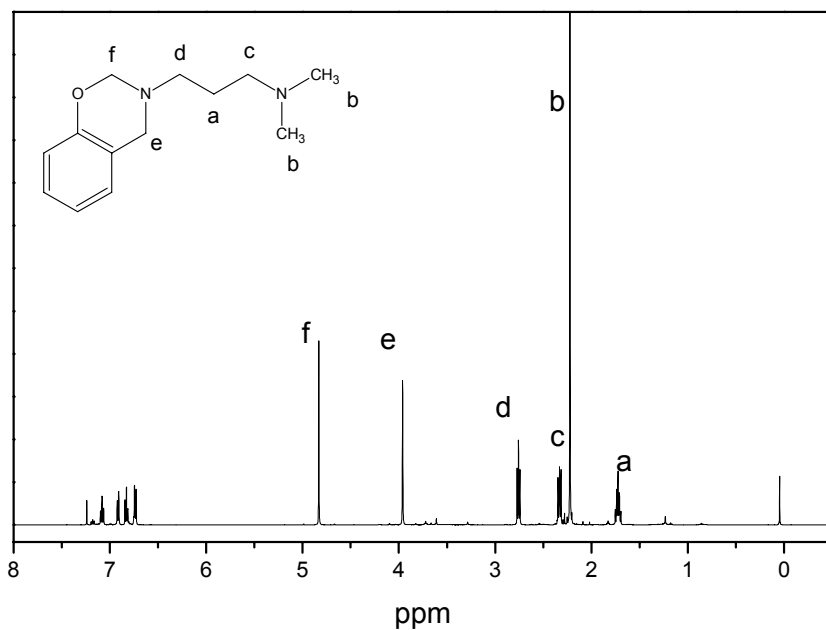


Figure 5-1. <sup>1</sup>H NMR spectrum of MBM.

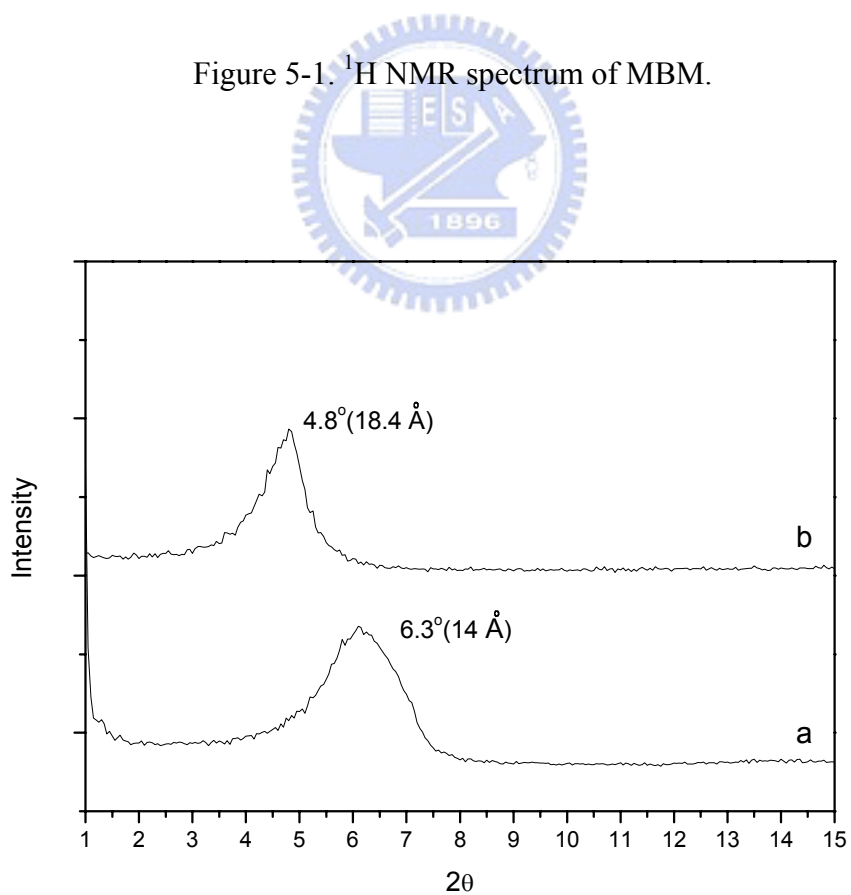


Figure 5-2. XRD patterns of (a) pure clay and (b) the clay intercalated by MBM.

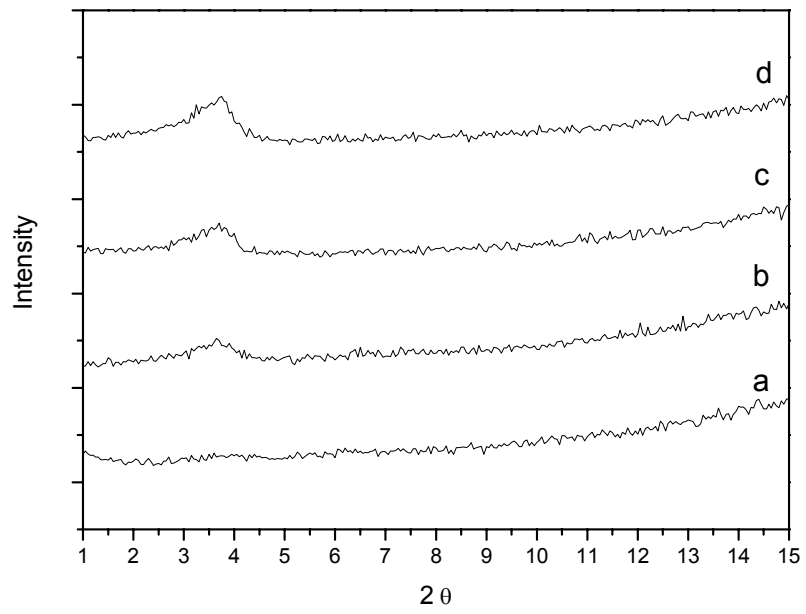


Figure 5-3. XRD patterns of the (a) 3, (b) 6, (c) 10, and (d) 15% clay nanocomposites.



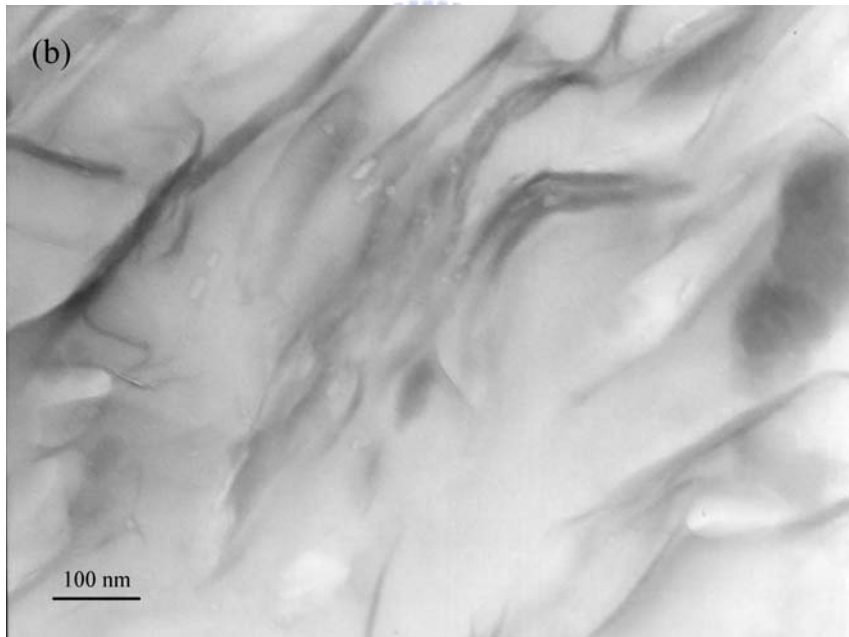
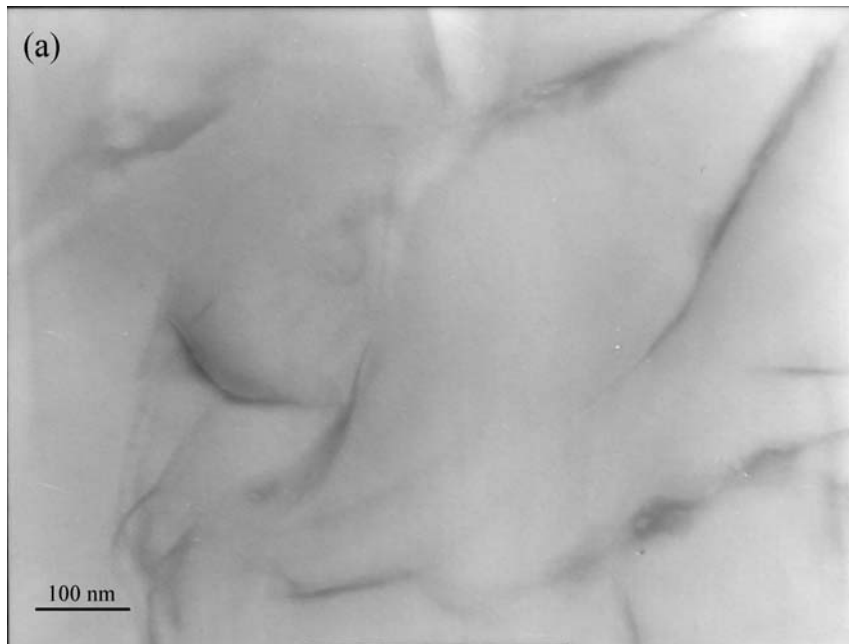


Figure 5-4. TEM micrographs of the (a) 3 and (b) 6% clay nanocomposites.

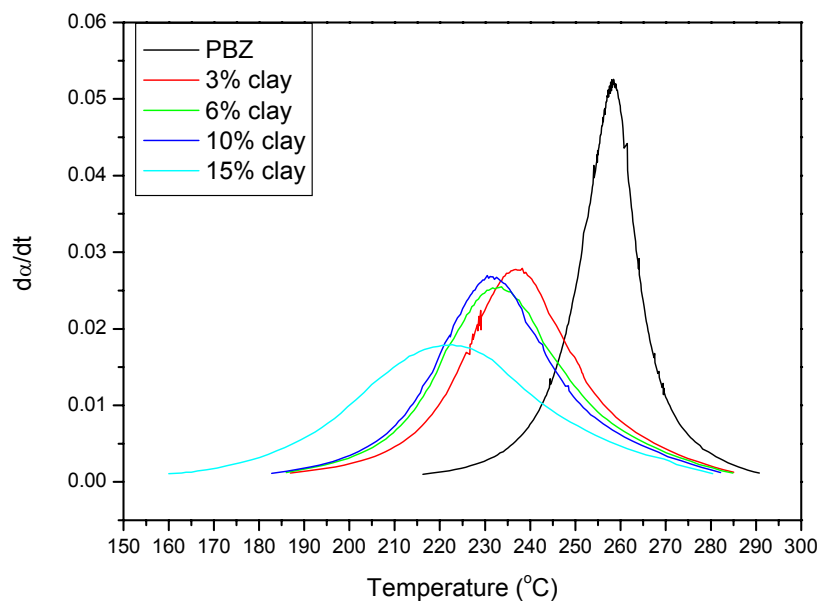


Figure 5-5. Dynamic exothermal curves of the PBZ/clay nanocomposites recorded at a heating rate of 20°C/min.

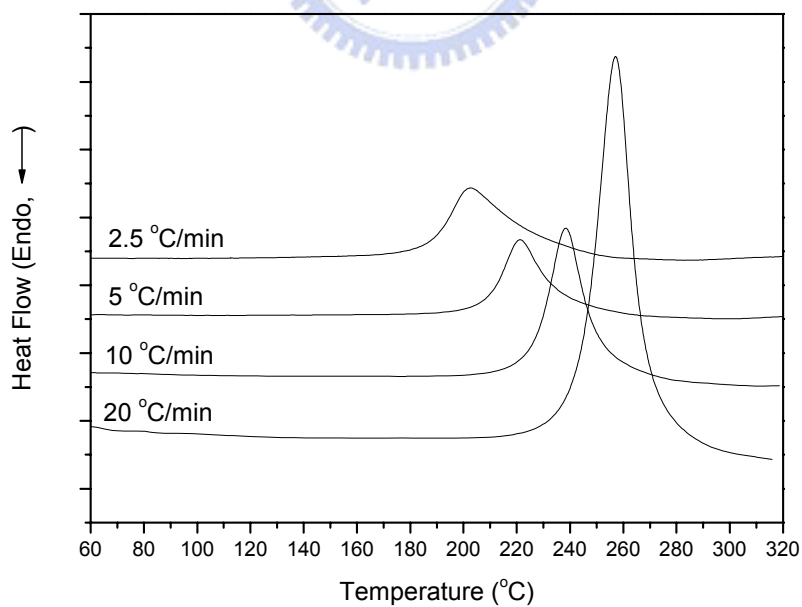


Figure 5-6. Dynamic DSC exothermic curves of pure PBZ recorded at different scan rates.

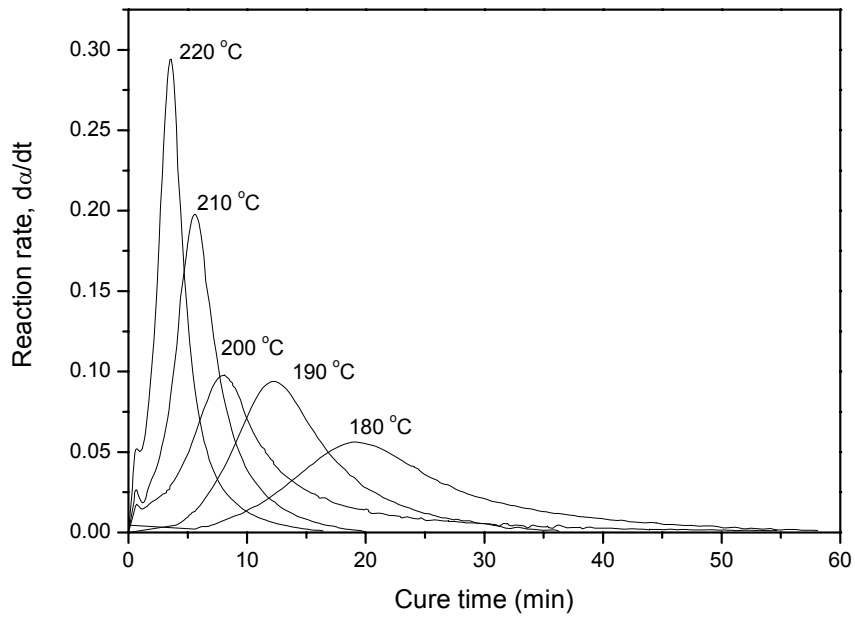


Figure 5-7. Plots of reaction rate versus curing time for pure PBZ at different curing temperatures.

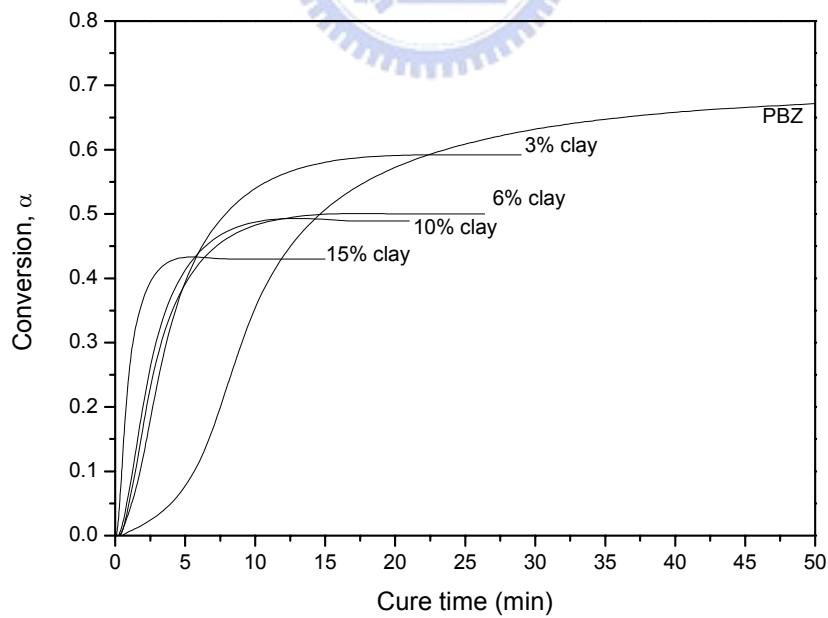


Figure 5-8. Plots of conversion as a function of cure time for the PBZ/clay nanocomposites cured at isothermal curing temperature of 200 °C.



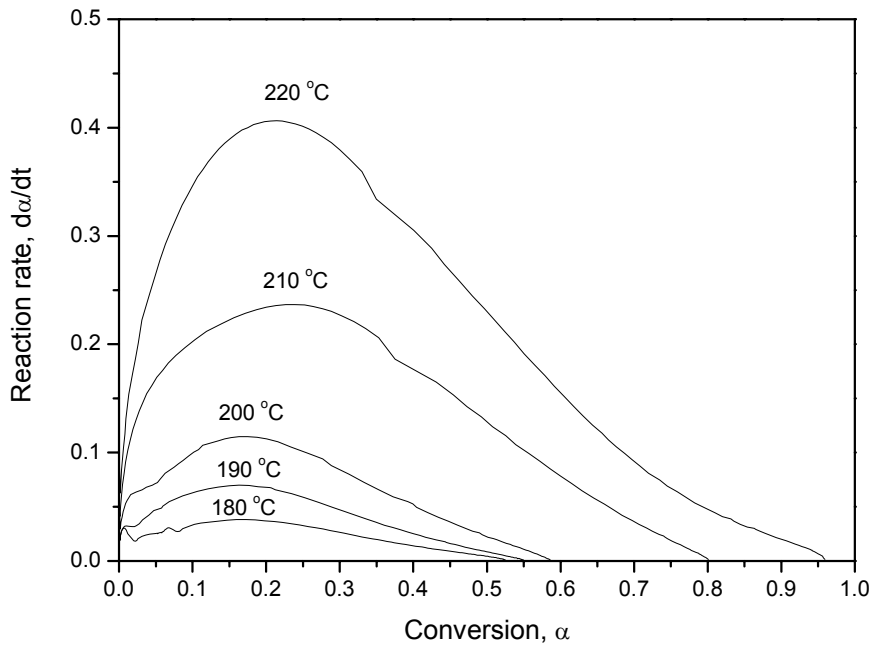


Figure 5-9. Plots of reaction rate as a function of conversion for the nanocomposites cured at different temperatures.

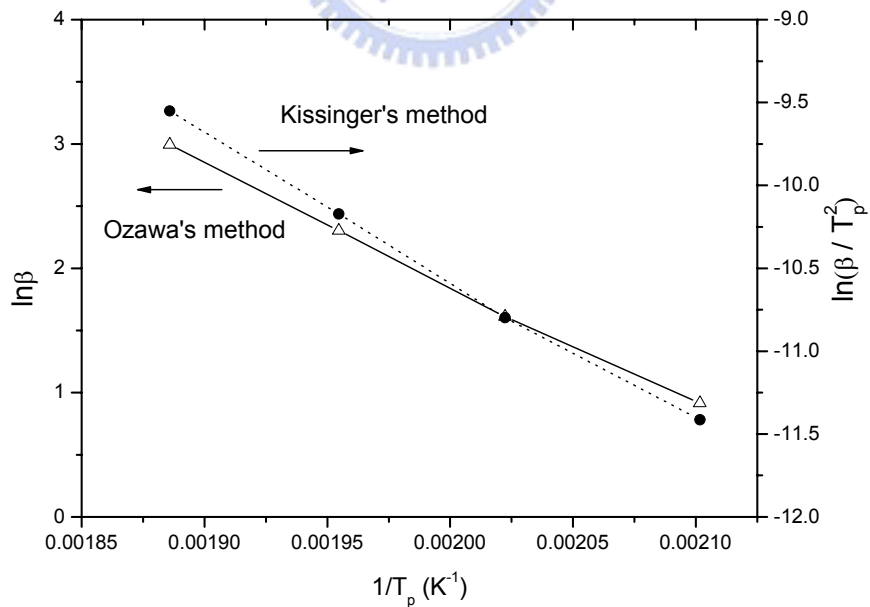


Figure 5-10. Representations of Ozawa's and Kissinger's methods of calculating the activation energy from non-isothermal data for pure PBZ ( $T_p$ , temperature at maximum reaction rate;  $\beta$ , heating rate).

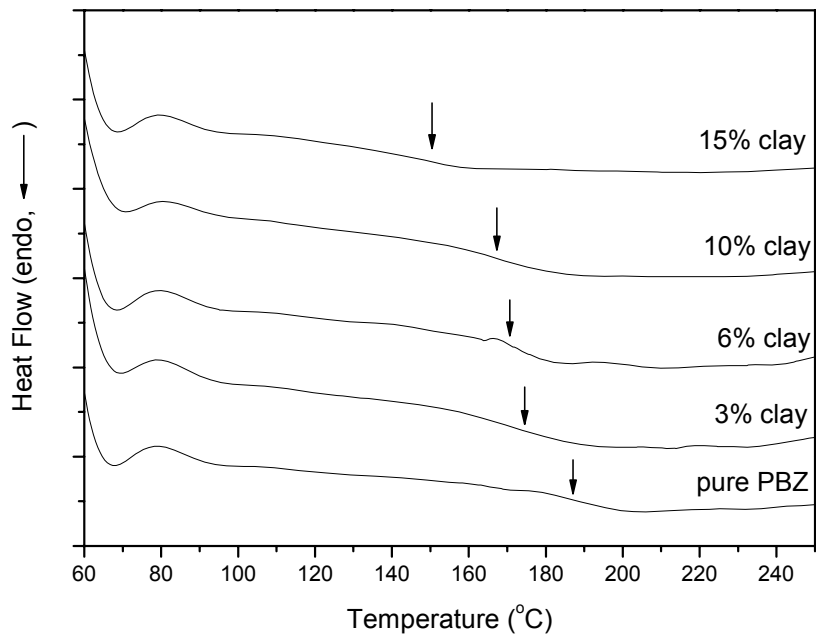


Figure 5-11. DSC curves for determining the glass transition temperatures of the nanocomposites.

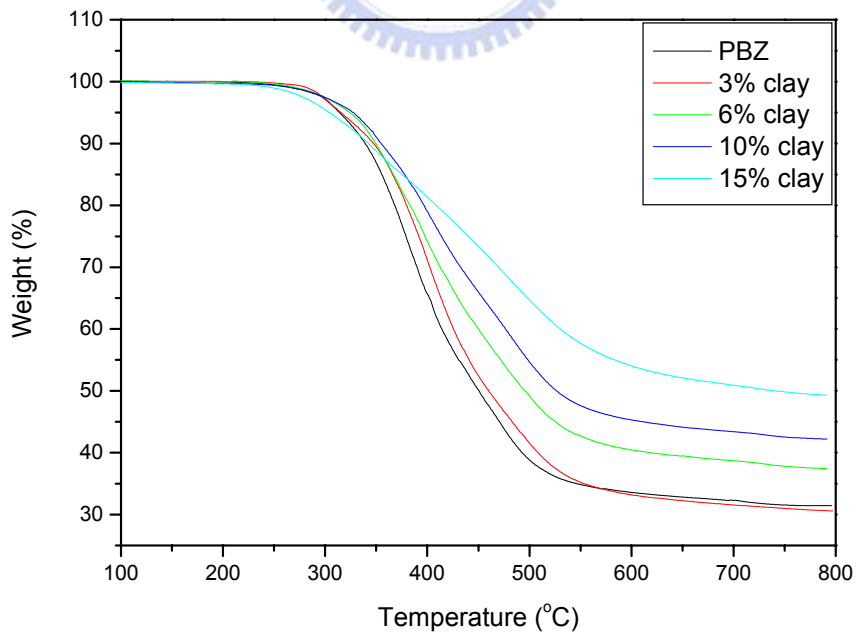


Figure 5-12. TGA curves of the PBZ/clay nanocomposites recorded under a nitrogen atmosphere.

## Chapter 6

### Conclusions and Future Outlook

#### *Conclusions*

We have prepared polystyrene/clay nanocomposites that have (a) an exfoliated structure when derived from POSS treatment and (b) an intercalated forms when treated with CPC. TGA of the nanocomposites suggests that the onset of thermal degradation occurs at a higher temperature for the nanocomposite formed from POSS than for either the virgin PS or the nanocomposite derived from CPC treatment. It appears that the presence of the POSS in the clay enhances the thermal stability of polystyrene.

We successfully synthesized intercalation agent of APB and prepared PS/clay nanocomposites with a fully exfoliated structure. Results of TGA indicated that intercalation agent containing rigid adamantane also has high thermal stability besides phosphonium group. The polymer adding silica layer can reduce CTE and provide good dimensional stability for the nanocomposites.

We have prepared polystyrene/clay nanocomposites that have (a) a mainly exfoliated structures with some portions intercalated when treated with CPC and (b) a fully exfoliated structure when treated with CPC/ $\alpha$ -CD. The  $^1\text{H}$  NMR spectra of the complexes demonstrate that the stoichiometry of the complexes is 1:2 (one CPC molecule to two  $\alpha$ -CD units). TGA revealed that the inclusion complex possesses increased thermal stability relative to that of the virgin CPC.

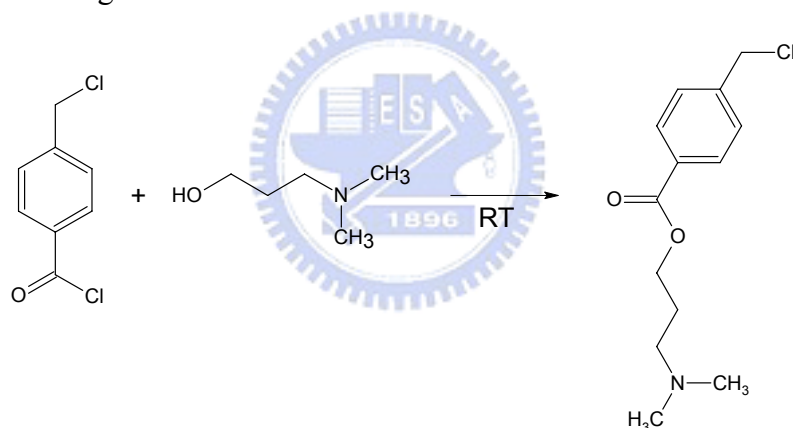
We successfully synthesized the intercalation agent MBM and prepared PBZ/clay hybrid nanocomposites. The sample had a fully exfoliated structure at a 3% clay content. The MBM intercalating agent, which contains a benzoxazine functional group that can undergo ring opening polymerization within the galleries of the clay,

promotes the exfoliated structure of nanocomposite. This finding suggests that the clay surface has a catalytic effect on the ring opening polymerization. The activation energy decreased upon increasing the clay content as a result of a lower conversion. The Kamal method—based on an autocatalytic model—suggested that the total order of the reaction was between 2.4 and 2.8.

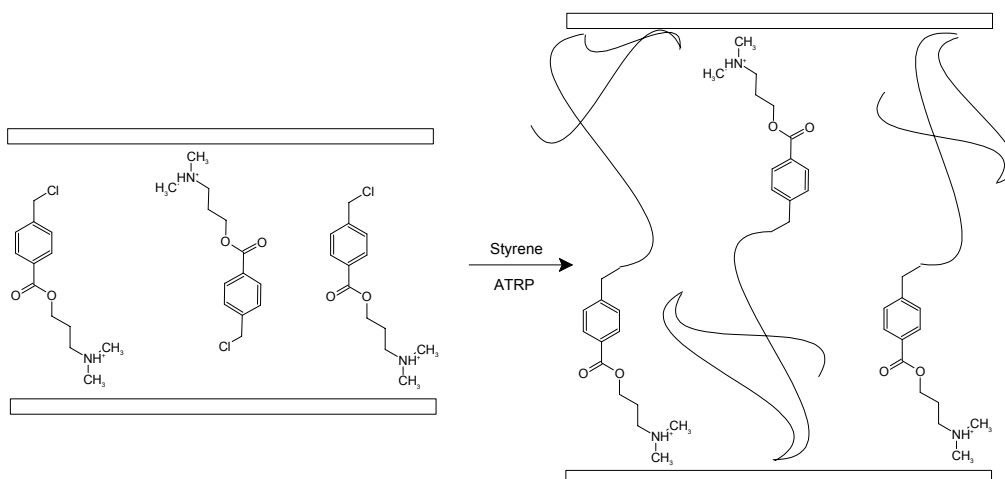
### Future Outlook

- Preparation of polystyrene/clay nanocomposite via in situ free radical surface-initiated polymerization.

The first, we synthesize initiator of ATRP, and then initiator intercalated clay via cation exchange.

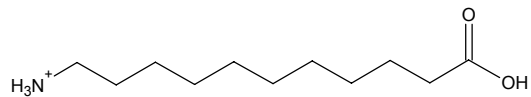
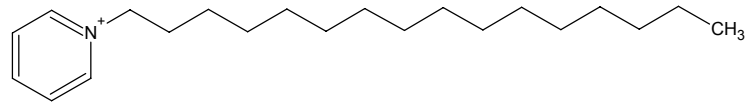


The second, intercalation agent of the initiator was polymerized via ATRP in the galleries of the clay.

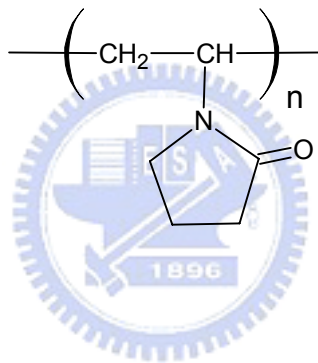


- The dispersing level of the clay in the matrix depends on hydrogen bond between intercalation agent and polymer.

We choose two intercalation agents: one could provide hydrogen bond with polymer; the other one could not.



Polymer matrix is poly(N-vinylpyrrolidone), PVP, and it could provide hydrogen bond with intercalation agent.



## List of Publications

1. **Ting-Ju Yeh**, Shiao-Wei Kuo, Yi-Che Su, Feng-Chih Chang\*, “**Enhanced Thermal Properties of PS Nanocomposites formed from Inorganic POSS-Treated Montmorillonite**”, *Polymer* 2004, 45, 2633.
2. **Ting-Ju Yeh**, Shiao-Wei Kuo, Huei-Kuan Fu, Feng-Chih Chang\*, “**Enhanced thermal properties of PS nanocomposites formed from Surfactant-cyclodextrin inclusion complex treated montmorillonite**”, *Polymer* 2005, 46, 741.
3. **Ting-Ju Yeh**, Huei-Kuan Fu, Wen-Yi Chen, Feng-Chih Chang\*, “**Synthesis of a Novel Benzoxazine Monomer-Intercalated Montmorillonite and the Curing Kinetics of Polybenzoxazine/clay Hybrid Nanocomposites**”, *J. Polym. Sci. Part B: Polym. Phys.* 2005, submitted.
4. **Ting-Ju Yeh**, Jieh-Ming Huang, Huei-Kuan Fu, Feng-Chih Chang\*, “**Thermal Properties of Exfoliated Polystyrene Nanocomposites Formed from Rigid Intercalated Agents-Treated Montmorillonite**”, *Polymer* 2005, submitted.
5. **Ting-Ju Yeh**, Feng-Chih Chang\*, “**Polystyrene/Clay Nanocomposite**”, Woodhead Publishing, Chapter 5, 2005.
6. Yi-Che Su, Shiao-Wei Kuo, **Ting-Ju Yeh**, Feng-Chih Chang\*, “**Thermal Properties and Hydrogen Bonding in polymer blend of polybenzoxine/poly(N-vinyl 2-pyrrolidone)**”, *Polymer* 2003, 44, 2187.

7. Yi-Che Su, **Ting-Ju Yeh**, Feng-Chih Chang\*, “**The Kinetics of B-a and P-a Type Copolybenzoxanine via Ring Opening Process**”, *J. Appl. Polym. Sci.* 2005, 95, 730.
  
8. **Ting-Ju Yeh**, Huei-Kuan Fu, Feng-Chih Chang\*, “**Synthesis of Initiator of Atom Transfer Radical Polymerization to Intercalate Clay via Situ Polymerization**” in preparation.
  
9. **Ting-Ju Yeh**, Huei-Kuan Fu, Feng-Chih Chang\*, “**Evolution of Surface Free Energy in Polymer/Clay Nanocomposite**” in preparation.



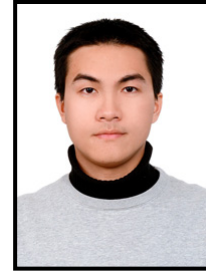
## Introduction to Author

English name: Ting-Ju Yeh

Chinese name: 葉定儒

Birthday: 1978. 09. 13

Address: 台中縣大甲鎮幸福里黎明路 2-2 號



### Education:

1997.09 ~ 2001.06      **B.S.**, Department of Chemical Engineering, National Taipei University of Technology, Taipei, Taiwan.

2001.07 ~ 2003.02      **M.S.**, Institute of Applied Chemistry, National Chiao Tung University, Hsinchu, Taiwan.

2003.03 ~ 2005.09      **Ph.D.**, Institute of Applied Chemistry, National Chiao Tung University, Hsinchu, Taiwan.